Final Report
NJCSCR Fellowship Award

Principal Investigator: Helen M. Buettner

NJCSCR Graduate Fellow: Margaret Julias

Department of Biomedical Engineering
Rutgers, The State University of New Jersey
599 Taylor Road
Piscataway, NJ 08854
(732) 445-4500

A Novel Micromechanical Method for Controlling Microstructure in Nerve Grafts

Grant Number: 05-2912-SCR-E-0
Grant Period: 6/15/2005 – 6/30/2009
Date: June 16, 2010

ORIGINAL AIMS OF THE PROJECT

The original aims of this project were:

1. To establish a micromechanical methodology for aligning 3D ECM gel models of an artificial nerve graft lumen.
2. To use the aligned gels developed in SA 1 to create 3D matrices containing oriented Schwann cells.

Our goal was to provide an alternative method for orienting the nerve graft matrix. Previously proposed methods require specialized facilities, increase the use of non-biological materials in the graft, or produce only large scale orientation. Toward this end, we employed a novel micromechanical method based on the needling technique used in acupuncture to create a field of matrix alignment around the needle in collagen-based matrices.

PROJECT SUCCESSES

The basic biomaterial system used for this work consisted of collagen-based, three-dimensional gels prepared from lyophilized collagen dissolved in acetic acid, neutralized with NaOH, and diluted to the desired strength in M199 and 10XMEM media to obtain physiological pH and ionic strength, then placed in a 37°C incubator to permit gelation. The gels were prepared in 35-mm glass bottom culture dishes with porous polyethylene (PPE) and poly(dimethyl siloxane) (PDMS) inserts used to modify the size and shape of some gels (1, 2). In some cases, gel composition was varied by adding fibrin or hyaluronic acid to the collagen.

Construction of a precision needling instrument. After multiple attempts and prototypes, we successfully developed a device consisting of a computer controlled micromotor to which a 250-μm stainless steel acupuncture needle (Seirin, Tokyo, Japan) was attached. With this apparatus, the needle could be inserted a specified depth into the gel using a calibrated micromanipulator and automatically rotated for a fixed number of revolutions at a constant, predetermined speed to produce matrix alignment (1, 6).

Methodology for measurement of matrix alignment. Although preliminary experiments were conducted using fluorescence confocal microscopy, that became prohibitively expensive and time consuming for larger sample numbers. Instead, we a devised a system to record the evolution of matrix alignment using polarized light microscopy. In this system, the collagen gel was situated between cross-polarizers. As the needle was rotated, a pattern of birefringence emerged due to the alignment of fibers creating bright regions when aligned 45° off-axis relative to the cross-polars. The brightness and area of the birefringence increased with needle rotation until gel failure, after which it sharply declined, thus enabling a quantitative measure of alignment and point-of-failure, which we analyzed using algorithms we developed as a means of characterizing matrix performance (1, 9).

Effects of matrix properties. In the course of developing the system, it became clear that variations in matrix properties represented a degree of tunability in matrix alignment and failure. To identify the appropriate parameter space for subsequent experiments, we examined key properties of interest to nerve guidance applications:

Matrix composition. In pure collagen gels, increasing collagen concentration within a relevant range (1.5-2.5 mg/ml) increased matrix alignment (1, 3, 5; Figure 1). For a given collagen concentration, adding fibrin (3, 11; Figure 2) or hyaluronic acid (7; Figure 3) decreased alignment. The final degree of alignment that could be achieved in the matrix was limited by the maximum number of needle revolutions possible before the gel broke. For collagen-only gels, the average number of revolutions was 5. Adding fibrin, which

decreased the stiffness of the matrix, doubled that number to 10; hyaluronic acid had a similar effect. This variation offers a reasonable range for tuning matrix characteristics through composition.

Matrix crosslinking. Crosslinking the collagen matrix increased matrix stiffness, reduced matrix alignment, and produced gels that failed at a lower degree of alignment (Figure 4). Gels were examined in a range of 1.5-2.0 mg/ml collagen. Alignment increased with increasing collagen concentration, but decreased with crosslinking. Cone-and-plate rheometry demonstrated that the crosslinking increased the storage modulus in shear by an order of magnitude. No differences in the failure point were observed when changing collagen concentration. However, crosslinked collagen failed with significantly fewer needle revolutions than untreated gels (1, 8).

Matrix geometry. Using collagen gels of different size and shape we demonstrated that geometrical asymmetry significantly influences alignment characteristics of the matrix. Small diameter circular gels generated more alignment per revolution than larger gels, but also failed earlier, and the alignment at failure was greater for the larger gels. Asymmetrical gels aligned faster than symmetrical ones; increasing anisotropy resulted in the greatest alignment at failure (2, 5, 12).

Cellular studies. After establishing the properties of the matrix, we showed quantitatively using fibroblasts as a model cell system that matrix alignment results in cell alignment (Figure 5) and changes in cell morphology (2, 3, 5, 7, 8, 10). With assistance from Dr. Li Cai in the Department of Biomedical Engineering we also adapted a procedure for labeling chick embryos with GFP as a source of GFP-labeled Schwann cells.

Discovery. An unanticipated success in the course of this work was the discovery of a new way to create nerve guides from collagen-based materials using the system we developed but separate from the proposed methods. This will not be described here due to the fact that we are in the process of filing a patent disclosure, but it is an avenue that we are continuing to pursue.

PROJECT CHALLENGES

Instrumentation. While we were successful in building a needling instrument, it was a more difficult task than we initially envisioned. Even with considerable expertise in micro-instrumentation contributed by collaborators, this required a significant development stage; we conceived and constructed three completely different prototypes before achieving a workable design for needle rotation. Although we had hoped to also incorporate bi-directional translational needling motion to produce linear alignment of the collagen matrices, this proved less straightforward and ultimately we opted to defer that goal in favor of obtaining some results on the biomaterial and biological features of the system that we believed would enable us to achieve our aims more quickly in the long run. Too late for the current project but helpful for future work, we learned of another group who has recently developed new micro-instrumentation along the lines that we need to extend the capabilities of our system to accomplish our original goal.

Biomaterials. The fact that alignment is sensitive to matrix properties introduces a means of controlling its performance characteristics, but also a sensitivity to variability in experimental conditions. In the process of developing the needling methodology, we initially encountered reproducibility issues that we eventually traced to variability in the collagen stock, purchased in lyophilized form. This was resolved by choosing one supplier, purchasing stock in large batches, and fine-tuning our own procedures to maintain the greatest consistency in performance. These difficulties are not unusual for biological materials and simply represented a learning curve in

working with our particular system. Our decision to do a more thorough characterization of the biomaterials matrix was motivated by the observation of this variability in the system.

Cellular studies. Our initial plan was to use our system to promote Schwann cell alignment in nerve graft models. This remains an objective but was delayed by the instrumentation and biomaterials issues. We developed the means to provide a steady source of GFP-labeled Schwann cells for this part of the study. However, we opted to use an easier cell source, fibroblasts, while working out the biomaterials procedures to avoid unnecessarily wasted effort in cell preparation. With a reliable, efficient, and reproducible methodology established on the biomaterials end now, we are ready to move forward with Schwann cells.

IMPLICATIONS FOR FUTURE RESEARCH AND/OR CLINICAL TREATMENT

Micromechanical needling represents a new and novel way to control the microarchitecture of collagen-based matrices for nerve graft applications. Our results indicate that this simple, inexpensive technique can produce cell alignment and change cell shape within these matrices, and that the material properties of the matrix may offer fine control over the degree of response. As such, this may ultimately be a way not only to orient cells in nerve grafts, but also to promote other mechanically sensitive cell behavior, such as spreading, proliferation, differentiation, and gene expression. This work forms a strong basis for further work on biomaterials with spatially graded cues for controlling neural cell behavior.

PLANS TO CONTINUE THIS RESEARCH

We are currently extending this research along three lines: 1) creation of longitudinal matrix and cell alignment, 2) investigation of cellular responses to matrix manipulation by needling, 3) application of the new methodology for creating nerve guide tubes that we discovered in the course of this project (now undergoing patent disclosure). We believe that our initial goal of producing matrix alignment along the axis of the nerve graft to align Schwann cells in the lumen is a viable one and are continuing with that aim. At the same time, we have begun exploring other ways in which cells may be affected by needling of the matrix, and we are also working with the new nerve guide tubes we have created. Although our earliest attempts to obtain other funding were near misses, we have subsequently been able to support the work through various funding sources, including both NSF and NIH. The project has greatly benefitted from the participation of Prof. David Shreiber, who co-supervised Ms. Julias and has taken the lead in continuation of the work.

Grants funded:
6/1/09 – 5/31/14
Grant Amount: $400,000
NSF-CBET
"CAREER: Engineered biomaterial gradients for control of neural cells"
PI: D. Shreiber

06/2008 - 05/2010
Grant Amount: $425,000
NIH - National Institute of Biomedical Imaging and Bioengineering

NIH - National Institute of Biomedical Imaging and Bioengineering
"Role of connective tissue geometry in acupuncture"
PI: H. Buettner

8/2006 - 8/2007
Grant Amount: $100,000
NJ Center for Military Biomaterials Research
"Biomaterials for improved peripheral nerve regeneration"
PI: H. Buettner

Submitted but not funded:
Application ID: 1R03NS055270-01
Proposal Title: Micropatterned surfaces for directing neural organization
Proposal Receipt Date: 06/2005
Amount: $151,375
PI: H. Buettner

Application ID: 1T32EB001649-01A2
Proposal Title: Training Program in Engineered Tissue Systems
Submitted: 09/2005
$1,595,193
PI: H. Buettner
(Nerve tissue systems were one of three major thrust areas of this proposal.)

PUBLICATIONS

Journal Articles

1. Julias M, Edgar LT, Buettner HM, and Shreiber DI. An in vitro assay of collagen fiber alignment by acupuncture needle rotation. Biomedical Engineering Online, 2008. 7:19.

2. Julias M, Buettner HM, Shreiber DI. Varying assay geometry to emulate connective tissue planes in an in vitro model of acupuncture. Submitted to The Anatomical Record (December 2009). In Review.

Conference Proceeding Papers & Abstracts

3. Julias M, Shreiber DI, and Buettner HM. Alignment of tissue equivalents by acupuncture needling (Poster). 2005 Biomedical Engineering Society Meeting, Baltimore, MD.

4. Señeres AW, Julias M, Patel N, Shreiber DI, and Buettner HM. A finite element model of acupuncture needling. 2005 ASME Summer Bioengineering Conference, Vail, CO.

5. Julias M, Shreiber DI, and Buettner HM. Extracellular matrix alignment using micromechanical needle manipulation. 2006 ASME Summer Bioengineering Conference, Amelia Island, FL.
   **Received Honorable Mention in PhD Student Paper Competition, Poster Division*

6. Señeres AW, Tamba A, Julias M, Shreiber DI, Buettner HM, and Bouzit M. A microrobotic needling instrument for an in vitro acupuncture model. 2006 ASME Summer Bioengineering Conference, Amelia Island, FL.

7. Julias M, Shreiber DI, and Buettner HM. Matrix Concentration Affects Alignment of Tissue Equivalents (Poster). 2006 Biomedical Engineering Society Meeting, Chicago, IL.

8. Julias M, Edgar LT, Shreiber DI, and Buettner HM. Collagen content and stiffness affect the biomechanical response of collagen gels to acupuncture in vitro. 2008 ASME Summer Bioengineering Conference, Marco Island, FL.
   **Received second place in PhD Student Paper Competition, Podium Division*

9. Edgar LT, Julias M, Shreiber DI, and Buettner HM. Polarized light microscopy for analyzing tissue mechanics during in vitro acupuncture. 2008 ASME Summer Bioengineering Conference, Marco Island, FL.

10. Julias M, Edgar LT, Buettner HM, and Shreiber DI. Emulating The Anatomy Of Acupuncture Points With In Vitro Models. 2009 ASME Summer Bioengineering Conference, Lake Tahoe, CA.

11. Julias M, Buettner HM, and Shreiber DI. The biophysical response of collagen-fibrin composite gels to in vitro acupuncture. 2010 ASME Summer Bioengineering Conference, Naples, FL.

12. Julias M, Buettner HM, and Shreiber DI. The geometry of connective tissue planes accentuates the biophysical response to traditional acupuncture: an in vitro study. 2010 ASME Summer Bioengineering Conference, Naples, FL.

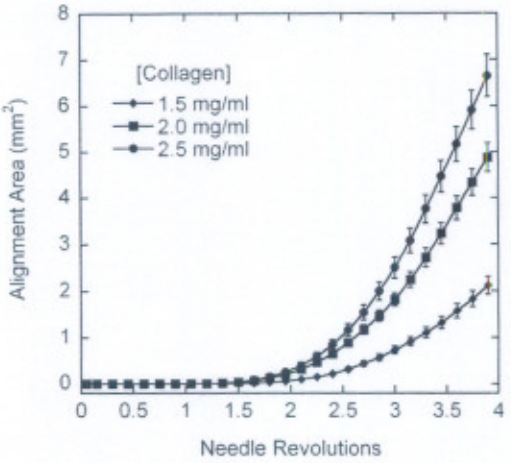

Figure 1. Effects of collagen concentration on matrix alignment. The birefringent area of alignment was identified from image sets obtained during needling using polarized light microscopy and plotted as a function of needle revolution. Alignment Increased with increasing collagen concentration.

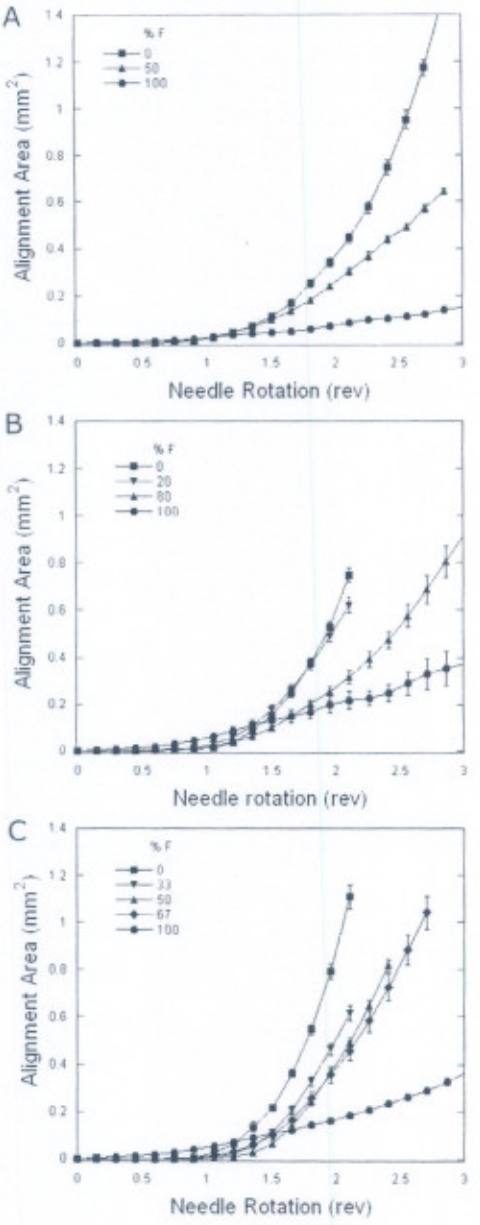

Figure 2. Effects of fibrin content on collagen matrix alignment. The birefringent area of alignment was identified from image sets and plotted as a function of needle revolution. Composition effects were observed in gels with total protein concentrations of 2.0mg/ml (A) 2.5mg/ml (B) and 3.0mg/ml (C). At the same total protein content, the alignment decreased with increasing fibrin content. Uneven curve lengths were due to gel failure at a different number of needle rotations for different compositions. F: fibrinogen.

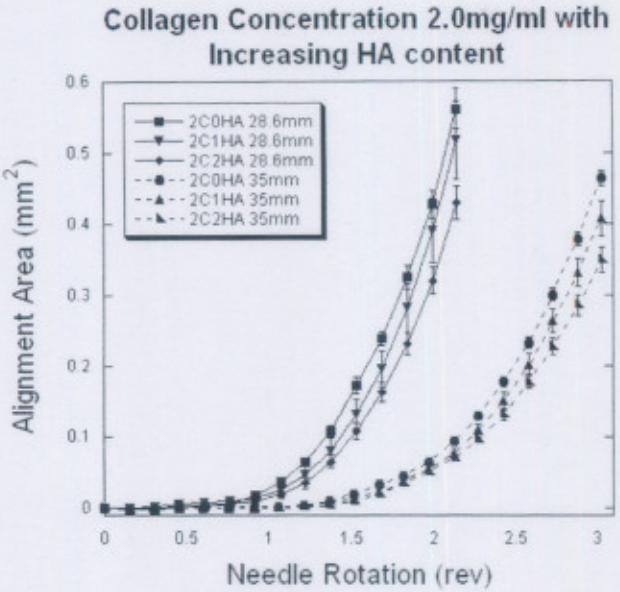

Figure 3. Effects of hyaluronic acid on matrix alignment in gels of different thickness. In general, alignment decreased with increasing HA concentration. C: [Collagen](mg/ml), HA: [Hyaluronic Acid](mg/ml).

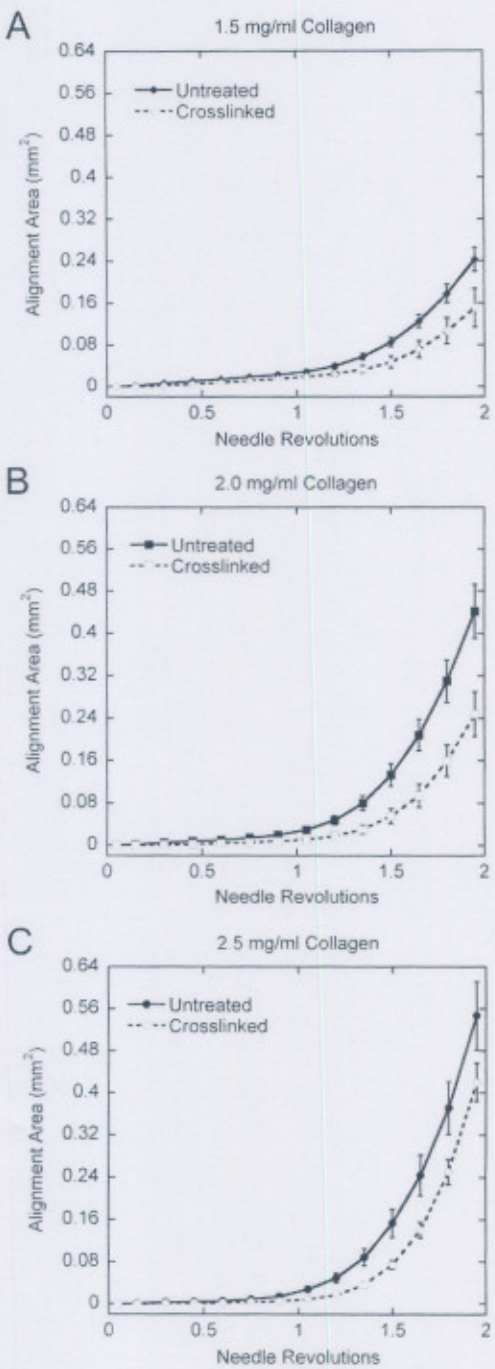

Figure 4: Effects of crosslinking on matrix alignment. Needle rotation in crosslinked collagen gels generated less alignment than untreated collagen gels at each collagen concentration. The area of alignment increased with increasing collagen concentration for both untreated and crosslinked collagen.

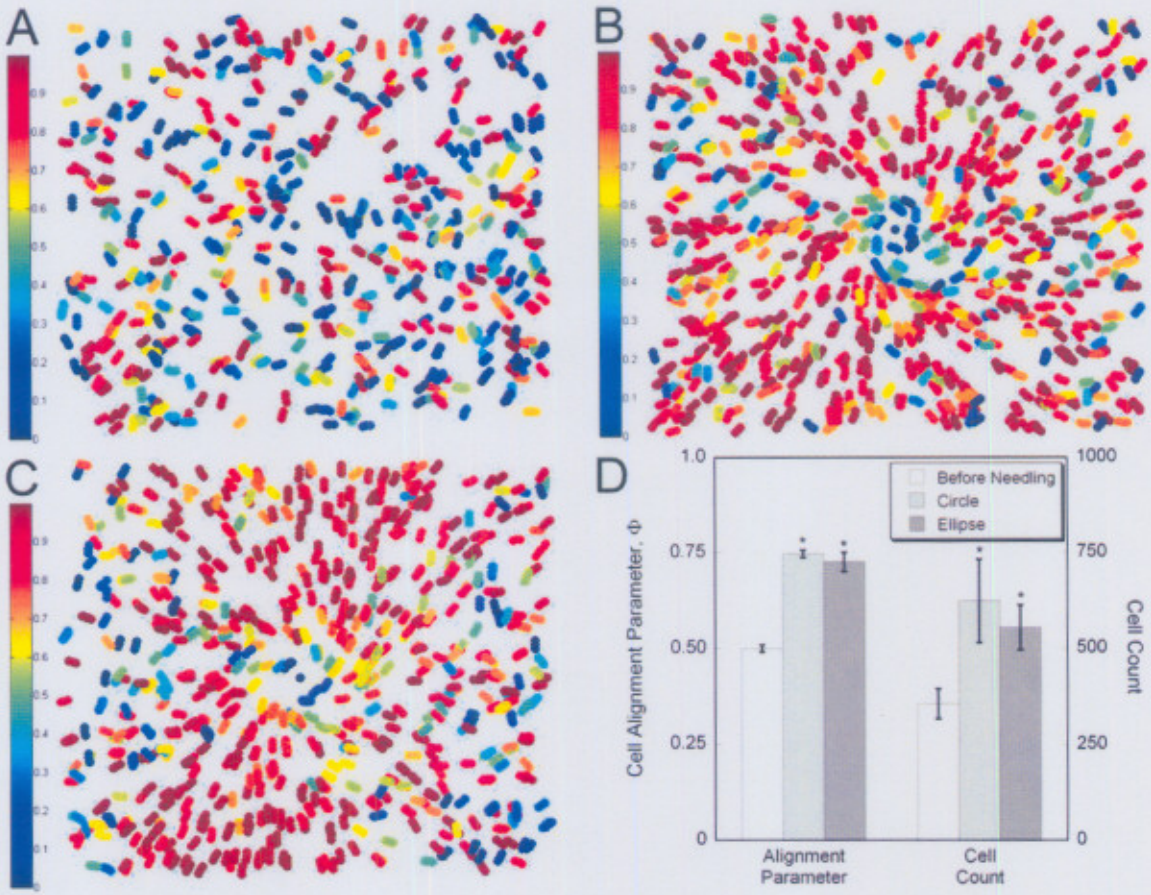

Figure 5: Quantitative assessment of the cell alignment parameter, F, which ranges from 0 (circumferential alignment – blue) to 1 (radial alignment – red). The alignment parameter was calculated for each cell in a stack of images and projected onto the same plot. Representative plots are shown for gels before needling (A), and after needling in circular (B) and elliptical (C) gels, where the major axis is oriented horizontally. Before needling, cells are randomly oriented. After needling, alignment increases in both circular and elliptical gels. The average cell count in the imaged area also increased after acupuncture needle rotation, demonstrating the significant displacement of cells and collagen towards needle as the fibers align.

BioMedical Engineering OnLine

BioMed Central

Research

Open Access

An *in vitro* assay of collagen fiber alignment by acupuncture needle rotation

Margaret Julias[1], Lowell T Edgar[2], Helen M Buettner[1,2] and David I Shreiber*[2]

Address: [1]Department of Chemical and Biochemical Engineering, Rutgers, The State University of New Jersey, Piscataway, NJ, USA and [2]Department of Biomedical Engineering, Rutgers, The State University of New Jersey, Piscataway, NJ, USA

Email: Margaret Julias - tikus@eden.rutgers.edu; Lowell T Edgar - honor51@eden.rutgers.edu; Helen M Buettner - buettner@rci.rutgers.edu; David I Shreiber* - shreiber@rci.rutgers.edu

* Corresponding author

Published: 7 July 2008

BioMedical Engineering OnLine 2008, **7**:19 doi:10.1186/1475-925X-7-19

Received: 8 February 2008
Accepted: 7 July 2008

This article is available from: http://www.biomedical-engineering-online.com/content/7/1/19

© 2008 Julias et al; licensee BioMed Central Ltd.
This is an Open Access article distributed under the terms of the Creative Commons Attribution License (http://creativecommons.org/licenses/by/2.0), which permits unrestricted use, distribution, and reproduction in any medium, provided the original work is properly cited.

Abstract

Background: During traditional acupuncture therapy, soft tissues attach to and wind around the acupuncture needle. To study this phenomenon in a controlled and quantitative setting, we performed acupuncture needling in vitro.

Methods: Acupuncture was simulated in vitro in three-dimensional, type I collagen gels prepared at 1.5 mg/ml, 2.0 mg/ml, and 2.5 mg/ml collagen, and either crosslinked with formalin or left untreated. Acupuncture needles were inserted into the gels and rotated via a computer-controlled motor at 0.3 rev/sec for up to 10 revolutions while capturing the evolution of birefringence under cross-polarization.

Results: Simulated acupuncture produced circumferential alignment of collagen fibers close to the needle that evolved into radial alignment as the distance from the needle increased, which generally matched observations from published tissue explant studies. All gels failed prior to 10 revolutions, and the location of failure was near the transition between circumferential and radial alignment. Crosslinked collagen failed at a significantly lower number of revolutions than untreated collagen, whereas collagen concentration had no effect on gel failure. The strength of the alignment field increased with increasing collagen concentration and decreased with crosslinking. Separate studies were performed in which the gel thickness and depth of needle insertion were varied. As gel thickness increased, gels failed at fewer needle revolutions. For the same depth of insertion, alignment was greater in thinner gels. Alignment increased as the depth of insertion increased.

Conclusion: These results indicate that the mechanostructural properties of soft connective tissues may affect their response to acupuncture therapy. The in vitro model provides a platform to study mechanotransduction during acupuncture in a highly controlled and quantitative setting.

Background

In traditional acupuncture therapy, fine needles are inserted into the skin at specific points on the body and manipulated manually, typically by needle rotation. During this process, it is important to achieve the characteristic of "de qi", a physical sensation experienced by the patient, and a biomechanical phenomenon experienced by the acupuncture therapist that is also known as needle grasp. In needle grasp, the therapist feels a resistance to further needle manipulation, which has been described as

a fish biting on a line (see [1]). Recent studies by Langevin et al suggest that needle grasp results when collagen fibers of the loose, subcutaneous connective tissue couple to and wind around the rotating needle [2-4]. The connective tissue experiences significant deformation during this process. In addition, acupuncture needle manipulation in connective tissue explants induces cytoskeletal remodeling by fibroblasts [5,6], the predominant cell type in loose connective tissue, supporting the hypothesis that tissue deformation due to needle manipulation mechanically stimulates fibroblasts, resulting in mechanotransduction effects that may contribute to therapeutic benefits [2,3].

These in vivo and ex vivo findings have pioneered an exciting focus on connective tissue involvement in acupuncture, but also raise interesting questions about acupuncture needling and collagen fiber winding that motivate the need for in vitro tools. From a therapeutic perspective, if fiber winding does play an important role then parameters that affect winding would be expected to alter the therapeutic response. Candidate parameters include ones that would affect tissue mechanics, such as matrix composition, density, and stiffness, as well as the thickness of the tissue layer(s). Identifying relationships among tissue properties, winding, and therapeutic effects through in vivo experiments alone, however, is complicated by normal in vivo variations in tissue properties. For example, the collagen content in skin is known to differ with location, tissue type, and skin layer [7-9]. Additionally, collagen content decreases with aging [10-12], potentially due to an increase in collagen crosslinking [13], and the thickness of the subcutaneous connective tissue is variable in humans, which may also affect the response to needling [14]. Accounting for these variations significantly increases the sample number required to obtain statistically meaningful in vivo data.

With this in mind, we have developed an in vitro approach to examine the first part of the proposed therapeutic mechanism, i.e., the link between tissue properties and collagen fiber winding, which can be used to guide further in vivo investigation. Specifically, we used type I collagen gels to study the effects of matrix properties on collagen fiber response to acupuncture needle rotation. We subjected gels with different collagen concentrations and degrees of crosslinking to computer-controlled needle rotation and used polarized light imaging to monitor the change in collagen fiber alignment during needle rotation. In separate gels, we varied the thickness and depth of needle insertion. Our results demonstrate that the winding response of fibrillar collagen to needle rotation resembles that of loose connective tissue and varies with network density and stiffness and the depth of needle insertion. The quantitative approach developed in this work provides a useful new tool to aid in elucidating tissue-level mechanisms of acupuncture.

Methods

Collagen gel preparation

Acellular collagen gels were prepared from lyophilized collagen (Elastin Products, Owensville, MO) as previously described [15]. A stock solution was prepared by dissolving 3.75 mg/ml collagen in 0.02 N acetic acid. The stock solution was diluted with 0.02 N acetic acid, neutralized with 0.1 N NaOH, and further diluted with M199 and 10XMEM media (Sigma Aldrich, St Louis, MO) to achieve the desired final collagen concentration of 1.5, 2.0, or 2.5 mg/ml (see below). A 3-ml gel solution was poured into a 35-mm glass bottom MatTek dish with a 20-mm glass microwell (MatTek Corporation) and incubated at 37°C for 2 hr to ensure complete fibril formation. After self assembly, 1 ml of fresh phosphate buffered saline (PBS) was added on top of the gel. In some samples, the collagen solution was spiked with FITC-labeled collagen (Elastin Products, Owensville, MO) in a 1:9 ratio of fluorescent collagen:collagen to permit visualization of collagen fibers using confocal microscopy. For crosslinking studies, gels were incubated in 1 ml of 10% neutral buffered formalin solution for 15 min on a rocker plate. The formalin solution was then replaced with PBS. The final height of gel was 4 mm and did not vary significantly with crosslinking.

In vitro acupuncture

A computer-controlled motor (MicroMo Electronics, Inc.) was used to needle the collagen gels. A 250-μm stainless steel acupuncture needle (Seirin, Tokyo, Japan) was attached to the motor and inserted perpendicular to the surface of the gel to a depth of 3 mm using a calibrated micromanipulator. The needle was rotated at 0.3 rev/s for either 2 or 4 revolutions in samples used for confocal imaging, or for 10 revolutions in samples used for continuous recording of the evolution of fiber alignment with polarized light microscopy.

A separate series of experiments was performed to investigate the influence of the depth of needle insertion on the response of the gel. Collagen solution was prepared at 2.0 mg/ml as described above, and gels were prepared such that the final gel height at the middle of the gel was 2 mm, 4 mm, or 6 mm. These gels were subjected to in vitro acupuncture as described above, with the depth of needle insertion varying from 1.5 mm to 4.5 mm and 25%–75% of the thickness of the gel (Table 1).

Confocal imaging

Confocal microscopy was used to examine the fibril alignment pre- and post- needle rotation. The MatTek dish was covered with a 3 mm-thick sheet of poly(dimethyl

Table 1: Conditions for investigating effects of needle insertion depth

Gel Height (mm)	Insertion Depth (mm)	Insertion Depth/Gel Height (%)
2	1.50	75.0
4	1.50	37.5
4	2.25	56.3
4	3.00	75.0
6	1.50	25.0
6	2.25	37.5
6	3.00	50.0
6	4.50	75.0

siloxane) (PDMS), through which the acupuncture needle was inserted prior to entering the gel. The needle was rotated either 2 or 4 revolutions with the motor, after which the needle was de-coupled from the motor. Insertion through the PDMS prevented the needle from recoiling when detached from the motor and allowed the transfer of the dish to the confocal microscope. The gel was imaged with a 63× objective using a laser wavelength of 488 nm to visualize the fluorescent collagen fibers (excitation 497 nm, emission 520 nm). The confocal images were compared to bright field and polarized light images taken during the needling procedure.

Polarized light imaging

Polarization light microscopy (PLM) was used to observe and image the evolution of fiber alignment continuously in real time. A dissection stereomicroscope (Carl Zeiss Microimaging, Thornwood, NY) with a USB camera (Matrix Vision, GmbH, Oppenweiler, Germany) was physically inverted and clamped to a benchtop, such that the base of the microscope provided a platform to hold the motor stand and MatTek dish (Figure 1). A fiber-optic ring light (Edmund Optics, Barrington, NJ) was attached to the motor housing. The gel was placed between two polarizers, which were positioned as 'cross-polars' with their respective angles of polarization 90° apart. In this arrangement, as the light passes through the filter-sample-filter optic train, the darkest area of the resulting image occurs where collagen fibers are oriented parallel or perpendicular to the optical axis of either polarizing element; the brightest area occurs where collagen fibers are oriented 45° to the filter optical axis. The collagen gel was needled for 10 revolutions. Images were captured at 6 frames per second during needle rotation and were analyzed with MATLAB (The Mathworks, Inc, Natick, MA), as described below. Six experiments, each comprising three replicates, were performed for untreated collagen gels, and five experiments were performed for crosslinked gels, also in triplicate.

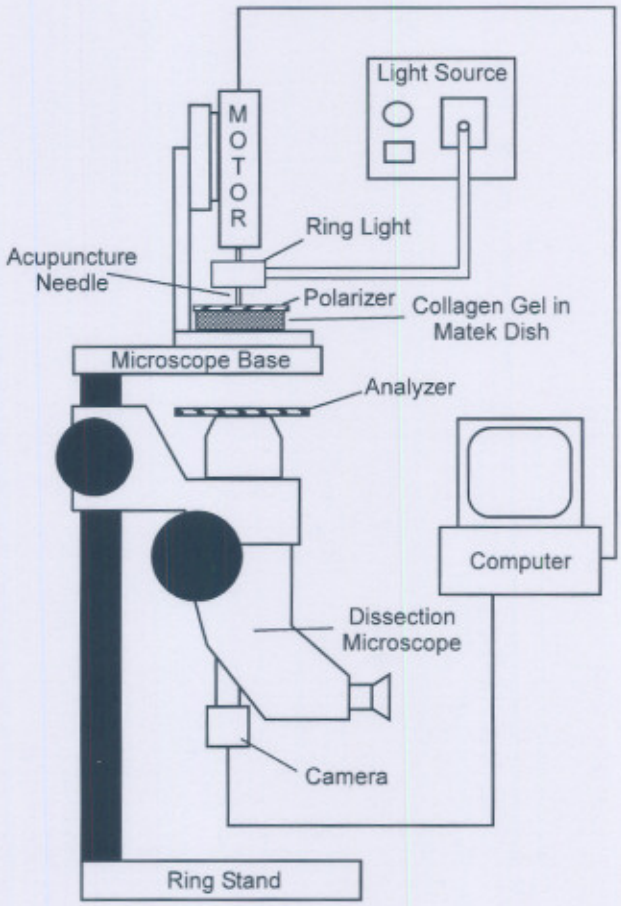

Figure 1
Schematic of polarized light microscopy system. A dissection stereomicroscope with a USB camera was mounted upside-down to a bench top. A fiber-optic ring light was attached to the motor housing providing a light source to the sample without hindrance from the motor. The polarizer was placed on top of the sample dish, and the analyzer was placed on the microscope as shown with the axis of polarization orthogonal to the axis for the polarizer. A small hole in the polarizer allowed free insertion and rotation of the acupuncture needle in the sample.

Image analysis

In all cases, PLM generated images with a '4-leaf clover' morphology of birefringence that emerged and increased in area with increasing needle rotation, extending beyond the field of the captured image, until gel failure, at which point the intensity decreased (Figure 2). The PLM images were imported into MATLAB to quantify the birefringence. First, the failure point for each individual experiment was identified by plotting the number of pixels with intensity greater than a given threshold value, determined as described below, against the number of needle revolutions and identifying the global maximum of the curve

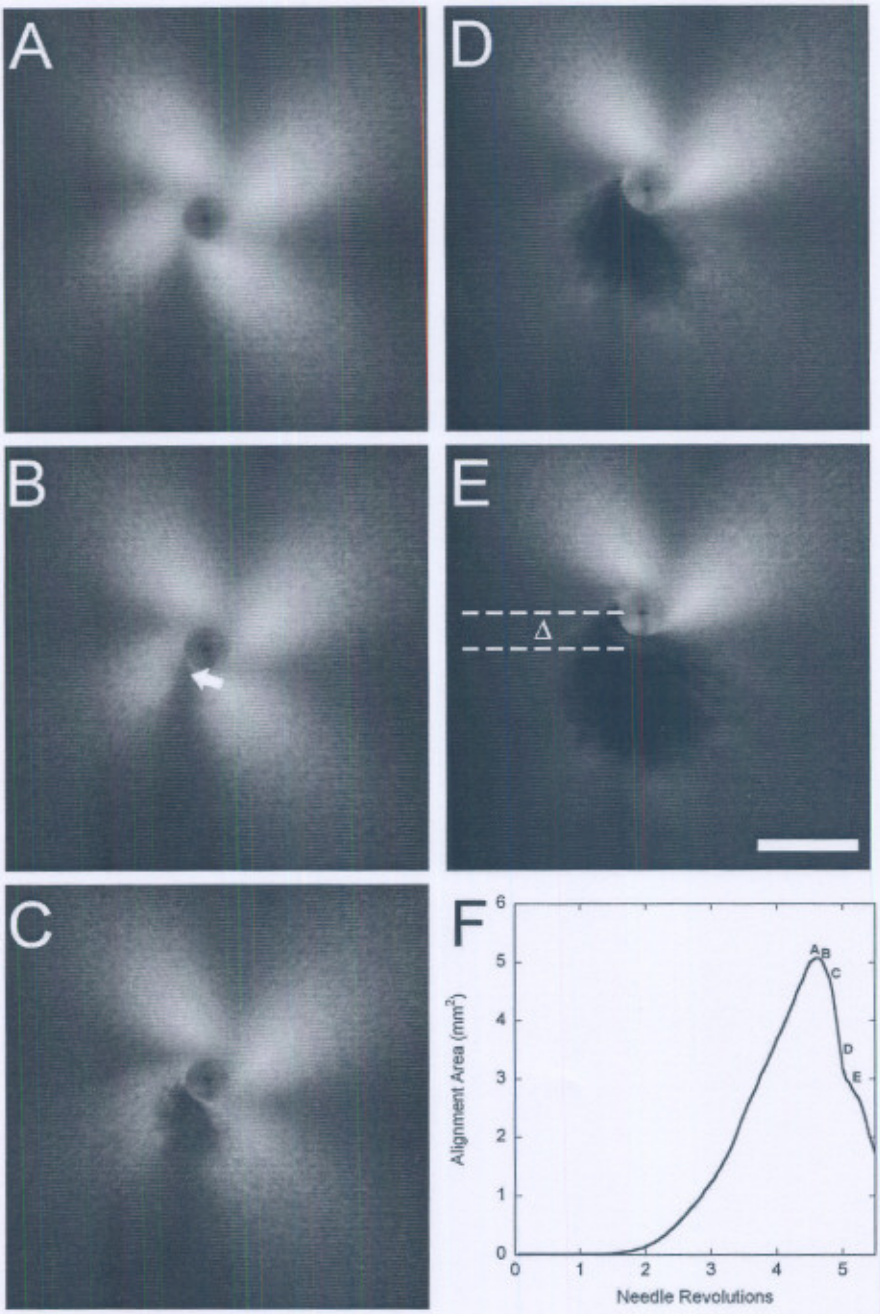

Figure 2
Winding and failure of collagen gels during in vitro acupuncture. (A) PLM image of the gel immediately before the onset of tearing. The characteristic '4-leaf clover' pattern of birefringence increases in size up to the point of failure as the gel becomes increasingly aligned due to winding around the needle. (B-E) Development of gel failure at 0.5 sec (0.15 rev) intervals. At the onset of tearing (B), a weakening of the birefringence can be observed near the needle where the dense, circumferentially wound center transitions to radially aligned fibers (arrow). As failure ensues, a hole is observed in the gel (C-E), and the residual stress in the remainder of the gel is enough to bend the needle, as indicated by the shift in needle position, Δ, directed away from the tear. The increasing size of the tear results in a decreasing area of birefringence. (F) Images A-E marked on a plot of the area above a threshold intensity vs. needle revolutions. The peak represents the image taken at maximum alignment immediately prior to the onset of failure. Bar: 1 mm.

(Figure 2F). This point was confirmed by visual inspection of the image sequence. Failure points were compared statistically using a two-way ANOVA, with collagen concentration and crosslinking as fixed effects (SPSS 12.0, Chicago, IL). Significance levels were set at $P < 0.05$. The earliest failure point (rounded down to the nearest integer) among all experiments was 4 revolutions for untreated samples and 2 revolutions for crosslinked samples.

The evolution of birefringence with needle rotation, reflecting the increase in fiber alignment, was quantified by determining a continuous index of the area of alignment. To apply a consistent criterion for comparing alignment across different conditions, the image sequence for each experiment was first normalized by subtracting the mode intensity value of the first image, which was taken prior to needle rotation and represented the background intensity level, from all remaining images in the sequence. This removed background differences among different collagen concentrations and smoothed out minor day-to-day fluctuations.

To determine the operating threshold intensity for each experimental set of images, the image at 2 (crosslinked samples) or 4 (untreated samples) revolutions was binarized at decreasing threshold intensity levels, beginning with the maximum intensity present in the image. As the threshold value decreased, the binarized image began to resemble a 4-leaf clover. The operating threshold value was identified as the maximum value for which a complete clover structure was observed (Figure 3). Using this threshold value, each frame in the image set was converted to a binary image, and the area of pixels greater than or equal to that intensity was calculated. Comparisons among untreated collagen gels were made up to 4 revolutions, and comparisons among crosslinked collagen gels, or between crosslinked and untreated gels, were made up to 2 revolutions, the earliest failure points observed among all experiments within these respective conditions.

Collagen gel rheology

Parallel plate rheometry was used to assess the mechanical properties of the collagen gels. Mechanical testing was done using a Rheometrics SR-2000 parallel plate rheometer with a temperature-controlled incubation chamber maintained at 37°C (TA Instruments, New Castle, DE). A sample well was formed by punching a 25 mm diameter hole in a 4 mm thick layer of PDMS. Type I collagen solutions were prepared at concentrations of 1.5, 2.0, and 2.5 mg/ml, as described above, and 2 ml were pipetted into the well, which was then transferred to a 37°C incubator. After self assembly, the gels were carefully removed with a spatula and transferred to the bottom plate of the rheometer. The top plate was lowered to a height of 2.0 mm. The dynamic storage and loss moduli of the gels were evaluated at 1% shear strain amplitude at frequencies ranging from 0.1 – 10 Hz. Five samples were tested for each of the 6 conditions. The moduli were analyzed statistically with a two-way ANOVA. Significance levels were set at $P < 0.05$.

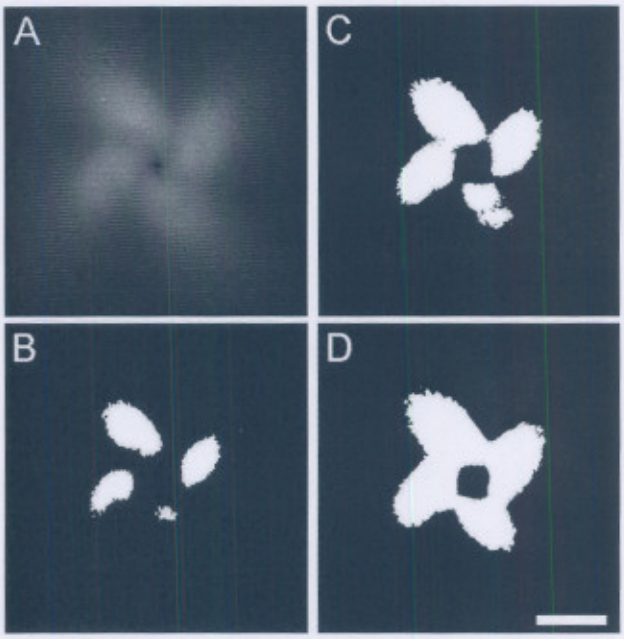

Figure 3
Methodology for identifying threshold criteria. From each image set, the image at 2 or 4 revolutions was extracted (A) and sequentially binarized with a decreasing grayscale value, beginning with the maximum intensity present in the image. As the threshold value decreased, the binarized image began to resemble a 4-leaf clover (B, C). The threshold value for the gel was set as the maximum grayscale value that produced a complete clover structure with no interruptions in the 4 leaves (D). Bar: 1 mm.

Results

General observations

During continuous needle rotation, all gels exhibited tearing prior to 10 revolutions. Whereas collagen concentration did not affect the failure of the gels ($P = 0.274$), crosslinked gels failed at a significantly lower number of revolutions than untreated gels ($P < 0.001$) (two-way ANOVA) (Figure 4). Therefore, to compare different conditions, quantitative analyses were performed up to a standardized number of revolutions that represented the lowest integer number before failure among all samples.

Collagen imaging

Gel morphology before and after 2 revolutions is shown in brightfield (Figure 5A &5B), PLM (Figure 5C &5D), and

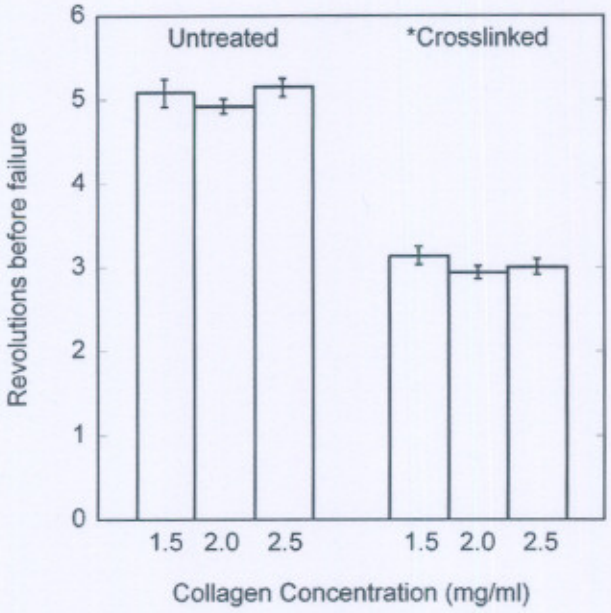

Figure 4
Revolutions to failure (average +/- standard error) during in vitro acupuncture. The number of revolutions before gel tearing was identified from alignment area curves and verified visually from the image sets. Crosslinking the collagen significantly decreased the ability of the collagen gels to withstand needle rotation without tearing (*, 2-way ANOVA, $P < 0.001$), whereas changing the collagen concentration had no effect ($P = 0.274$)

confocal (Figure 5E &5F) images. Collagen fiber winding was not obvious in bright field images, but could be inferred from PLM images (see below), and was directly observed in confocal images. Prior to needle rotation, collagen fibers were randomly oriented. After needle rotation, circumferential alignment was observed close to the needle, which evolved into radial alignment as the distance from the needle increased (Figure 5F). The effect was similar but more pronounced after 4 revolutions (data not shown).

Quantitative PLM

The alignment pattern observed with confocal microscopy was evident in PLM images as a clover-leaf pattern of birefringence, where fiber alignment 45° off-axis generates an intensity peak. The area of alignment at the same number of revolutions was visually greater with increasing collagen concentration and in untreated collagen gels vs. crosslinked gels (up to 2 revolutions) (Figure 6). A continuous index of the area of alignment was generated by binarizing the complete set of images in each run using a threshold intensity as described above. For untreated collagen gels, the average area of alignment increased more rapidly and to a higher final value with increasing concentration (Figure 7). Crosslinked samples aligned more gradually than untreated gels (Figure 8), and also demonstrated the trend of increased area of alignment with increasing collagen concentration.

Depth of needle insertion

The depth of insertion study was performed with a new shipment of collagen, and preliminary experiments with collagen from the crosslinking and collagen concentration studies indicated that the new batch presented significantly less alignment than the old batch, but that trends in the response were the same. As such, experiments in the depth of insertion studies were performed exclusively with the new batch of collagen and analyzed separately from the crosslinking and collagen concentration studies. Changing the depth of needle insertion significantly affected the failure of the gels (Figure 9). Thicker gels failed at fewer revolutions than thinner gels. For 4 mm-thick gels, increasing the depth/percentage of needle insertion decreased the revolutions before failure, but this was not observed consistently with the 6 mm-thick gels. The alignment of gels was also affected by insertion depth and percentage (Figure 10). In vitro acupuncture with needles inserted the same depth in gels of different thickness generated more alignment in thinner gels, indicating that the fraction of the gel that is subjected to needle rotation is an important parameter in dictating the response. Maintaining the same percentage of insertion at gels of different thickness produced greater alignment in thicker gels than thinner gels. For example, inserting a needle 3 mm into a 4 mm-thick gel and rotating the needle produced more alignment than the same procedure in a 6 mm-thick gel (inverted triangles, Figure 10A and 10B). However, inserting a needle 75% into a 6 mm-thick gel (squares, Figure 10B) produces more alignment than 75% into a 4 mm gel (inverted triangles, Figure 10A).

Rheology measurements

Storage and loss moduli were determined using parallel plate rheometry. The storage modulus showed a gradual increase with increasing frequency, before sharply dropping (Figure 11A). Inspection of gels revealed damage to the samples, which did not occur if experiments were run only at lower frequencies (data not shown), and we assumed that the damage was responsible for the apparent decrease in stiffness. In general, increased collagen concentration and crosslinking delayed this damage. The loss modulus for untreated gels showed a gradual increase at low frequencies, particularly for untreated collagen (Figure 11B). The loss modulus for crosslinked collagen decreased at moderate frequencies, and increased more sharply for all cases concurrent with the decrease in storage modulus. Two-way ANOVA revealed significant increases in the storage and loss moduli at all frequencies

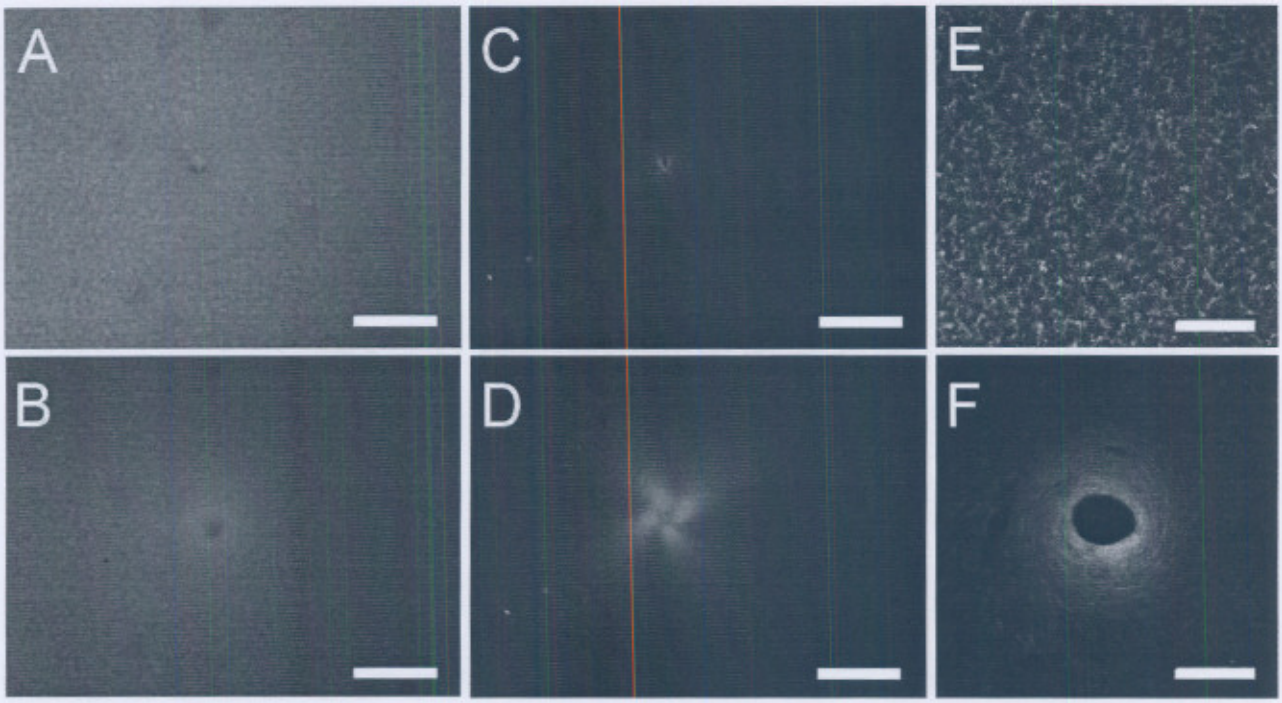

Figure 5
Images of 2 mg/ml fluorescently spiked collagen gels before needling and after 2 revolutions. (A) Brightfield imaging of the gel with needle inserted before needling shows a small hole in an otherwise uniform field. (B) After needle rotation, the collagen fiber density appears to change around the needle. (C) Under cross-polars, the needle hole is again evident in an otherwise random field before needle rotation. (D) After rotation, the significant bright regions indicating collagen fiber alignment 45° off-axis. (E) Using confocal microscopy, the random orientation of collagen fibers is apparent. (F) After needling, the fiber density increases around the needle. Fibers near the needle are aligned circumferentially and transition to radial alignment away from the needle. Bars: A-D, 1 mm; E-F, 50 μm.

with increasing collagen concentration and crosslinking (all $P < 0.001$).

Discussion

During treatment, acupuncture therapists aim to achieve "needle grasp" as a sensory marker of an appropriate degree of needle manipulation. Recent studies suggest that needle grasp occurs when collagen fibers in the subcutaneous connective tissue attach to and wind around the needle, thus imposing a local stress and strain field on the surrounding tissue [6]. In this paper, we imaged a simple, in vitro, acellular collagen gel system using polarized light microscopy during acupuncture needle rotation and measured the degree of winding in terms of fiber alignment to identify relationships between collagen concentration, crosslinking, and winding, as well as the failure of the gels.

We found that both collagen concentration and crosslinking influenced the response to controlled acupuncture needle rotation. Alignment increased with increasing collagen concentration, but decreased in gels that were crosslinked with formalin. Crosslinked gels also failed at a significantly lower number of needle rotations than untreated gels. Failure consistently occurred ~0.25 mm-1.0 mm away from the needle, and corresponded to the point where circumferential alignment of collagen fibers wound around the needle transitioned to radial alignment from fibers in the periphery of the gel being pulled into the needled area. The acute change in fiber geometry likely introduced a stress concentration that ultimately caused a tear in the collagen gel.

Altering the collagen concentration increases fiber density, which has potential indirect and direct consequences on the polarized light microscopy. First, the increase in fiber density could affect the mechanical properties simply by increasing the number of structural elements to carry load and/or by increasing fiber-fiber interactions, which would affect the tissue response to needle rotation. The increase in fiber density would also influence the degree of alignment, as measured with polarized light microscopy. An increase in fiber density implies that a greater number of fibers would be aligned for the same

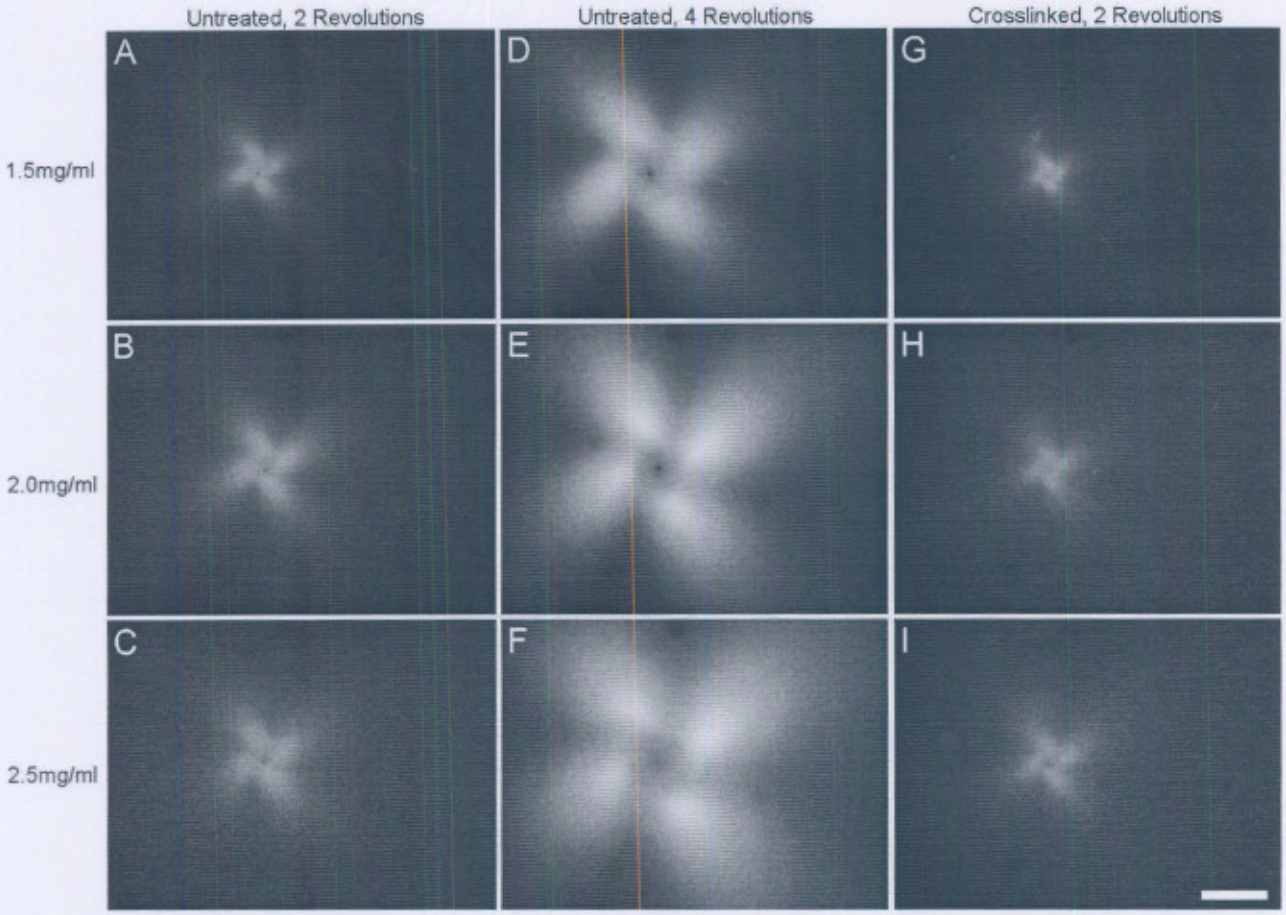

Figure 6
Polarized light images of collagen gel response to in vitro acupuncture after 2 needle revolutions (A-C), and 4 revolutions (D-F) in untreated collagen gels and 2 revolutions (G-I) in crosslinked gels. The birefringent area increased with increasing revolutions, and was greater in untreated collagen compared to crosslinked collagen at the same number of revolutions. This area also increased with increasing collagen concentration for each condition (A, D, G – 1.5 mg/ml; B, E, H – 2.0 mg/ml; C, F, I – 2.5 mg/ml). Bar = 1 mm.

number of revolutions, and could therefore more efficiently rotate the polarization state of the incident light.

Crosslinking the gel decreases the flexibility of individual and aggregate fibers, which had a marked effect on the mechanical properties of the gels, increasing the storage modulus in shear by about an order of magnitude. The increased rigidity of crosslinked fibers increased the resistance to winding and deformation, and also increased the stress generated with winding, thereby leading to less alignment and earlier failure compared to untreated gels of the same concentration.

In addition to altering the mechanical properties of the gels, changing collagen concentration and crosslinking the gels could have influenced interactions and adhesion with the needle and/or the polystyrene dish. However, no gels failed at either the needle interface or the dish interface, and we believe that differences in adhesion among conditions played a minimal role in the bulk of the observed temporal response, except, perhaps, for the initial lag period in the alignment curves that represents initiation of alignment.

The differences between the response of untreated and crosslinked collagen gels to in vitro acupuncture, and particularly the earlier failure of crosslinked gels, suggests that mechanostructural differences in the soft tissues that contact an acupuncture needle during therapy may be responsible for the selective coupling and winding of collagen fibers in specific soft tissue layers during needle rotation. In vivo and explant studies have demonstrated

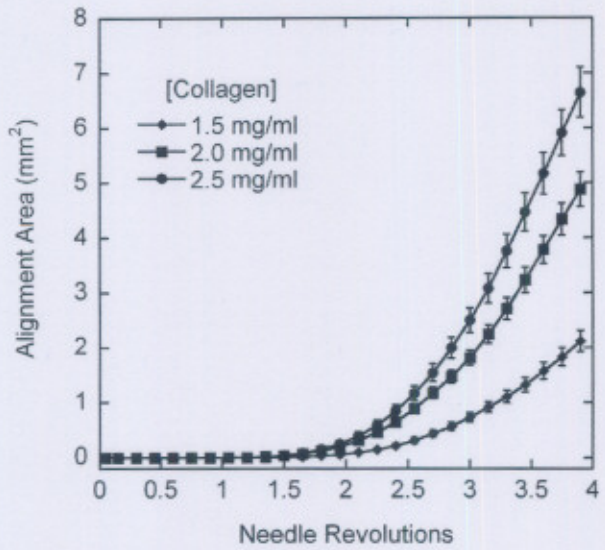

Figure 7
Effects of collagen concentration on area of alignment (average +/- standard error). The birefringent area of alignment was identified from image sets binarized based on the image at 4 revolutions, and plotted as a function of needle revolution. Increasing the collagen concentration increased the area.

that, although an acupuncture needle is inserted through the epidermis and dermis and into subcutaneous fat and muscle, only the subcutaneous loose connective tissue appears to specifically wind around the needle [3]. The resulting recruitment of loose connective tissue fibers towards the needle can thicken that layer and subsequently compress the overlying and underlying tissue layers, but the characteristic whorl pattern is only seen in the loose connective tissue.

The tissue properties that govern this selective adherence and winding are not yet known. However, a recent study by Iatridis et al. documented the mechanical properties in uniaxial tension of loose connective tissue from mouse explants, and noted important distinctions between loose connective tissue and other load bearing soft tissues, including skin [16]. Most soft tissues demonstrate significant non-linear stiffening above a certain strain – typically between 1% and 20%. For example, skin has a low strain modulus on the same order as loose connective tissue (2.75 kPa) up to about 10% strain [17], after which the modulus increases to ~240 kPa [17,18]. In contrast, loose connective tissue demonstrated a highly linear elastic response up to 50% strain [16]. Thus, as tissue begins to wind around the needle and deform, significantly greater stress will be generated in skin vs. loose connective tissue, and, similar to the response of our crosslinked gels, we

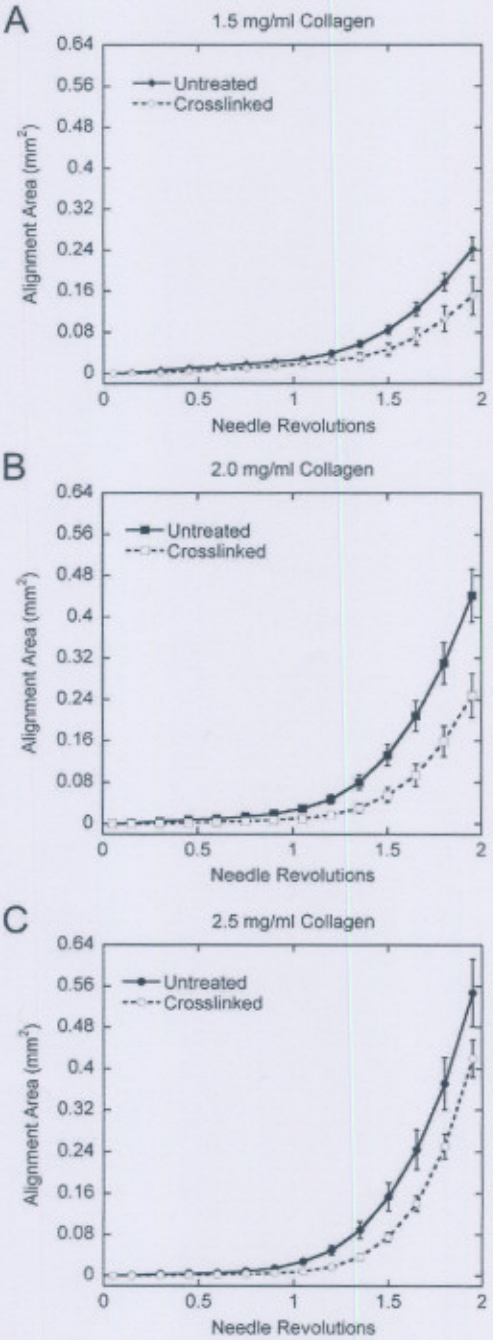

Figure 8
Effects of crosslinking on area of alignment (average +/- standard error). The birefringent area of alignment was identified from image sets binarized based on the image at 2 revolutions. Needle rotation in crosslinked collagen gels generated less alignment than untreated collagen gels at each collagen concentration. The area of alignment increased with increasing collagen concentration for both untreated and crosslinked collagen.

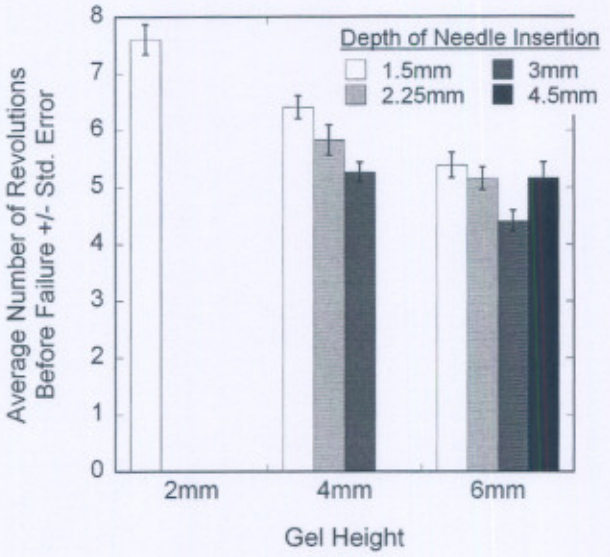

Figure 9
Effects of gel height and depth of needle insertion on revolutions to failure during in vitro acupuncture. Thin gels were able to withstand significantly more needling than thick ones ($P < 0.001$). For 4 mm-thick gels, revolutions to failure decreased as the depth of needle insertion increased, but this was not observed for 6 mm-thick gels.

would expect the failure stress to be reached at a lower number of revolutions. The network of collagen fibers in the dermis may be too stiff to effectively respond to acupuncture needle rotation.

In clinical acupuncture, the thickness of the connective tissue layer varies, often with the thickness of subcutaneous fat, and it is especially thick at intermuscular cleavage planes. These planes correlate anatomically to acupuncture points and meridians[14], and Langevin has shown that the resistant force to needle rotation at acupuncture points is greater than at control points, where the connective tissue layer is thinner. It was suggested that needling in locations where connective tissue is more pronounced enhances the mechanical response of fibroblasts residing within this tissue [1]. In investigating how the depth of needle insertion and gel thickness may affect the response of a homogeneous tissue, we found that both the relative depth as well as the absolute depth of insertion into the collagen gel were important factors in the failure and alignment responses. Thinner gels were able to withstand more needle rotations than thick ones. Interestingly, the failure point was reached earlier as the depth of insertion was increased in 4 mm-thick gels, but no real trend was observed in 6 mm-thick gels. For both 4 mm-thick and 6 mm-thick gels, more alignment was recorded when the depth of insertion was greater. The last observation is consistent with an increase in the number of fibers subjected to rotation via contact with the needle. We also observed that more alignment was generated for the same depth of insertion in thin gels versus thick ones. The greatest amount of alignment was observed with the greatest absolute coverage of the needle by the collagen gel – 4.5 mm insertion into a 6 mm-thick gel. We believe that the increase in thickness of collagen below the needle increases the physical resistance to drawing individual fibers up and in towards the needle, thereby creating more stress to stimulate resident cells. We also note that the tip of the acupuncture needle is tapered. The length of the tapered tip represents a greater proportion of the inserted needle at shallower insertion depths than deeper insertions. The biomechanical response of the gel, particularly the initial adhesion of the collagen fibers to the needle, may be influenced by needle diameter [14], which would be embedded in our needle depth results.

The differences with collagen concentration and crosslinking, as well as the empirical differences in alignment from separate batches of collagen (compare 2.0 mg/ml plot in Figure 6 to 3 mm insertion into 4 mm-thick gels in Figure 10A), suggest that subtle changes in tissue composition and structure may affect the biomechanical response to needle rotation in vivo, and potentially the efficacy of acupuncture therapy. It is well known that the collagen content of human skin throughout the body is non-uniform [9], and the matrix components of skin can be crosslinked, degraded, and or damaged by any number of environmental factors, including exposure to ultraviolet light, disease states, such as glycation associated with type 1 diabetes mellitus [19], and normal physiological processes, such as wound healing. There have been relatively few studies of loose connective tissue of any kind, though it is likely that the biophysical properties of this tissue also vary among individuals and with location in one individual, and may dictate, in part the efficacy of acupuncture in a particular patient or at a particular location.

It is important to keep in mind that the in vitro system developed in this work is only a first step and differs significantly from the loose connective tissue involved in acupuncture, a cellular tissue comprising primarily fibroblasts embedded in an extracellular matrix of collagen and elastin fibers and proteoglycans. We chose to begin with an acellular collagen gel, representing the most significant structural component of the extracellular matrix, to establish a baseline for further study before proceeding to the more complex cellular system, in which a number of variables can change dynamically due to fibroblast-mediated compaction, matrix synthesis, and degradation. We also chose a rotational velocity (0.3 rev/sec) significantly slower than typically applied clinically

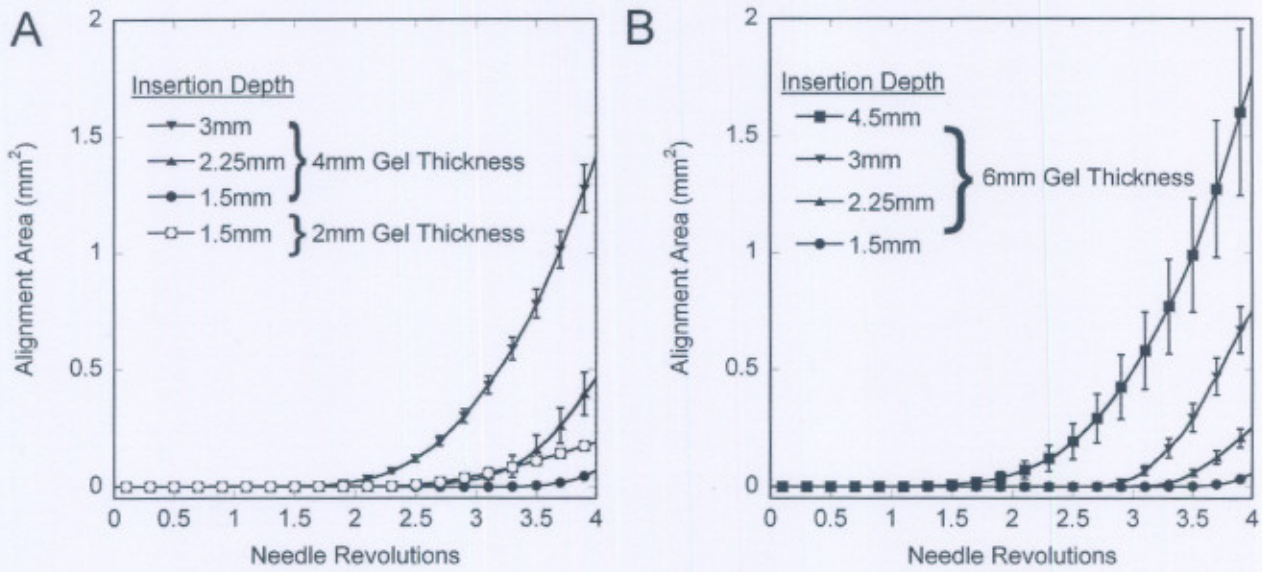

Figure 10
Effects of gel thickness and depth of needle insertion on the measured area of fiber alignment (average +/- std. error). (A) 2 mm-thick and 4 mm-thick gels; (B) 6 mm-thick gels. For the same depth of insertion, thin gels demonstrated more alignment than thick gels. For both 4 mm- and 6 mm-thick gels, the alignment area increased as depth of insertion increased.

to facilitate image acquisition and reduce viscoelastic effects.

Conclusion

The in vitro model provides a platform to study mechanotransduction during acupuncture in a highly controlled and quantitative setting. The results indicate that the mechanostructural properties of soft connective tissues may affect their response to acupuncture therapy. Based on the results of this work, the biofidelity of our in vitro system can now be systematically improved by introducing cells and additional matrix components, such as elas-

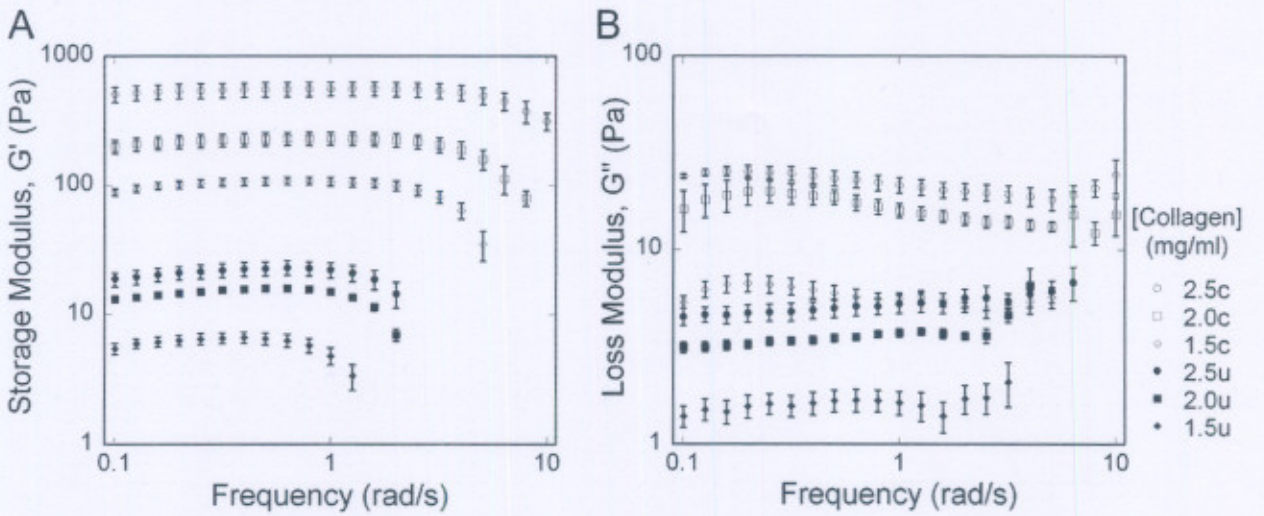

Figure 11
Frequency sweep of collagen gels under 1% controlled strain (average +/- standard error). (A) Storage Modulus; (B) Loss Modulus. Both the storage and loss moduli demonstrated significant increases with increasing collagen concentration and crosslinking (2-way ANOVA, $P < 0.001$). Key: c: crosslinked, u: untreated.

tin and proteoglycans, to better mimic features of loose connective tissue, and by applying needle rotation protocols consistent with clinical practice. The incorporation of additional instrumentation to record the resistive torque that develops in the gel during needle manipulation and the strain within the gel would also significantly improve our ability to study the biomechanics associated with acupuncture. It is likely that the torque and strain, which may be transmitted to resident cells in vivo and in cellular assays in vitro to initiate mechanotransduction, are strongly influenced by gel or tissue composition as well as the rate and number of needle rotations. The system can then be used to aid in the determination of the quantitative biological response to biomechanical signals introduced during acupuncture needling.

Competing interests

The authors declare that they have no competing interests.

Authors' contributions

MJ carried out the in vitro experiments and helped draft the manuscript. LTE developed the image processing algorithms and analyzed the polarized light images. HMB and DIS conceived of the study, designed the experiments, and drafted the manuscript. All authors read and approved the manuscript.

Acknowledgements

The authors thank Alice Señeres for her initial work on the controlled needle rotation instrumentation. Support for this research was provided by grants from the Charles and Johanna Busch Biomedical Research Foundation, a graduate fellowship to MJ from the New Jersey Commission on Spinal Cord Research (05-2912-SCR-E-0), the National Science Foundation (NSF-IGERT on Integratively Designed Biointerfaces – DGE 033196), and the National Institutes of Health (R03 EB006045-01A1).

References

1. Langevin HM, Churchill DL, Fox JR, Badger GJ, Garra BS, Krag MH: **Biomechanical response to acupuncture needling in humans.** *J Appl Physiol* 2001, **91(6):**2471-2478.
2. Langevin HM, Churchill DL, Cipolla MJ: **Mechanical signaling through connective tissue: a mechanism for the therapeutic effect of acupuncture.** *Faseb J* 2001, **15(12):**2275-2282.
3. Langevin HM, Churchill DL, Wu J, Badger GJ, Yandow JA, Fox JR, Krag MH: **Evidence of connective tissue involvement in acupuncture.** *Faseb J* 2002, **16(8):**872-874.
4. Langevin HM, Konofagou EE, Badger GJ, Churchill DL, Fox JR, Ophir J, Garra BS: **Tissue displacements during acupuncture using ultrasound elastography techniques.** *Ultrasound Med Biol* 2004, **30(9):**1173-1183.
5. Langevin HM, Bouffard NA, Badger GJ, Churchill DL, Howe AK: **Subcutaneous tissue fibroblast cytoskeletal remodeling induced by acupuncture: evidence for a mechanotransduction-based mechanism.** *J Cell Physiol* 2006, **207(3):**767-774.
6. Langevin HM, Bouffard NA, Churchill DL, Badger GJ: **Connective tissue fibroblast response to acupuncture: dose-dependent effect of bidirectional needle rotation.** *J Altern Complement Med* 2007, **13(3):**355-360.
7. Da Silva DFT, Vidal BC, Zezell DM, Zorn TMT, Nunez SC, Ribeiro MS: **Collagen birefringence in skin repair in response to red polarized-laser therapy.** *Journal of Biomedical Optics* 2006, **11(2):**024002-1-6.
8. Pierce MC, Strasswimmer J, Park BH, Cense B, de Boer JF: **Birefringence measurements in human skin using polarization-sensitive optical coherence tomography.** *Journal of Biomedical Optics* 2004, **9(2):**287-291.
9. Vitellaro-Zuccarello L, Cappelletti S, Dal Pozzo Rossi V, Sari-Gorla M: **Stereological analysis of collagen and elastic fibers in the normal human dermis: variability with age, sex, and body region.** *The Anatomical Record* 1994, **238(2):**153-162.
10. Debessa CRG, Maifrino LBM, de Souza RR: **Age related changes of the collagen network of the human heart.** *Mechanisms of Ageing and Development* 2001, **122:**1049-1058.
11. Mays PK, McAnulty RJ, Campa JS, Laurent GJ: **Age-related Alterations in Collagen and Total Protein Metabolism Determined in Cultured Rat Dermal Fibroblasts: Age-related Trends Parallel those Observed in Rat Skin In Vivo.** *Int J Biochem Cell Biol* 1995, **27(9):**937-945.
12. Vogel HG: **Influence of maturation and aging on mechanical and biochemical properties of connective tissue in rats.** *Mech Ageing Dev* 1980, **14(3-4):**283-292.
13. Takahashi M, Hoshino H, Kushida K, Inoue T: **Direct Measurement of Crosslinks, Pyridinoline, Deoxypyridinoline, and Pentosidine, in the Hydrolysate of Tissues Using Hign-Performance Liquid Chromatrography.** *Analytical Biochemistry* 1995, **232:**158-162.
14. Langevin HM, Yandow JA: **Relationship of acupuncture points and meridians to connective tissue planes.** *Anat Rec* 2002, **269(6):**257-265.
15. Shreiber DI, Enever PAJ, Tranquillo RT: **Effects of PDGF-BB on rat dermal fibroblast behavior in mechanically stressed and unstressed collagen and fibrin gels.** *Experimental Cell Research* 2001, **266:**155-166.
16. Iatridis JC, Wu J, Yandow JA, Langevin HM: **Subcutaneous tissue mechanical behavior is linear and viscoelastic under uniaxial tension.** *Connect Tissue Res* 2003, **44(5):**208-217.
17. Eshel H, Lanir Y: **Effects of strain level and proteoglycan depletion on preconditioning and viscoelastic responses of rat dorsal skin.** *Ann Biomed Eng* 2001, **29(2):**164-172.
18. Oxlund H, Manschot J, Viidik A: **The role of elastin in the mechanical properties of skin.** *J Biomech* 1988, **21(3):**213-218.
19. Vishwanath V, Frank KE, Elmets CA, Dauchot PJ, Monnier VM: **Glycation of skin collagen in type I diabetes mellitus. Correlation with long-term complications.** *Diabetes* 1986, **35(8):**916-921.

Publish with **BioMed Central** and every scientist can read your work free of charge

"BioMed Central will be the most significant development for disseminating the results of biomedical research in our lifetime."

Sir Paul Nurse, Cancer Research UK

Your research papers will be:

- available free of charge to the entire biomedical community
- peer reviewed and published immediately upon acceptance
- cited in PubMed and archived on PubMed Central
- yours — you keep the copyright

Submit your manuscript here:
http://www.biomedcentral.com/info/publishing_adv.asp

BioMedcentral

The Anatomical Record

Varying assay geometry to emulate connective tissue planes in an in vitro model of acupuncture needling

Journal:	*Anatomical Record*
Manuscript ID:	AR-09-0372.R1
Wiley - Manuscript type:	Full Length Article
Date Submitted by the Author:	30-Apr-2010
Complete List of Authors:	Julias, Margaret; Rutgers, the State University of New Jersey, Chemical & Biochemical Engineering Buettner, Helen; Rutgers, the State University of New Jersey, Chemical & Biochemical Engineering; Rutgers, the State University of New Jersey, Biomedical Engineering Shreiber, David; Rutgers, the State University of New Jersey, Biomedical Engineering
Keywords:	acupuncture, connective tissue, fascia, tissue mechanics

scholarONE™
Manuscript Central

Varying assay geometry to emulate connective tissue planes in an in vitro model of acupuncture needling

Margaret Julias[1], Helen M. Buettner[1,2], and David I. Shreiber[2]

1. Department of Chemical and Biochemical Engineering, Rutgers, The State University of New Jersey, Piscataway, NJ, USA

2. Department of Biomedical Engineering, Rutgers, The State University of New Jersey, Piscataway, NJ, USA

Running title: Tissue planes in an in vitro acupuncture model

Address Correspondence to:
David I. Shreiber
Associate Professor
Department of Biomedical Engineering
Rutgers, The State University of New Jersey
Piscataway, NJ, USA 08854
732-445-4500 x6312
732-445-3753 (fax)
shreiber@rci.rutgers.edu

Grant Sponsor: National Institutes of Health; Grant Number R03 EB006045-01A1

Grant Sponsor: New Jersey Commission on Spinal Cord Research; Grant Number 05-2912-SCR-E-0

For Peer Review

Abstract

During traditional acupuncture, fine needles are inserted subcutaneously and rotated, which causes loose fascial tissue to wind around the needle. This coupling is stronger at acupuncture points, which tend to fall above intermuscular fascial planes, than control points, which lay above skeletal muscle. These different anatomical constraints may affect the mechanical coupling. Fascia at acupuncture points is bounded on two sides by skeletal muscle, but at control points is essentially unbounded. These differences were approximated in simple in vitro models. To emulate the narrower boundary within the intermuscular plane, type I collagen was cast in circular gels of different radii. To model the channel-like nature of these planes, collagen was cast in elliptical gels with major and minor axes matching the large and small circular gels, respectively, and in planar gels constrained on two sides. Acupuncture needles were inserted into the gels and rotated via a computer-controlled motor while capturing the evolution of fiber alignment under cross-polarization. Small circular gels aligned faster, but failed earlier than large circular gels. Rotation in elliptical and planar gels generated more alignment-per-revolution than circular gels. Planar gels were particularly resistant to failure. Alignment in circular gels was isotropic, but was stronger in the direction of the minor axis in elliptical and planar gels. In fibroblast-populated gels, cells followed the alignment of the collagen fibers, and also became denser in regions of stronger alignment. These results suggest that the anatomy at acupuncture points may provide unique boundaries that accentuate the mechanical response to needle manipulation.

For Peer Review

Introduction

Although acupuncture has been clinically proven in treating conditions such as pain, nausea and hypertension (Acupuncture, 1997) and has been increasingly used by patients seeking alternative medical therapies (Eisenberg et al., 1998), the mechanisms that underlie the therapeutic benefits remain unknown. During treatment, fine needles are inserted and rotated at specific locations on the body known as acupuncture points based on empirical maps passed down for centuries. Manipulating these acupuncture points is believed to regulate the flow of energy or 'qi' through acupuncture meridians to produce local effects and specific, far-reaching results. Despite the evidence for clinical and functional efficacy, there has been little correlation of acupuncture points and meridians to neuroanatomical structures or, until recently, physiological features.

Clinically, practitioners locate acupuncture points by identifying a nearby anatomical landmark, such as a bony prominence, muscle, or tendon, and then using light palpation to precisely determine the final position (Langevin and Yandow, 2002). Recently, Langevin and Yandow identified a high correlation between inter- and intramuscular connective tissue cleavage planes and acupuncture points (~80%) and meridians (~50%) by mapping acupuncture points on a cadaver to serial gross sections from the Visible Human Project (Fig 1) (Langevin and Yandow, 2002). At these points, there is an abundance of loose, interstitial, connective tissue and no underlying skeletal muscle. After locating the points, practitioners insert and manipulate the needles until they feel 'needle grasp' – described as a "fish biting on a line" – at which time the patient senses 'de qi' (Langevin et al., 2001b). Using an instrumented needling apparatus, Langevin showed that this grasping force at acupuncture points was significantly greater

For Peer Review

than at control points, which did not lay above connective tissue planes. Separate work with full thickness rat abdominal wall explants, where acupuncture needles were inserted through epidermis, dermis, subcutaneous connective tissue and fat, and subcutaneous muscle and then rotated, demonstrated that only the loose, subcutaneous connective tissue wound around the needle to evoke a grasping force (Langevin et al., 2002). Working with explants of subcutaneous connective tissue alone, Langevin also showed that fibroblasts residing several millimeters away respond to the mechanical perturbation produced by acupuncture needle rotation with distinct morphological and cytoskeletal changes (Langevin et al., 2005).

Taken together, these results suggest that mechanical forces may contribute to the cellular and tissue changes leading to therapeutic benefits following acupuncture needling, and that the anatomical organization of soft tissues strongly influences the biomechanical response. However, untangling the contributions of these and other factors to the biophysical responses of tissues and cells in clinical settings or in explant studies, which present complex tissue environments, is difficult. We have developed a three-dimensional (3D) in vitro approach to examine the biophysical and, ultimately, the cellular responses to acupuncture needling in a controlled setting. Using type I collagen gels as tissue mimics, we demonstrated previously that the winding response of fibrillar collagen to needle rotation resembles that of loose connective tissue and varies with network density and stiffness and the depth of needle insertion (Julias et al., 2008).

In the current study, we used this in vitro approach to investigate the influence of fascial plane geometry on fiber winding. In vivo, the tissue in these planes is bounded on two sides by skeletal muscle, and generally becomes narrower with increasing depth to

For Peer Review

resemble a 'V' shaped channel, thereby presenting distinct boundary conditions compared to locations above a muscle, which resembles an infinite plane (Fig 1). We prepared circular gels of different radii to emulate the narrower boundary within the intermuscular plane, and elliptical gels and planar gels constrained on only two sides to model the anisotropic boundary conditions presented within these planes. We quantified the alignment response of these gels to controlled needling, and we examined cell alignment in fibroblast-populated gels.

For Peer Review

Materials and Methods

Collagen gel preparation

Collagen gel solutions were prepared from lyophilized collagen (Elastin Products, Owensville, MO) as previously described (Shreiber et al., 2001) to achieve a final concentration of 2.5mg/ml. The 'V' shaped geometry of a fascial plane presents two variations in geometry that affect the distance from the needle to the muscle wall, which in essence is the width of the loose connective tissue layer. These variations were emulated in vitro. First, the decrease in fascial plane width with increasing needle depth was modeled by casting collagen gels within circular hydrophilic porous polyethylene (PPE – Small Parts, Miramar, FL) annular inserts with different inner diameters – 28.6mm and 19.1mm. Second, the bounded plane, which presents a narrow channel of connective tissue, was modeled by preparing 'planar' gels than extended farther in one axis than the other. These gels were either cast gels between two long (~35 mm – the width of the dish), thin strips of PPE placed 19.1mm apart to capture the channel, or within elliptical PPE inserts with major (28.6mm) and minor (19.1mm) diameters matching the large and small circular inserts, respectively (Fig 1).

The collagen solution was poured into a 35-mm glass bottom MatTek dish with a 20-mm glass microwell (MatTek Corporation, Ashland, MA) containing the PPE inserts and incubated at 37°C for 4hrs to ensure complete fibril formation. The imaging approach (polarized light microscopy, described below) was strongly dependent on sample thickness within the imaged region. Accordingly, the gel centerline height was maintained at 4mm for all conditions.

For Peer Review

Cellular Gel Preparation

Cell populated gels were prepared using rat dermal fibroblasts (RDFs) that were isolated and expanded from neonatal transgenic rats engineered to express green fluorescent protein (GFP – 488nm excitation, 509nm emission). RDFs were cultured in Dulbecco's Modified Eagle's Medium (DMEM; Sigma Aldrich, St Louis, MO) supplemented with 10% fetal bovine serum (FBS; Atlanta Biologicals, Lawrenceville, GA), 2ml of 200mM L-glutamine (Sigma Aldrich, St Louis, MO), and 2ml of 5000 units/ml penicillin-5mg/ml streptomycin (Sigma Aldrich, St Louis, MO). Trypsinized cells were rinsed in culture medium and resuspended in a 2mg/ml collagen solution at a cell concentration of 100,000 cells/ml.

The in vitro setup was modified slightly to enhance cell viability within the tissue equivalent constructs by supporting PPE inserts holding the gels above the bottom surface of the culture dish, which essentially suspended the gels within culture medium. The approach to create the suspended gels was not amenable to the planar gels, and cellular gels were only generated within large circular or elliptical inserts. First, a poly(dimethyl siloxane) (PDMS) template was created with a 60-mm outer diameter and an inner profile matching the shape of the PPE inserts. The PDMS template was placed in a 60-mm dish, and the PPE inserts placed within the PDMS. The cell-containing collagen solution was poured into PPE ring and incubated at 37°C for 4hrs. Following self assembly, the PPE inserts with attached gels were removed from the PDMS and placed in a separate 60-mm dish on short PDMS support pegs, which introduced a small space between the bottom of the gel and the culture dish. The dish was filled with fresh culture

For Peer Review

medium, which allowed diffusive transport across both the top and bottom surfaces of the suspended gel and enhanced cell survival. After two days in culture, the PPE inserts and gels were transferred to a MatTek dish and covered with medium in preparation for controlled acupuncture needling.

In vitro acupuncture

A computer controlled motor (MicroMo Electronics, Inc., Clearwater, FL) was used to needle the acellular and cellular collagen gels. For acellular gels, a 250-μm stainless steel acupuncture needle (Seirin, Tokyo, Japan) was attached to the motor and inserted perpendicular to the surface of the gel to a depth of 3mm using a calibrated micromanipulator. The needle was rotated for ten revolutions at 0.3rev/s, during which time the evolution of fiber alignment was continuously recorded with polarized light microscopy (see below).

For cellular gels, the MatTek dish was first covered with a thin sheet of PDMS. The needle was inserted through the PDMS sheet and completely through the suspended gel. The cellular gels were needled for two revolutions at 0.3rev/s. After needling, the needle was detached from the motor but remained in place because of the PDMS sheet, thereby allowing the gel to be transferred to the stage of an inverted microscope for epifluorescent imaging of cell alignment without any unwinding or damage from needle removal.

Polarized Light Imaging

Polarization light microscopy (PLM) was used to observe and image the evolution of fiber alignment continuously in real time, as previously described (Julias et al., 2008). A dissection stereomicroscope (Carl Zeiss Microimaging, Thornwood, NY) with a USB

For Peer Review

camera (Matrix Vision, GmbH, Oppenweiler, Germany) was physically inverted and clamped to a benchtop, which allowed the base of the microscope to be used as a platform to hold the motor stand and MatTek dish (Fig 2). A fiber-optic ring light (Edmund Optics, Barrington, NJ) was attached to the motor housing. The gel was placed between two polarizers, which were positioned as 'cross-polars' with their respective angles of polarization 90° apart. In this arrangement, as the light passes through the filter-sample-filter optic train, the darkest area of the resulting image occurs where collagen fibers are oriented parallel or perpendicular to the optical axis of either polarizing element; the brightest area occurs where collagen fibers are oriented 45° to the filters' optical axes. Initially, the axes of the polarizer and analyzer were aligned with the major and minor axes of the ellipse. Images were captured at six frames-per-second during needle rotation and were analyzed with MATLAB (The Mathworks, Inc, Natick, MA), as described below. In cases where needling was stopped before gel failure, after the needle rotation was complete, samples were imaged under additional polarization states where the polarizer and analyzer were rotated to 22.5° and 45° off the ellipse's major axis to observe anisotropy in the alignment pattern due to the asymmetric boundaries (Fig 3).

PLM Image Analysis

PLM-generated images were imported into MATLAB (The Mathworks, Inc, Natick, MA) to quantify the birefringence (Julias et al., 2008). The evolution of birefringence with needle rotation, reflecting the increase in the fiber alignment, was quantified by determining a continuous index of the alignment area using a thresholding algorithm previously described (Julias et al., 2008), where the alignment area was the area of pixels greater than or equal to the threshold intensity. These alignment curves demonstrated a

For Peer Review

sharp decrease upon failure of the gel, which enabled determination of the number of revolutions before gel tearing. *Cell alignment quantification*

Cell-populated gels were imaged before and after needle rotation. Needling was limited to two revolutions to prevent gel tearing. Gels were imaged with an Olympus IX81 inverted microscope (Olympus, Melville, NY) using 4x magnification and standard FITC optics to collect the GFP-generated fluorescent signal of cells within a ~2.0mm^3 volume of gel. A motorized focus was used to capture ten images at 50μm intervals through the thickness of the sample in a ~2.25mm x 1.75mm region centered around the needle. The images were coded with filenames that allowed them to be analyzed in a blinded fashion. Elliptical assays were oriented with the major axis horizontal to the captured image. Cell alignment was quantified from the images by tracing the major axis of a cell and determining the projection (cos θ) of the cell-axis vector to the radial position vector of its location with respect to the needle position (Fig 4). These values were squared to produce an alignment index, $\Phi = \cos^2\theta$, for each cell, where $\Phi = 1$ indicated radial alignment and $\Phi = 0$ indicated circumferential alignment (Knapp et al., 1999). Only cells with distinct boundaries were traced, and the location of the cells within the image was marked and compared across images to ensure that a cell was not measured multiple times. Scatter plots of Φ with respect to centroid position were created to assess the spatial distribution of cell alignment. The total number of cells traced also served as a measure of cell density within the imaged volume.

Sample Sizes and Statistics

For acellular gel studies, 105 gels in total were subjected to in vitro acupuncture needling (n=17-30 per assay configuration). Of those 105, needle rotation was stopped at

For Peer Review

2.5 revolutions in 35 gels (n=8-10 per assay configuration) to assess alignment non-uniformity by rotating the polarization axes. The remainder (n=9-22 per configuration) were needled until failure. For cellular gel studies, cell alignment was quantified within the ~2.0mm^3 region around the needle in four circular gels and five elliptical gels for a total sample size of nine. Statistical comparisons were made among conditions using one-way ANOVA. When appropriate, post hoc pairwise comparisons were made with Tukey's test. Significance levels were set at $P < 0.05$.

For Peer Review

RESULTS

Effects of Assay Geometry on Fiber Winding

Rotating acupuncture needles within collagen gels cast in different geometries produced alignment that presented in a form of '4-leaf clover' using PLM (Fig 5), which increased in area with increasing needle rotation. Differences in alignment area at 2.4 revolutions were statistically significant (ANOVA, $P < 0.001$) (Fig 6A). The alignment curves indicated that gels with anisotropic dimensions demonstrated more alignment than gels with uniform dimensions (Tukey's test, max $P < 0.02$), except when the planar gels were compared to the small circles ($P = 0.162$). Differences between the planar and elliptical gels were indistinguishable ($P = 0.761$). Smaller circular gels produced more alignment area than larger circular gels, though the results were not statistically significant following post hoc comparison ($P = 0.176$). Failure of the gels consistently presented as a tearing within the body of the gel, and did not occur at the interface with the needle or at the interface with the PPE wall. The smaller circular gels failed at the lowest number of revolutions, followed by the elliptical gels, the large circular gels, and finally the planar gels (ANOVA followed by pairwise comparisons with Tukey's test, max $P = 0.002$) (Fig 6B). The planar gels has the greatest alignment at failure ($P < 0.001$ for all pairwise comparisons); alignment at failure between the elliptical and large circular assays was statistically indistinguishable ($P = 0.768$), and alignment was least in the small circular gels ($P < 0.001$ for all pairwise comparisons against other configurations) (Fig 6C).

Effects of Assay Geometry on Alignment Pattern

For Peer Review

The initial coincident orientation of the crossed-polars with respect to the assay axes generated a PLM image of fiber alignment with a prevailing orientation of 45° to the major and minor axes of the elliptical gel (or the vertical and horizontal axes of the circular gels) (Fig 4 & Fig 7). For these cases, each of the four 'clover leafs' was roughly equal in shape and size because of the symmetry of the four quadrants of alignment with respect to the geometry. By rotating the crossed-polars, alignment in other directions was assessed. The degree of anisotropy of the clover pattern was described as the ratio of the size of the leafs on perpendicular axes (Fig 7G). As the orientation was changed, the circular gels still presented largely uniform alignments. However, the alignment image in the planar and elliptical gels was non-uniform, with significantly stronger alignment occurring in the direction of minor axis when compared to the circular gels (max $P < 0.001$), which was consistent with a stronger alignment field in a smaller circular assay.

Effects of Assay Geometry on Cell Alignment

Fibril and cell alignment in cell-populated gels was consistent with the fiber alignment observed in acellular gels. Fibril and cell alignment appeared stronger along the minor axis of the elliptical gels, but was uniform in circular gels, and in both cases extended several millimeters away from the needle (Fig 8), and, in some cases, to the boundary of the assay (up to 14mm away from the needle) even though needling was limited to only two revolutions. To quantify cell alignment, an alignment index, Φ was calculated for each cell in a z-stack of images that encompassed a volume of 2.0mm^3 around the needle position and plotted at the cell centroid (Fig 9). Before needling, cells were randomly aligned, and the average value of Φ was close to the ideal value for

For Peer Review

random alignment of 0.5. After needling of circular gels, cells were primarily oriented radially, and the alignment was uniform with respect to angular position at the same radius. In elliptical gels, radial alignment occurred preferentially along the minor axis, and cells within the remainder of the gel appeared to be aligned randomly. Statistical comparison of average alignment values demonstrated that cells in both circular and elliptical gels became significantly more aligned after needling ($P < 0.001$). Cell number in the imaged region also increased significantly in the needled gels ($P < 0.001$), which coincided with the substantial displacement of fibers toward the needle. Within circular gels, cell density in the imaged region appeared to be uniform with respect to circumferential position, but was greater along the minor axis within elliptical gels.

For Peer Review

Discussion

Recent research has suggested a role for loose connective tissue located along inter- and intra-muscular fascial planes in transferring mechanical signals imparted by needle manipulation to resident cells via displacement and deformation of the tissue. In humans, in addition to increased amounts of loose connective tissue, these planes also present a distinct geometry compared to 'control' locations (Langevin and Yandow, 2002). For the same number of needle rotations, the 'grasping' force is greater when therapy is applied at acupuncture points located above a fascial plane than control points located above skeletal muscle (Langevin et al., 2001b). Using simple in vitro analogs, we demonstrated that the geometrical constraints present in the narrowing channels of connective tissue at fascial cleavage planes may act to accentuate the mechanical response of the tissue to needle manipulation.

When considering the anatomical organization of loose connective tissue (eg Fig 1), the tissue at control points above skeletal muscle is effectively unbounded, whereas the connective tissue at acupuncture points is bounded by muscle groups. Although not to the same disparity, we believe we captured the essence of this distinction in boundary conditions by altering the shape and size of the collagen gel. We used two metrics as indices of the mechanical response - collagen fiber alignment and gel failure. The strength of alignment – demonstrated as brighter regions in PLM – is a function of the orientation of fibers and the number/density of oriented fibers. We found that alignment was stronger when boundaries were closer to the needle, which is not surprising. It is well documented that anisotropic deformations of fibrillar materials, such as collagen gels, generates fiber alignment that is dependent on the magnitude of the disparity of

For Peer Review

deformation in different directions (Barocas and Tranquillo, 1997b, 1997a). Needle rotation in circular gels causes uniform winding of collagen fibers around the needle, drawing in fibers from the surrounding gel. At the perimeter, these fibers are constrained via intercalation with the PPE wall, thereby preventing circumferential movement. As a result, the fibers throughout the bulk of the gel straighten radially, and the closer the boundary is to the needle, the faster these fibers align. Since the distance to the boundary constraint is uniform around the perimeter, the alignment field is isotropic with respect to radial position. Coincident with development of the uniform alignment is an increase in stress in the system that is also uniform. Accordingly, the circular gels with smaller diameter fail after fewer needle revolutions than the larger circular gels.

When the boundary is non-uniform, as with the ellipse or planar gels, there is greater resistance to displacement along the minor axis or across the plane. The fibers still align radially, but also accumulate along the minor axis to become denser and generate a stronger alignment signal, thereby resulting in non-uniform alignment measurements with respect to angular position, as was demonstrated by rotating the polarization axes. The stronger alignment in the 'shorter' direction was consistent with results from the circular gels and the anisotropy predicted by simple mechanics. The allowance for displacement appeared to shield the gel from failure as well. Elliptical gels failed after a greater number of needle revolutions than the small circular gels, despite demonstrating greater alignment. Planar gels demonstrated an even greater resistance to failure, surpassing even the larger circle. As in our previous study (Julias et al., 2008), in all gels, the failure occurred within the belly of the gel, approximately where

For Peer Review

circumferential alignment transitions to radial alignment, which places the fibers under a significant shear load.

When fibroblasts were included in the gels, the cells aligned to follow the collagen fibers, similarly to that observed in rat and mouse full thickness tissue explants (Langevin et al., 2001a). This phenomenon is known as contact guidance, which is generally defined as the tendency for cells to align and/or migrate preferentially in the direction of the prevailing orientation of the underlying substrate or surrounding network. As such, fiber alignment produced by an anisotropic mechanical strain field will also induce alignment of cells via contact guidance (Girton et al., 2002). Cell alignment in the circular gels was circumferential near the needle, and then became radial, and was uniform with respect to angular position. The elliptical gels also produced circumferentially aligned cells near the needle, but radial alignment was more prevalent in along the minor axis of the ellipse. Coincident with the significant increase in alignment was an increase in cell density in the volume of tissue near the needle, which resulted from the convective transport of cells along with the displaced tissue towards the needle. Despite large areas along the major axis that lacked alignment in this region, the average cell alignment and cell number in the elliptical gels were the same as the circular gels, which also points to the relatively greater displacement of the tissue towards the minor axis in the elliptical assay than in the circular ones. Cell alignment consistently extended several millimeters away from the needle, and in some cases to the boundary of the assay. This is particularly noteworthy, since the cellular gels were only subjected to two needle revolutions, where fiber alignment began to sharply increase with further needle rotation (Fig 6).

For Peer Review

Together with our previous in vitro study, these results provide quantitative illustrations of some of the distinct features of loose connective that help to explain its unique capabilities to transfer mechanical load during acupuncture therapy. Specifically, the anisotropic boundaries presented within connective tissue planes appear to allow a greater volume of fibrous tissue to be displaced and deformed and shields that tissue from tearing, thereby increasing the mechanical stimulus introduced during therapy. These locations also have more of the loose connective tissue, which can further accentuate the response. Another factor that may affect the biophysical response that may be added to the in vitro model is the extracellular matrix composition. Loose connective tissue maintains a significant proteoglycan content (Bode-Lesniewska et al., 1996; Stoeckelhuber et al., 2002), which can affect bulk and micro-mechanical properties and potentially cell-matrix adhesion. Thus, tissue composition may further distinguish connective tissue from surrounding tissues in vivo, and also may change with aging and disease to alter the tissue response of a particular patient (or a location on that patient) to needle manipulation.

Studies by Langevin (Langevin et al., 2005; Langevin et al., 2006; Langevin et al., 2007) have demonstrated that this mechanical stimulus can induce morphologic and phenotypic changes in fibroblasts, and there is a growing body of literature that substantiates the role of mechanotransduction in dictating cellular physiology and pathophysiology (Eshel and Lanir, 2001; Grinnell, 2003; Grinnell et al., 2003; Stegemann and Nerem, 2003; Bride et al., 2004). However, if these signals generated during acupuncture needling can be propagated along meridians, and whether the mechanical signals play a role in the therapeutic benefits, remain to be elucidated. In this study, even

For Peer Review

after only two needle revolutions, cells (and fibers) were aligned several millimeters away from the needle, and manipulations in vivo are typically more substantial (Langevin et al., 2004; Langevin et al., 2006). The results demonstrating stronger fiber alignment (and presumably mechanical signaling) in the narrower direction in our assays suggests that the signal generated by a single needle would be better propagated across a connective tissue plane rather than along the plane. However, the increase in cell and fiber density results from recruitment and displacement along the tissue plane. Moreover, these results point to the crucial role of boundary conditions in enabling fiber winding. Not every position along a connective tissue plane is recognized as an 'acupuncture point', and a more precise examination of the mechanical barriers at these locations is warranted. Furthermore, in a clinical setting, acupuncture therapy most often involves manipulation of multiple needles along a plane (Yamashita et al., 2001; Eshkevari, 2003), which could further introduce constraining boundaries to tissue displacement and alter the strength and direction of mechanical stimulation.

For Peer Review

Acknowledgements

Funding for this study was provided by the National Institutes of Health (R03 EB006045-01A1) and the New Jersey Commission on Spinal Cord Research (05-2912-SCR-E-0). Data from the Visible Human Project Initiative was made available through the National Library of Medicine and the University of Colorado.

For Peer Review

Literature Cited

Acupuncture NCSo. 1997. In: NIH.

Barocas VH, Tranquillo RT. 1997a. An anisotropic biphasic theory of tissue-equivalent mechanics: the interplay among cell traction, fibrillar network deformation, fibril alignment, and cell contact guidance. J Biomech Eng 119:137-145.

Barocas VH, Tranquillo RT. 1997b. A finite element solution for the anisotropic biphasic theory of tissue-equivalent mechanics: the effect of contact guidance on isometric cell traction measurement. J Biomech Eng 119:261-268.

Bode-Lesniewska B, Dours-Zimmermann MT, Odermatt BF, Briner J, Heitz PU, Zimmermann DR. 1996. Distribution of the large aggregating proteoglycan versican in adult human tissues. J Histochem Cytochem 44:303-312.

Bride J, Viennet C, Lucarz-Bietry A, Humbert P. 2004. Indication of fibroblast apoptosis during the maturation of disc-shaped mechanically stressed collagen lattices. Arch Dermatol Res 295:312-317.

Eisenberg D, Davis R, Ettner S, Appel S, Wilkey S, Rompay M, Kessler R. 1998. Trends in alternative medicine use in the United States, 1990-1997. JAMA 280:1569-1575.

Eshel H, Lanir Y. 2001. Effects of strain level and proteoglycan depletion on preconditioning and viscoelastic responses of rat dorsal skin. Ann Biomed Eng 29:164-172.

Eshkevari L. 2003. Acupuncture and pain: a review of the literature. Aana J 71:361-370.

Girton T, Barocas V, Tranquillo R. 2002. Confined compression of a tissue-equivalent: collagen fibril and cell alignment in response to anisotropic strain. Journal of Biomechanical Engineering 124:568-575.

Grinnell F. 2003. Fibroblast biology in three-dimensional collagen matrices. Trends in Cell Biology 13:264-269.

Grinnell F, Ho C, Tamariz E, Lee D, Skuta G. 2003. Dendritic fibroblasts in three-dimensional collagen matrices. Molecular Biology of the Cell 14:384-395.

Julias M, Edgar LT, Buettner HM, Shreiber DI. 2008. An in vitro assay of collagen fiber alignment by acupuncture needle rotation. Biomed Eng Online 7:19.

Knapp DM, Helou EF, Tranquillo RT. 1999. A fibrin or collagen gel assay for tissue cell chemotaxis: assessment of fibroblast chemotaxis to GRGDSP. Exp Cell Res 247:543-553.

Langevin HM, Bouffard NA, Badger GJ, Churchill DL, Howe AK. 2006. Subcutaneous tissue fibroblast cytoskeletal remodeling induced by acupuncture: evidence for a mechanotransduction-based mechanism. J Cell Physiol 207:767-774.

Langevin HM, Bouffard NA, Badger GJ, Iatridis JC, Howe AK. 2005. Dynamic fibroblast cytoskeletal response to subcutaneous tissue stretch ex vivo and in vivo. Am J Physiol Cell Physiol 288:C747-756.

Langevin HM, Bouffard NA, Churchill DL, Badger GJ. 2007. Connective tissue fibroblast response to acupuncture: dose-dependent effect of bidirectional needle rotation. J Altern Complement Med 13:355-360.

Langevin HM, Churchill DL, Cipolla MJ. 2001a. Mechanical signaling through connective tissue: a mechanism for the therapeutic effect of acupuncture. Faseb J 15:2275-2282.

Langevin HM, Churchill DL, Fox JR, Badger GJ, Garra BS, Krag MH. 2001b. Biomechanical response to acupuncture needling in humans. J Appl Physiol 91:2471-2478.

Langevin HM, Churchill DL, Wu J, Badger GJ, Yandow JA, Fox JR, Krag MH. 2002. Evidence of connective tissue involvement in acupuncture. Faseb J 16:872-874.

Langevin HM, Konofagou EE, Badger GJ, Churchill DL, Fox JR, Ophir J, Garra BS. 2004. Tissue displacements during acupuncture using ultrasound elastography techniques. Ultrasound Med Biol 30:1173-1183.

Langevin HM, Yandow JA. 2002. Relationship of acupuncture points and meridians to connective tissue planes. Anat Rec 269:257-265.

Shreiber D, Enever P, Tranquillo R. 2001. Effects of PDGF-BB on rat dermal fibroblast behavior in mechanically stressed and unstressed collagen and fibrin gels. Experimental Cell Research 266:155-166.

Stegemann J, Nerem R. 2003. Phenotype modulation in vascular tissue engineering using biochemical and mechanical stimulation. Annals of Biomedical Engineering 31:391-402.

Stoeckelhuber M, Stumpf P, Hoefter EA, Welsch U. 2002. Proteoglycan-collagen associations in the non-lactating human breast connective tissue during the menstrual cycle. Histochem Cell Biol 118:221-230.

Yamashita H, Tsukayama H, White AR, Tanno Y, Sugishita C, Ernst E. 2001. Systematic review of adverse events following acupuncture: the Japanese literature. Complement Ther Med 9:98-104.

For Peer Review

Figure Legends

Figure 1: A) Anatomical section of a thigh (adapted from Langevin and Yandow, 2002). The white dot located above the vastus lateralis (V. Lat) represents a control point. The black dot located between the V. Lat and the biceps femoris (B. Fem) above an intermuscular cleavage plane, or fascial plane, indicates an acupuncture point. B) Simplified schematic of a cross-section of the thigh indicating different tissue types and the location of fascial planes. C) Along the axis of the muscles, the fascial plane presents a geometry that is generally bounded on two sides and narrows with increasing depth. D) Simple assay geometries emulating the basic features of the fascial planes were generated out of porous polyethylene (PPE) to create geometric constraints: two circles of different diameter to examine the effects of a narrowing boundary condition, and elliptical and planar geometries to simulate the anisotropic boundary conditions where the distance to the PPE constraints is greater in one direction.

Figure 2: Schematic of polarized light microscopy system. A dissection stereomicroscope with a USB camera was mounted upside-down to a bench top. A fiber-optic ring light was attached to the motor housing providing a light source to the sample without hindrance from the motor. The polarizer was placed on top of the sample dish, and the analyzer was placed on the microscope as shown with the axis of polarization orthogonal to the axis for the polarizer. A small hole in the polarizer allowed free insertion and rotation of the acupuncture needle in the sample. From Julias et al, 2008.

For Peer Review

Figure 3: The orientation of the axes of polarization (solid lines) with respect to the major and minor axes of the elliptical assay were rotated to assess fiber alignment in different directions (dashed lines/clover leaf pattern). A) When the polarization axes are coincident with the axes of the ellipse (0°/90°), fiber alignment is evaluated at 45°, which is symmetric with respect to the ellipse. The polarization axes are rotated to be 22.5°/67.5° (B) and 45°/45° (C) off of the axes of the ellipse to examine anisotropy in alignment.

Figure 4: Alignment was quantified for individual cells by projecting the long axis of the cell onto a radial vector connecting the centroid of the cell to the needle position to determine cos θ. These projections were squared to create an index, $\Phi = \cos^2 \theta$ ranging from 0 (circumferentially aligned) to 1 (radially aligned).

Figure 5: Representative images of PLM-generated 'four-leaf clover' pattern of alignment following in vitro acupuncture. (A-D) Alignment at 2.4 revolutions; (E-H) Alignment at failure, with number of revolutions at failure indicated in lower-left hand corner. At 2.4 revolutions, alignment-induced birefringence is clearly weaker in the large circular gels (A) and small circular gels (B) when compared to elliptical gels (C) and planar gels (D). At failure, alignment was stronger in large circular gels (E) than small circular ones (F) and approached that in elliptical gels (G), because the large circles were able to withstand more needle rotation before failing. Planar gels (H) demonstrated the strongest field of alignment at failure. Bar: 1mm.

For Peer Review

Figure 6: Effects of assay geometry on gel failure and fiber alignment. (A) Evolution of alignment area (average +/- standard error) up to 2.4 revolutions, which represented the fewest revolutions before failure across all conditions. (B) Average revolutions (+/- standard error) before gel failure. (C) Average alignment area (+/- standard error) at failure. Small diameter circular gels generated more alignment per revolution that larger gels, but also failed earlier, and the alignment at failure was greater for the larger gels. Introducing a non-uniform boundary condition significantly affected both alignment and failure. Fibers in the elliptical geometry aligned faster than in either circular assay but failed in between the two. The net alignment at failure was the same statistically as that produced in the large circles. When the anisotropy was increased with the planar gels, gels aligned at the same rate as in the ellipses, but were able to withstand the most number of revolutions before failure (Tukey's test, $P<0.001$), which enabled the planar gels to demonstrate the greatest alignment at failure ($P<0.001$).

Figure 7: Effects of changing the orientation of the polarization axes (cross in upper right-hand corner) with respect to the assay geometry (large circle A-C; or ellipse D-F, shown) on the clover-leaf pattern after binarizing the images with the threshold algorithm. Within circular gels with uniform boundaries, the clover leaf patterns remained symmetric regardless of the polarization axes. Patterns within elliptical and planar gels were symmetric when the axes were coincident with the major and minor axes, but became increasingly asymmetric as the angle was changed to 22.5° (E) and 45° (F). The degree of asymmetry was expressed as the ratio of the length of perpendicular (opposite) leafs in each assay geometry (G). The elliptical and planar geometries became

For Peer Review

increasingly asymmetric as the polarization axis was rotated (* - significantly different than 0°, # - significantly different than 22.5°, ANOVA followed by Tukey's pairwise comparisons.) Bar: 1mm.

Figure 8: Epifluorescence images of GFP-expressing fibroblasts (top) and polarized light images of fiber orientation (bottom) in elliptical gels demonstrate that cell alignment follows fiber alignment. Before needle rotation, cells appeared randomly oriented (A), and PLM images are uniformly dark (B). After 2 needle rotations, significant alignment of cells (C) and fibers (D) is observed, particularly in the direction of the minor axis of the ellipse (shown in upper right-hand corner of C). A higher magnification image of cell alignment near the needle (E) demonstrates radial alignment that falls off faster in the major axis direction than the minor axis direction, which correlates to the corresponding PLM image of fiber alignment (F). The alignment is propagated along the minor axis several millimeters away from the needle (* in C & D, shown at high magnification in G & H). Bar: 1mm.

Figure 9: Quantitative assessment of the cell alignment parameter, Φ, which ranges from 0 (circumferential alignment – blue) to 1 (radial alignment – red). The alignment parameter was calculated for each cell in a stack of images encompassing a volume of ~2.0mm^3 taken with a 4X objective and projected onto the same plot (~2.25mm x 1.25mm). Representative plots are shown for gels before needling (A), and after needling in circular (B) and elliptical (C) gels, where the major axis is oriented horizontally. The black circle in the middle represents the needle location. Before needling, cells are

For Peer Review

randomly oriented. After needling, alignment increases in both circular and elliptical gels. Some circumferential alignment is apparent near the needle, but the prevailing orientation is radial. The radial alignment is uniform throughout the imaged field in circular gels. In elliptical gels, radial alignment is preferentially seen in the direction of the minor axis. (D) The average alignment in the different conditions was significantly greater after needling than before needling, where Φ was approximately the predicted value of 0.5 for random alignment. The average cell count in the imaged area also increased after acupuncture needle rotation, demonstrating the significant displacement of cells and collagen towards needle as the fibers wind around the needle. (* - significantly different than before needling, ANOVA followed by Tukey's pairwise comparisons.)

For Peer Review

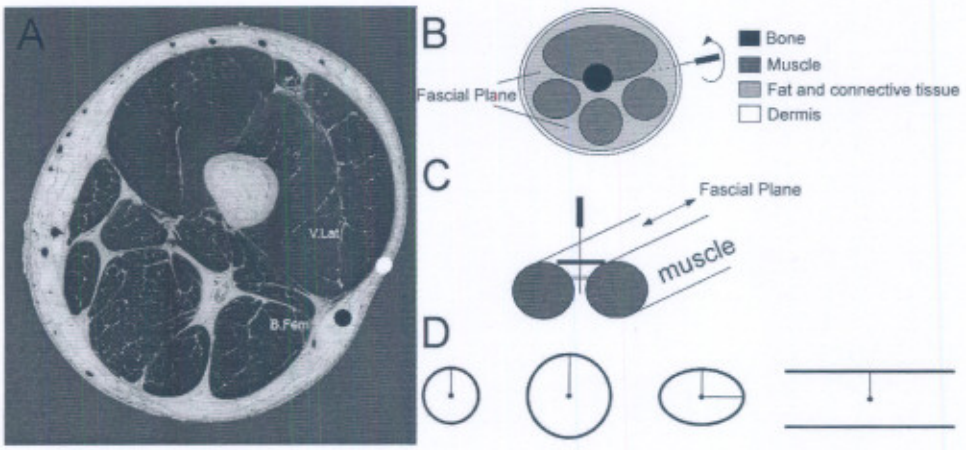

Figure 1: A) Anatomical section of a thigh (adapted from Langevin and Yandow, 2002). The white dot located above the vastus lateralis (V. Lat) represents a control point. The black dot located between the V. Lat and the biceps femoris (B. Fem) above an intermuscular cleavage plane, or fascial plane, indicates an acupuncture point. B) Simplified schematic of a cross-section of the thigh indicating different tissue types and the location of fascial planes. C) Along the axis of the muscles, the fascial plane presents a geometry that is generally bounded on two sides and narrows with increasing depth. D) Simple assay geometries emulating the basic features of the fascial planes were generated out of porous polyethylene (PPE) to create geometric constraints: two circles of different diameter to examine the effects of a narrowing boundary condition, and elliptical and planar geometries to simulate the anisotropic boundary conditions where the distance to the PPE constraints is greater in one direction.
90x41mm (600 x 600 DPI)

For Review

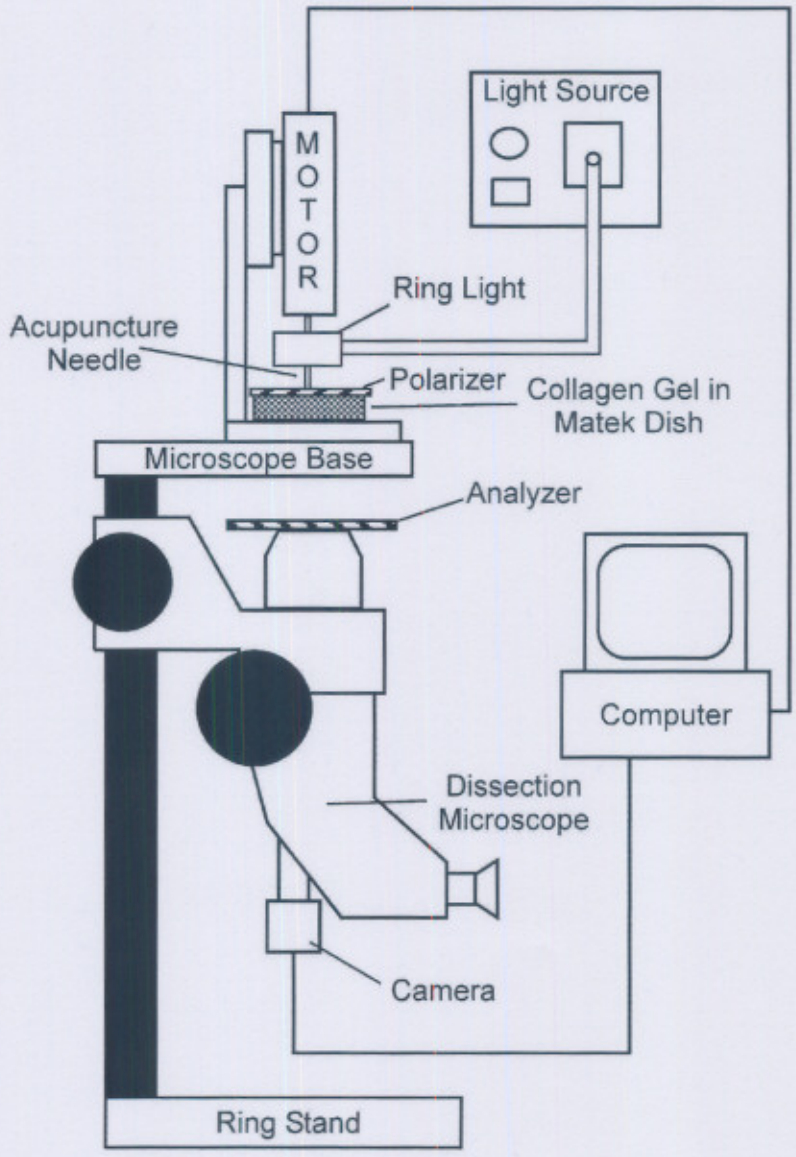

Figure 2: Schematic of polarized light microscopy system. A dissection stereomicroscope with a USB camera was mounted upside-down to a bench top. A fiber-optic ring light was attached to the motor housing providing a light source to the sample without hindrance from the motor. The polarizer was placed on top of the sample dish, and the analyzer was placed on the microscope as shown with the axis of polarization orthogonal to the axis for the polarizer. A small hole in the polarizer allowed free insertion and rotation of the acupuncture needle in the sample. From Julias et al, 2008.
120x174mm (600 x 600 DPI)

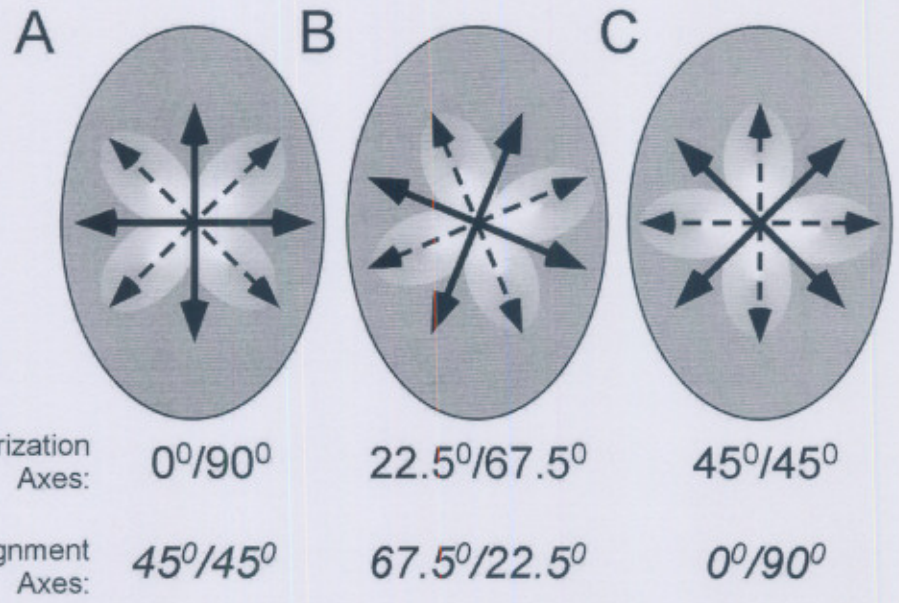

Figure 3: The orientation of the axes of polarization (solid lines) with respect to the major and minor axes of the elliptical assay were rotated to assess fiber alignment in different directions (dashed lines/clover leaf pattern). A) When the polarization axes are coincident with the axes of the ellipse (0°/90°), fiber alignment is evaluated at 45°, which is symmetric with respect to the ellipse. The polarization axes are rotated to be 22.5°/67.5° (B) and 45°/45° (C) off of the axes of the ellipse to examine anisotropy in alignment.°
68x43mm (600 x 600 DPI)

Review

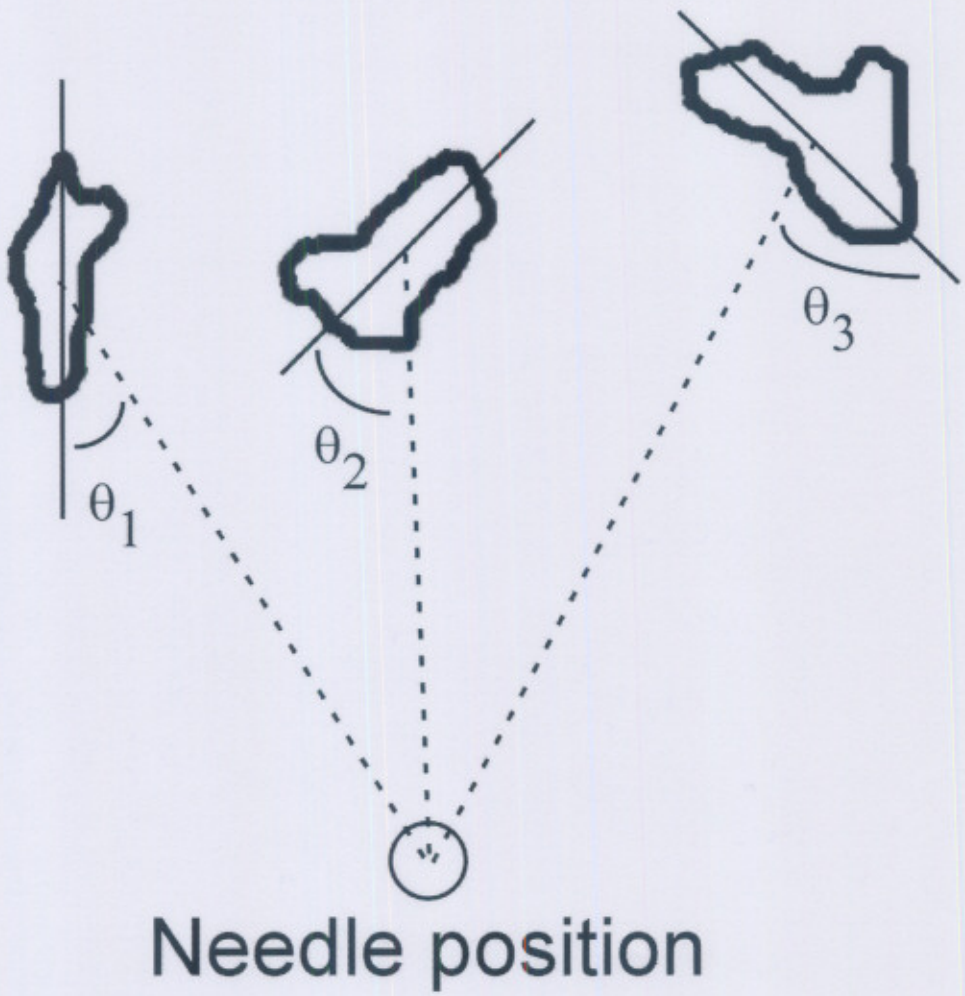

Figure 4: Alignment was quantified for individual cells by projecting the long axis of the cell onto a radial vector connecting the centroid of the cell to the needle position to determine cos θ. These projections were squared to create an index, $\Phi=\cos^{\theta}$ ranging from 0 (circumferentially aligned) to 1 (radially aligned).
78x80mm (600 x 600 DPI)

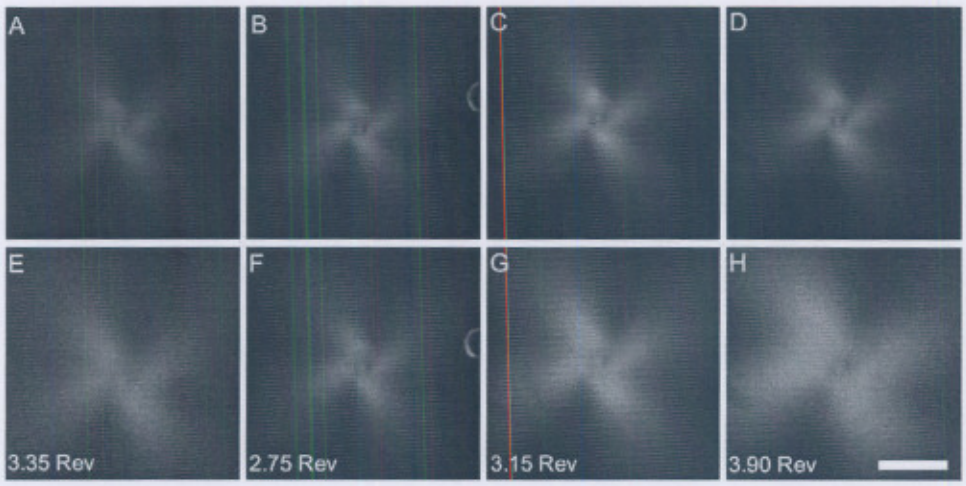

Figure 5: Representative images of PLM-generated 'four-leaf clover' pattern of alignment following in vitro acupuncture. (A-D) Alignment at 2.4 revolutions; (E-H) Alignment at failure, with number of revolutions at failure indicated in lower-left hand corner. At 2.4 revolutions, alignment-induced birefringence is clearly weaker in the large circular gels (A) and small circular gels (B) when compared to elliptical gels (C) and planar gels (D). At failure, alignment was stronger in large circular gels (E) than small circular ones (F) and approached that in elliptical gels (G), because the large circles were able to withstand more needle rotation before failing. Planar gels (H) demonstrated the strongest field of alignment at failure. Bar: 1mm.
103x51mm (300 x 300 DPI)

For Review

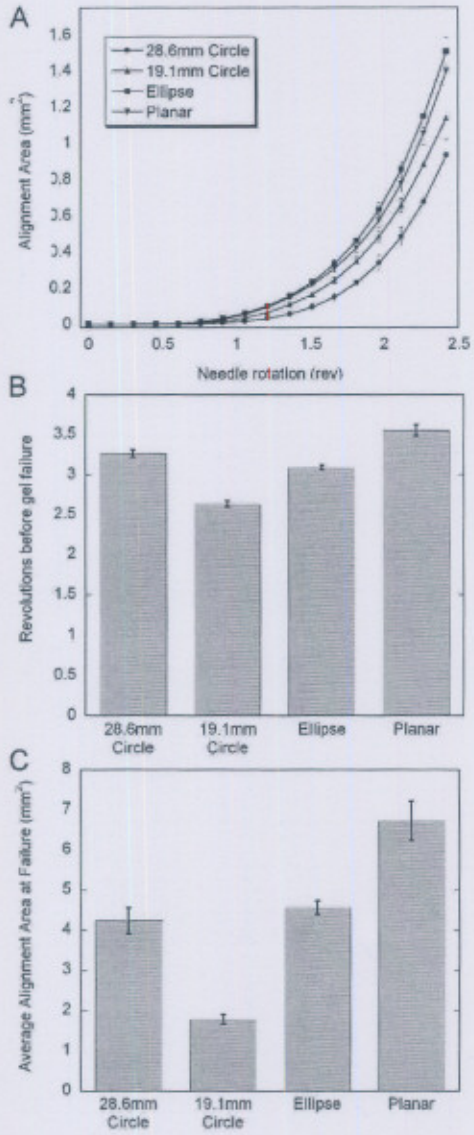

Figure 6: Effects of assay geometry on gel failure and fiber alignment. (A) Evolution of alignment area (average +/- standard error) up to 2.4 revolutions, which represented the fewest revolutions before failure across all conditions. (B) Average revolutions (+/- standard error) before gel failure. (C) Average alignment area (+/- standard error) at failure. Small diameter circular gels generated more alignment per revolution that larger gels, but also failed earlier, and the alignment at failure was greater for the larger gels. Introducing a non-uniform boundary condition significantly affected both alignment and failure. Fibers in the elliptical geometry aligned faster than in either circular assay but failed in between the two. The net alignment at failure was the same statistically as that produced in the large circles. When the anisotropy was increased with the planar gels, gels aligned at the same rate as in the ellipses, but were able to withstand the most number of revolutions before failure (Tukey's test, $P<0.001$), which enabled the planar gels to demonstrate the greatest alignment at failure ($P<0.001$).

135x326mm (300 x 300 DPI)

For Peer Review

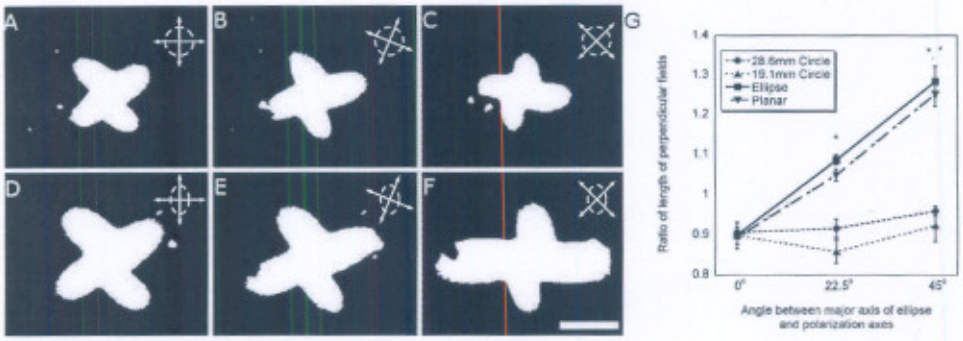

Figure 7: Effects of changing the orientation of the polarization axes (cross in upper right-hand corner) with respect to the assay geometry (large circle A-C; or ellipse D-F, shown) on the clover-leaf pattern after binarizing the images with the threshold algorithm. Within circular gels with uniform boundaries, the clover leaf patterns remained symmetric regardless of the polarization axes. Patterns within elliptical and planar gels were symmetric when the axes were coincident with the major and minor axes, but became increasingly asymmetric as the angle was changed to 22.5º (E) and 45º (F). The degree of asymmetry was expressed as the ratio of the length of perpendicular (opposite) leafs in each assay geometry (G). The elliptical and planar geometries became increasingly asymmetric as the polarization axis was rotated (* - significantly different than 0º, # - significantly different than 22.5º, ANOVA followed by Tukey's pairwise comparisons.) Bar: 1mm.
363x125mm (300 x 300 DPI)

For Review

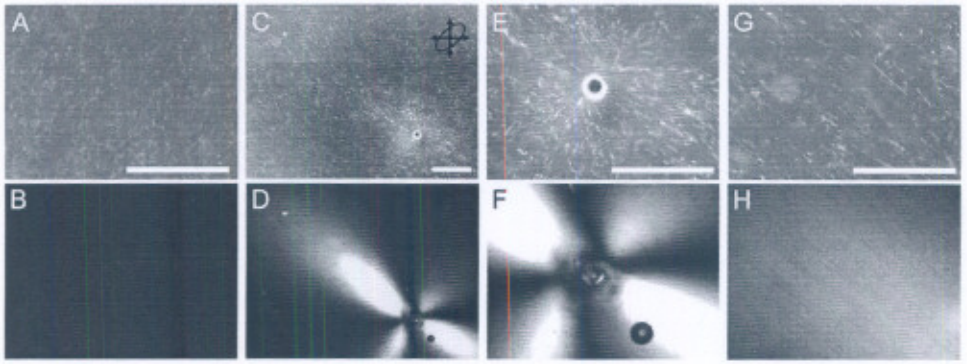

Figure 8: Epifluorescence images of GFP-expressing fibroblasts (top) and polarized light images of fiber orientation (bottom) in elliptical gels demonstrate that cell alignment follows fiber alignment. Before needle rotation, cells appeared randomly oriented (A), and PLM images are uniformly dark (B). After 2 needle rotations, significant alignment of cells (C) and fibers (D) is observed, particularly in the direction of the minor axis of the ellipse (shown in upper right-hand corner of C). A higher magnification image of cell alignment near the needle (E) demonstrates radial alignment that falls off faster in the major axis direction than the minor axis direction, which correlates to the corresponding PLM image of fiber alignment (F). The alignment is propagated along the minor axis several millimeters away from the needle (* in C & D, shown at high magnification in G & H). Bar: 1mm.
203x76mm (300 x 300 DPI)

For Review

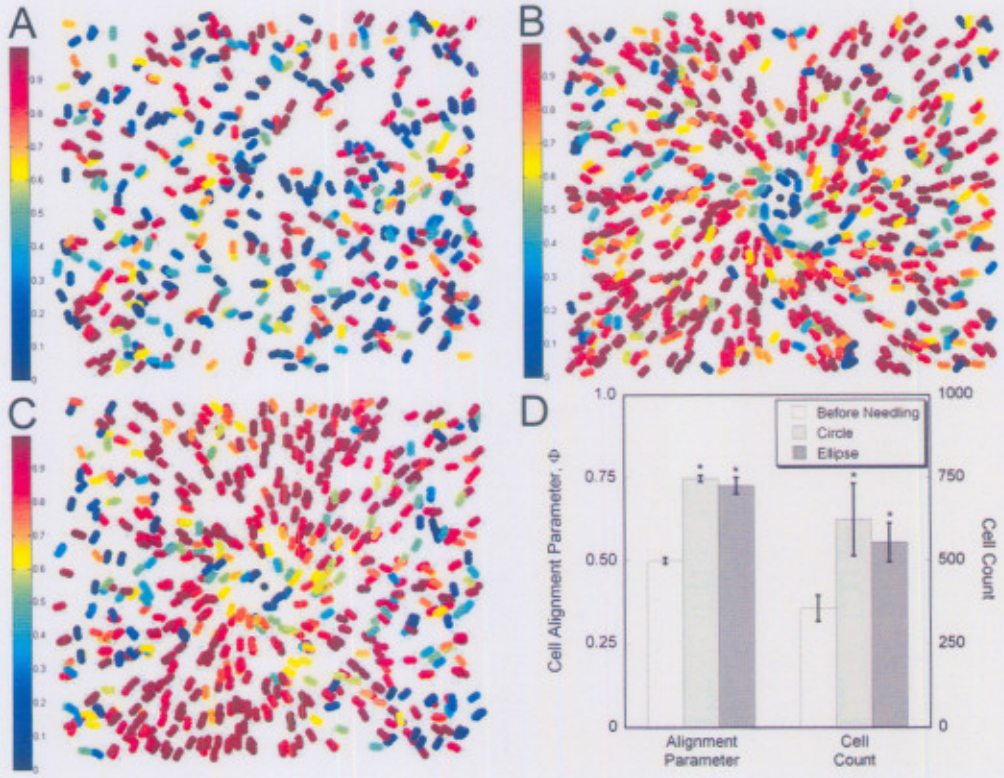

Figure 9: Quantitative assessment of the cell alignment parameter, Φ, which ranges from 0 (circumferential alignment – blue) to 1 (radial alignment – red). The alignment parameter was calculated for each cell in a stack of images encompassing a volume of ~2.0mm^3 taken with a 4X objective and projected onto the same plot (~2.25mm x 1.25mm). Representative plots are shown for gels before needling (A), and after needling in circular (B) and elliptical (C) gels, where the major axis is oriented horizontally. The black circle in the middle represents the needle location. Before needling, cells are randomly oriented. After needling, alignment increases in both circular and elliptical gels. Some circumferential alignment is apparent near the needle, but the prevailing orientation is radial. The radial alignment is uniform throughout the imaged field in circular gels. In elliptical gels, radial alignment is preferentially seen in the direction of the minor axis. (D) The average alignment in the different conditions was significantly greater after needling than before needling, where Φ was approximately the predicted value of 0.5 for random alignment. The average cell count in the imaged area also increased after acupuncture needle rotation, demonstrating the significant displacement of cells and collagen towards needle as the fibers wind around the needle. (* - significantly different than before needling, ANOVA followed by Tukey's pairwise comparisons.)
203x157mm (300 x 300 DPI)

ALIGNMENT OF TISSUE EQUIVALENTS BY ACUPUNCTURE NEEDLING

2005 BMES Conference, Baltimore, MD

Margaret Julias[1], David I. Shreiber[2], Helen M. Buettner[1,2]
[1]Department of Chemical and Biochemical Engineering, and [2]Department of Biomedical Engineering,

During acupuncture therapy, fine acupuncture needles are inserted into the skin and manipulated by hand, by rotating or pistoning the needle in place. Recent studies have shown that acupuncture needle rotation in vivo and ex vivo causes a field of connective tissue alignment around the needle, suggesting that it may be possible to achieve a similar effect in engineered tissues. To test this hypothesis, needle rotation was performed on collagen and fibrin gels and cell-populated tissue equivalents. Collagen gels were spiked with FITC-collagen to visualize individual collagen fibers. Fibrin gels were incubated in FITC solution to visualize fibrin fibers. Fiber alignment in the direction of needle rotation was observed by confocal microscopy and was similar to the previously reported connective tissue response to acupuncture. When needling was performed on GFP-fibroblast populated collagen or fibrin gels, the cells reoriented in the direction of fiber alignment as observed ex vivo. These results suggest that it is possible to mimic the connective tissue response to acupuncture needling with an in vitro system, and enable further investigation of the local tissue effects of acupuncture. In addition, they provide insight into a minimally invasive way to direct cell and tissue behavior in engineered tissue constructs. Currently, we are working on a complementary in vitro design for translational needling of ECM gels, which mimics the pistoning mode of acupuncture needling. Supported by the Charles and Johanna Busch Memorial Fund, a NJ Center for Biomaterials Summer Fellowship, and the New Jersey Commission on Spinal Cord Research.

A FINITE ELEMENT MODEL OF ACUPUNCTURE NEEDLING

Alice W. Señeres (1), Margaret Julias (2), Natasha Patel (1), David I. Shreiber (1), Helen M. Buettner (1,2)

(1) Department of Biomedical Engineering
Rutgers University
Piscataway, NJ

(2) Department of Chemical and Biochemical Engineering
Rutgers University
Piscataway, NJ

ABSTRACT

Acupuncture is a centuries-old treatment that has been gaining popularity and acceptance with Western medicine in recent decades. Though it is a low-cost and low-risk treatment for various physical ailments, very little is known about the mechanisms by which acupuncture works. Ex vivo needle rotation in subcutaneous tissue causes the connective tissue fibrils near the needle to reorient in a spiral pattern as shown by Langevin et al [1]. There is a mechanical coupling between the needle and tissue that is demonstrated by the increased force required to remove the needle from the tissue after rotation [2]. This coupling is believed to allow mechanical forces to be transmitted from the needle to the tissue, initiating a mechanotransduction mechanism that triggers the body's healing response. An in vitro system is being designed using a collagen-based tissue equivalent to investigate this hypothesis. To aid in designing this in vitro assay, a finite element model was created to study the tissue deformation caused by needling. The collagen gel was modeled as a viscoelastic material, with the acupuncture needle being represented as a rigid body. A contact model was created in which the acupuncture needle is inserted into the collagen gel and then rotated, mimicking the therapeutic procedure. The finite element model shows deformation gradients in the same pattern as the observed fibril alignment. The model will serve as an aid in designing the in vitro model with appropriate dimensions so that the inherent boundary conditions experienced by the collagen gel do not affect the results obtained.

INTRODUCTION

Acupuncture has been successfully used for thousands of years, yet little is known about the mechanisms by which it works. There are specific locations on the body that are historically known as acupuncture points. When acupuncture is performed, a needle is inserted into one of the acupuncture points and then rotated. Rotating the needle causes the extracellular matrix and the cells of the subcutaneous tissue to deform. To investigate the possibility that this deformation of the cells causes a mechanotransduction event that initiates the body's healing response, an in vitro tissue engineered model is being created to mimic the in vivo acupuncture process. To understand the physical dimensions needed for this in vitro model, a finite element model of collagen was created to predict material behavior.

METHODS

The finite element model was created using the software package ABAQUS. The tissue equivalent and needle were both modeled using cylindrical geometries, as shown in Figure 1. Boundary conditions were put in place to simulate the boundary conditions that the collagen gel experiences in a petri dish. The bottom surface of the cylinder was bounded in the z direction, and the outer rim of the cylinder was bounded in the r and θ direction. Adaptive meshing was used to prevent excessive element deformation.

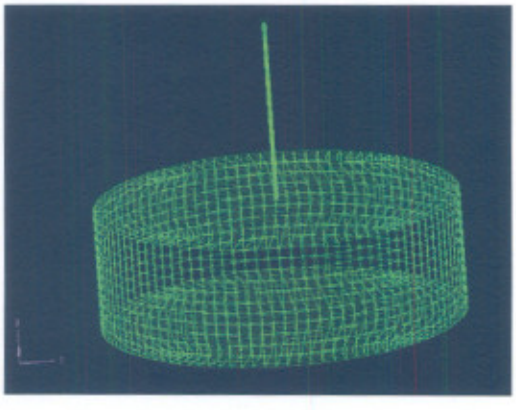

Figure 1. Finite element mesh of collagen gel and needle

Needling of the gel occurs in two steps. In step one, the needle is inserted into the gel by moving in the negative z direction, as shown in

Figure 2. In step two, a rotational velocity is applied to the needle, causing it to rotate about its z-axis.

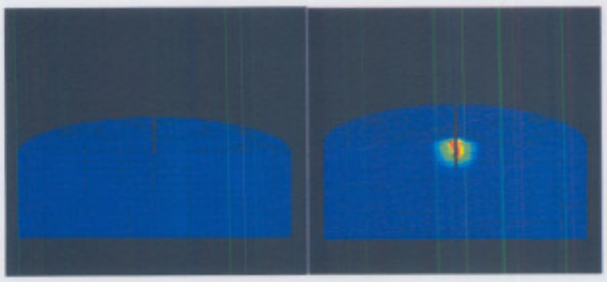

Figure 2. Needle is inserted into collagen gel

The boundary conditions in step one prevent rotation of the needle about the r, θ, or z axis, and movement of the needle in the r and θ direction. This ensures that the needle is inserted straight down. The boundary conditions in step two prevent movement in the r and z direction to ensure there is no unwanted translation.

Finite element model captures in vitro behavior

Rotating the acupuncture needle in tissue explants causes connective tissue fiber alignment over an immediate radius of a few millimeters. Since cells adhere to fibers, the fiber alignment can be seen by visualizing the cells, as shown in Figure 3. The finite element model is able to demonstrate this fiber alignment by mapping the maximum principal stress.

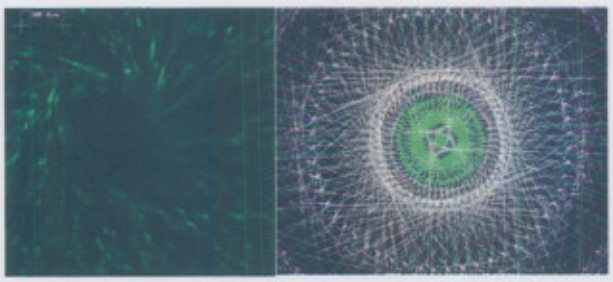

Figure 3. Fiber alignment reflected by cell orientation in vitro (left) and with the finite element model (right) after needle rotation

Due to its viscoelastic nature, the connective tissue climbs up the acupuncture needle as the needle is being rotated. This behavior can also be demonstrated in the finite element model by plotting the displacement in the z direction, as shown in Figure 4.

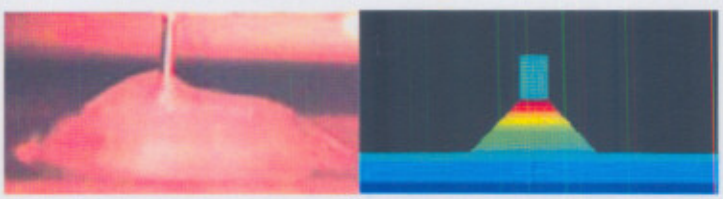

Figure 4. Tissue climb in vitro (left) and in finite element model (right)

Applications to experimental system

The in vitro assay has to be designed so that the inherent boundary conditions of the petri dish do not influence the tissue behavior and consequently the results. It is intuitively understood that basic parameters such as the height or radius of the gel have an effect on how the tissue behaves. The gel must be deep enough so that the bottom of the petri dish does not affect the material behavior. The radius of the collagen gel must be large enough so that the side boundary conditions do not affect the results. Early results from the finite element model demonstrate that when the same needling force is applied to gels with different radii, the gels exhibit different amounts of tissue climb. Similar observations were made for gels of different heights. This indicates that the dimensions of the assay need to be increased.

The finite element model can also be used to determine how the depth of needle insertion affects the results, so that an appropriate range of interest can be determined and studied. The speed with which the needle is rotated will also affect the material behavior since collagen is a viscoelastic material. The finite element model can be used to determine the range of needle rotational velocities of interest, so that they can be studied with the in vitro assay.

Unlike an in vitro assay, the parameters of the finite element model can easily be altered. Therefore it is clearly time efficient and cost effective to use a finite element model to understand how different parameters affect the material behavior. The parameters needed for the in vitro assay can then be quantified. The finite element model will also be used to study in vivo response in future work.

SUMMARY

Though acupuncture is a centuries-old treatment, the mechanisms by which acupuncture works have yet to be quantified. To aid in the in vitro investigation of mechanotransduction mechanisms, a finite element model of collagen undergoing acupuncture needling has been created. This finite element model mimics the behavior of collagen in vitro – the collagen climbs up the needle during rotation, and fiber alignment is demonstrated by plotting maximum principal stress. Different cases of the finite element model will be examined to quantify the dimensional needs of the in vitro collagen assay. An assay can then be built with appropriate dimensions so that boundary conditions will not influence material behavior.

ACKNOLWEDGEMENTS

We would like to thank the Charles and Johanna Busch Memorial Fund and NSF IGERT on Integratively Engineered Biointerfaces (DGE 033196) for their support.

REFERENCES

1. Langevin, H.M., Churchill, D.L., Wu, J., Badger, J., Yandow, J.A., Fox, J.R., and Krag, M. H., 2002, "Evidence of Connective Tissue Involvement in Acupuncture," *The FASEB Journal*, 15:2275.
2. Langevin, H.M., and Yandow, J.A., 2002, "Relationship of Aucupuncture Points and Meridians to Connective Tissue Planes," *The Anatomical Record*, 269: 257-265.

Proceedings of BIO2006
2006 Summer Bioengineering Conference
June 21-25, Amelia Island Plantation, Amelia Island, Florida, USA

BIO2006-XXXXX

EXTRACELLULAR MATRIX ALIGNMENT USING MICROMECHANICAL NEEDLE MANIPULATION

Margaret Julias (1), David I. Shreiber (2), Helen M. Buettner (1,2)

(1) Department of Chemical and Biochemical Engineering
Rutgers, The State University of New Jersey
New Brunswick, NJ

(2) Department of Biomedical Engineering
Rutgers, The State University of New Jersey
New Brunswick, NJ

INTRODUCTION

Aligned extracellular matrix (ECM) is a critical element of natural and bioartifical tissues. For example, oriented ECM affects cell morphology and provides a contact guidance field to direct cell migration [1, 2], which is important in many processes such as wound healing and nerve regeneration. It also provides critical mechanical anisotropy to optimally allow tissues to respond to mechanical loading. Cells interact with ECM chemically and mechanically via integrins and focal adhesions, which connect the ECM to intracellular cytoskeletal elements. Thus, a natural feedback exists between the intracellular and extracellular environment, where cells can exert traction and reorganize their ECM environment through cytoskeletal reorientation and reorganization, and can also experience forces transmitted through the ECM by other cells or extrinsic factors. The biophysical cues also affect protein synthesis, such as ECM proteins or metalloproteinases, to further contribute to the composition and structure of the ECM [3, 4].

As such, orienting ECM and cells has become an important component of many tissue engineering strategies. Methods to extrinsically align ECM include applying a controlled magnetic field to rotate fibrillar proteins during self-assembly of a gel network [1], or applying a mechanical force to the bulk bioartificial tissue to create a homogeneous anisotropic strain field, with alignment generally following the principal directions of the deviatoric strain tensor [2]. In certain applications, such as generating regions for fasciculation of white matter or muscle, finer control over the spatial profile of regions of alignment may be warranted.

Recent studies show that acupuncture needling, which includes needle insertion and rotation, causes subcutaneous local connective tissue deformation and alignment [5]. We believe that similar needling of tissue equivalents – cell populated collagen gels – in vitro may provide a simple, effective means of generating controlled alignment in ECM-based, 3D, engineered constructs to influence cell migration as well as mechanical properties. Herein, we report on how tissue equivalent geometry and needling parameters influence the magnitude of tissue realignment.

MATERIALS AND METHOD

Cell Culture

Rat dermal fibroblasts isolated and expanded from neonatal transgenic rats engineered to express GFP (a gift from the WM Keck Center for Collaborative Neuroscience at Rutgers) were cultured in Dulbecco's Modified Eagle's Medium (DMEM; Sigma Aldrich, St Louis, MO) supplemented with fetal bovine serum (FBS; Atlanta Biologicals, Lawrenceville, GA), L-glutamine (Sigma Aldrich, St Louis, MO), and penicillin-streptomycin (Sigma Aldrich, St Louis, MO)

Tissue Equivalent Preparation

Acellular collagen gels were prepared from lyophilized collagen (MP Biomedicals, Inc, Solon, Ohio). Collagen was dissolved in 0.02N acetic acid, neutralized with 0.1N NaOH, and diluted using M199 and 10XMEM media (Sigma Aldrich, St Louis, MO). To permit visualization of collagen fibers using fluorescence-mode confocal microscopy, the collagen solution was spiked with FITC-labelled collagen (Elastin Products, Owensville, MO) in a 9:1 ratio of collagen:fluorescent collagen. Cellular collagen gels were prepared by seeding fibroblasts into the collagen solution using the same method described above. A 5 mm thick gel was prepared in a Petri dish and incubated at 37°C. The diameter of the collagen gel was varied using porous polyethylene (PPE) ring inserts while keeping the gel thickness at 5 mm; diameters of 10, 15, and 35 mm were evaluated.

Copyright © 2006 by ASME

Needling Procedure

Collagen gels were needled manually using 410 μm stainless steel syringe needles (Becton Dickinson, Franklin Lakes, NJ). Needles were inserted 5 mm into the gel perpendicular to the gel surface and rotated at an approximate rate of 20 rev/min for 0, 5 and 10 revolutions. Gels were imaged with confocal microscopy with the needle in place.

RESULTS

Needle rotation caused the normally isotropic collagen fibers to wind and become denser around the needle (Fig 1). The change in collagen alignment resulted in rearrangement of resident fibroblasts (Fig 2). Increasing the number of rotations increased the zone of alignment (Fig 3). Increasing the diameter of the gel also increased the zone of alignment, although the intensity decreased (Fig 4). In no case was slip of the gel observed at the gel-plate or gel-PPE interface.

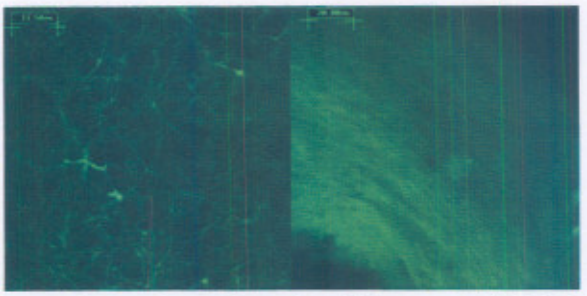

Figure 1. Random orientation of fluorescently labeled collagen fibers (left) and fibril alignment after needling (right) were visualized using 100x objective.

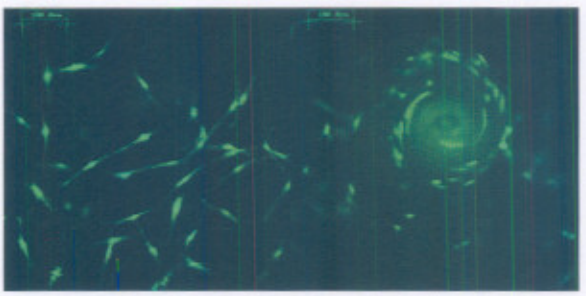

Figure 2. Random orientation of cell (left) and cell alignment after needling (right) were visualized using 20x objective.

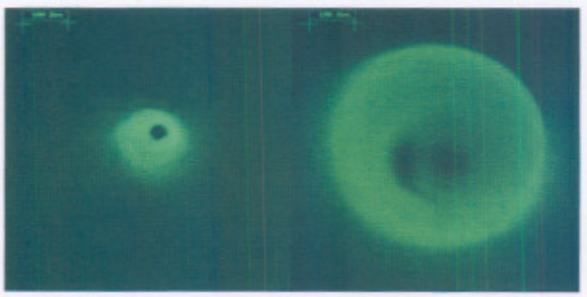

Figure 3. Fibril alignment after needling for 5 rev (left) and 10 rev (right) were visualized using 20x objective.

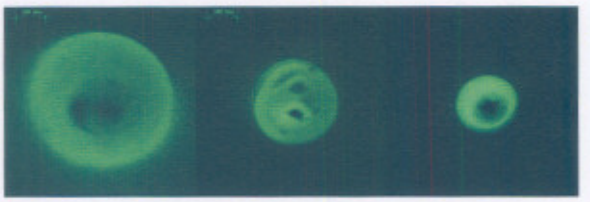

Figure 4. Fibril alignment after needling of collagen with diameter of 35 mm (left), 15 mm (middle), and 10 mm (right) was visualized using 20x objective.

DISCUSSION

The results demonstrate that circumferential alignment of tissue equivalents can be achieved with needle insertion and rotation akin to acupuncture therapy. As the collagen gel was needled, individual fibril alignment along with cell alignment were observed, with alignment much stronger near the needle. This is similar to the connective tissue response to acupuncture needling, where tissue aligns, deforms, and thickens around the needled area. The area of tissue reorganization could be controlled by the number of needle rotations and/or by the geometry of the gel.

This micromechanical method provides a minimally invasive way to achieve and manipulate alignment and, subsequently, cell migration in the tissue equivalents through variation of needle rotation and needle location. Another type of needle manipulation is through needle pistoning, where the needle is manipulated by moving the needle repeatedly in up-down motion after insertion. This method may create a linear alignment along the needle axis.

ACKNOWLEDGEMENTS

The work is supported by New Jersey Commission on Spinal Cord Research, Charles and Johanna Busch Memorial Fund, and NJ Center for Biomaterials Summer Fellowship.

REFERENCES

1. Guido, S. and Tranquillo, R. T., 1993, "A Methodology for the Systematic and Quantitative Study of Cell Contact Guidance in Oriented Collagen Gels," Journal of Cell Science, 105, pp. 317-331.
2. Atance, J., Yost, M. J., and Carver, W., 2004, "Influence of the Extracellular Matrix on the Regulation of Cardiac Fibroblast Behavior by Mechanical Stretch," Journal of Cellular Physiology, 200, pp. 377-386.
3. Alberts, B., Johnson, A., Lewis, J., Raff, M., Roberts, K., and Walter, P., 2002, "Molecular Biology of the Cell," 4th edition.
4. Friedl, P., and Brocker, E. B., 2000, "The Biology of Cell Locomotion within Three-Dimensional Extracellular Matrix," Cell Mol Life Sci., 57, pp. 41-64.
5. Langevin, H. M., Churchill, D. L., and Cipolla, M. J., 2001, "Mechanical Signaling Through Connective Tissue: A Mechanism for the Therapeutic Effect of Acupuncture," The FASEB Journal, 15, pp. 2275-2282.

Copyright © 2006 by ASME

Proceedings of BIO2006
2006 Summer Bioengineering Conference
June 21-25, Amelia Island Plantation, Amelia Island, Florida, USA

BIO2006-152599

A MICROROBOTIC NEEDLING MACHINE FOR AN IN VITRO ACUPUNCTURE MODEL

Alice W. Señeres (1), Abhijit Tamba (3), Margaret Julias (2), David I. Shreiber (1), Helen M. Buettner (1,2), Mourad Bouzit (1,3)

(1) Department of Biomedical Engineering
Rutgers University
Piscataway, NJ

(2) Department of Chemical and Biochemical Engineering
Rutgers University
Piscataway, NJ

(3) Department of Electrical and Computer Engineering
Rutgers University
Piscataway, NJ

INTRODUCTION

Acupuncture is an ancient Eastern technique that has gained popularity in the U.S. in recent decades. Acupuncture is performed by inserting and rotating fine needles in the skin at specific points on the body. This technique has been shown to be beneficial for addressing a variety of health conditions in clinical studies [1-3]. Despite these positive results, the use of acupuncture in this country is controversial since its underlying mechanisms are not well understood.

Acupuncture involves applying a mechanical force to the body via an acupuncture needle. Though this force is extremely localized, needling at a given point is purported to influence parts of the body that are located some distance from the needling site. Previous work done by Langevin et al determined that needling elicits a connective tissue response, including a significant thickening of the connective tissue layer [5], an increased mechanical linkage to the needle [4-6], and a rearrangement of tissue architecture [5]. However, for long-range healing to be possible, the effects of acupuncture clearly must be propagated further than just the connective tissue. It is hypothesized that the connective tissue response to needling prompts the nearby fibroblasts to activate the mechanotransductive pathway. This pathway allows the cells to convert mechanical forces into biochemical signals and alter short and long term phenotypic behavior, as well as tissue composition and organization. To quantitatively evaluate the mechanotransduction mechanism, we are studying the connective tissue response to acupuncture in vitro using a tissue equivalent comprising a cell-populated collagen gel.

Acupuncture is normally performed manually by a licensed practitioner. However, manual needling introduces a degree of uncertainty in needling parameters (i.e. insertion speed, rotation speed, number of needle rotations), and lacks the desired reproducibility for quantitative experiments. Therefore, a microrobotic needling machine was designed to perform acupuncture needling with a high degree of accuracy and repeatability. The requirements of the design were that the machine be lightweight and small for ease of use, allow for fine motor control (minimum rotation speed of 1 rev/sec and a minimum translation speed of 5 mm/sec), and have the ability to measure the force and torque acting on the needle. By designing this microrobotic needling machine, acupuncture needling can now be performed on the in vitro tissue equivalent with the necessary scientific rigor

METHODS

Overview of needling machine design

To operate the needling machine, the user inputs the desired parameters into a C code, which is sent to the PIC Microcontroller (Fig 1). The PIC microcontroller, with help from the driver, sends the necessary current to the motors to drive them. The motors are outfitted with optical encoders, which records 1200 light pulses for every revolution of the needle. This information is sent through the counter chip to the PIC microcontroller, which calculates the distance and speed of the needle, and adjusts the current being sent to the motors accordingly. The needling instrument also contains a sensor unit to measure the force and torque acting on the needle. This information is sent to the PIC microcontroller and displayed on the computer real-time during the experiment.

Microfabrication

The structural elements of the needling machine were designed using Mechanical Desktop software. Once the design was finalized, the parts were built using stereo lithography (Fig 2), which allows parts to be built quickly and inexpensively.

Copyright © 2006 by ASME

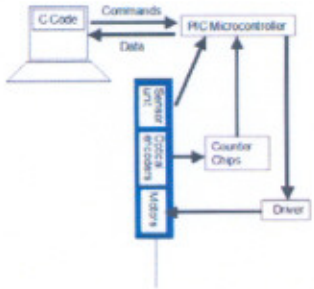

Figure 1. Overview of Needling Machine

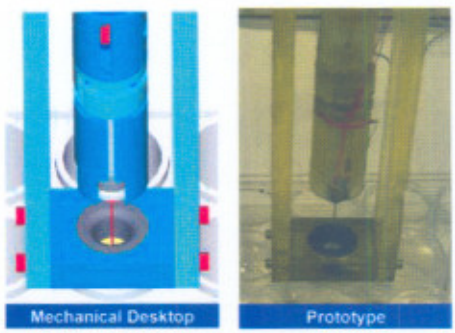

Figure 2. Design (left) and prototype (right) of the needling machine

Needling Unit

The needling machine (Fig 3) utilizes two motors – the translational motor to drive the insertion and removal of the needle in the assay, and the rotational motor to rotate the needle. Each motor is equipped with an optical encoder, which provides feedback regarding the speed, distance, and number of rotations the needle has moved. This allows the amount of current being sent to the motors to be adjusted to ensure the user-requested needling parameters are being met.

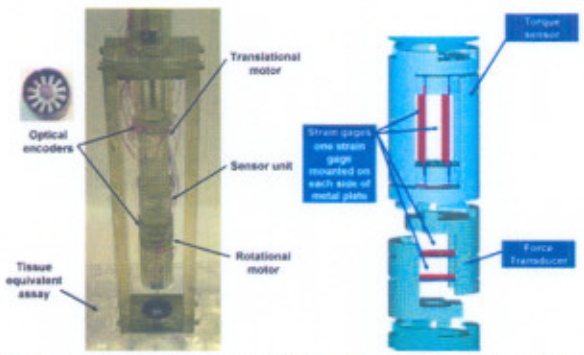

Figure 3. Needling unit (left) and sensor units (right)

Sensor Unit

Custom force transducers and torque sensors were designed to be small enough for mounting on the needling machine yet still provide the sensitivity required to measure the force and torque acting on the needle (Fig 3). The force transducer has only one degree of freedom in the axial direction, and contains four strain gages mounted in a Wheatstone bridge configuration to give the transducer a sensitivity of 0.2 mN. The torque sensor has only one degree of freedom in the rotational direction, and also uses four strain gages in a Wheatstone bridge configuration to give the torque sensor a sensitivity of 0.5 mN•mm.

RESULTS

This microrobotic needling machine allows force and torque data to be taken during in vitro acupuncture needling of the collagen gel (Fig 4). This data can then be compared to previously conducted in vivo work [4] to validate the experimental setup. When the needle is first inserted into the gel, the needle is going into compression (as seen by the positive force) because the gel is resisting the entry of the needle. Once rotation begins, the needle quickly goes into tension due to the 'tissue grasp' phenomenon of the tissue pulling down on the needle [4]. The torque increases as the needle is rotated due to greater resistance to movement as the tissue climbs up the needle and essentially stabilizes it. When rotation stops and the needle is removed, the force and torque drop back down to zero as expected.

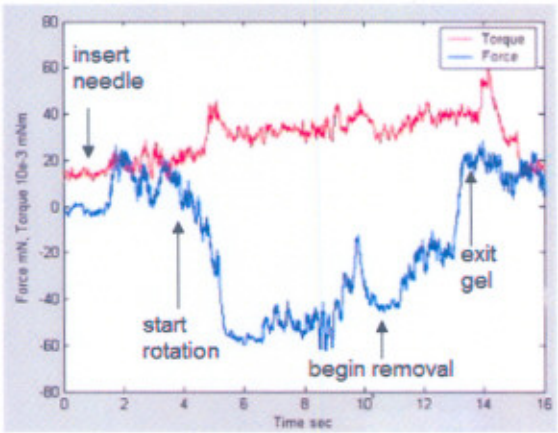

Figure 4. Force and torque data

SUMMARY

The microrobotic needling machine provides an accurate and reproducible needling protocol. In addition, the needling machine allows the force and torque acting on the needle to be measured and recorded. These force and torque measurement correspond with previous work conducted be Langevin et al [4].

ACKNOWLEDGMENTS

We would like to thank the Charles and Johanna Busch Memorial Fund and the NSF IGERT on Integratively Engineering Biointerfaces (DGE 033196) for their support.

REFERENCES

[1] Birch S, Hesselink JK, Jonkman FAM, Hekker TAM. Clinical research on acupuncture: Part 1. What have reviews of the efficacy and safety of acupuncture told us so far? Journal of Alternative & Complimentary Medicine 10: 468-480, 2004.

[2] NIH. Acupuncture consensus statement. 1997.

[3] World Health Organization. Acupuncture: Review and analysis of reports on controlled clinical trials. Geneva: WHO, 2002.

[4] Langevin H, Churchill D, Fox J, Badger G, Garra B, Krag M. Biomechanical response to acupuncture needling in humans. Journal of Applied Physiology 91: 2471-2478, 2001.

[5] Langevin H, Churchill D, Wu J, Badger G, Yandow J, Fox J. Krag M. Evidence of connective tissue involvement in acupuncture. The FASEB Journal 16: 872-874, 2002.

[6] Langevin H, Yandow J. Relationship of acupuncture points and meridians to connective tissue planes. The Anatomical Record 269: 257-265, 2002.

Copyright © 2006 by ASME

Matrix Concentration Affects Alignment of Tissue Equivalents

2006 BMES Conference, Chicago, IL

Margaret Julias[1], David I. Shreiber[2], Helen M. Buettner[1,2]
[1]Department of Chemical and Biochemical Engineering, and [2]Department of Biomedical Engineering

Aligned extracellular matrix (ECM) has been utilized to affect cell morphology and provide a contact guidance field to direct cell migration in wound healing and nerve regeneration. Orienting ECM and cells has become an important component of many tissue engineering strategies. Studies have shown acupuncture needling causes local subcutaneous connective tissue deformation and alignment. Needling of cell populated collagen gels may provide a simple, effective way of generating controlled alignment in ECM assemblies to influence cellular responses as well as mechanical properties. Collagen gels were prepared and subjected to needle rotation and translation. To visualize collagen fiber alignment, the collagen solution was spiked with FITC-labelled collagen. To observe cell alignment, GFP rat dermal fibroblasts were incorporated into the gels. Gels were prepared with different concentrations of collagen and hyaluronic acid (HA). Stainless steel needles were inserted into the gel and rotated at an approximate rate of 20 rev/min, or drawn through the gel at 10 mm/min. The number of needle rotations or translations was varied to observe the effect of needling. Individual fibril alignment and cell alignment were observed; changing the collagen concentration and addition of HA affected the intensity of alignment. Manipulation of matrix components along with micromechanical needling provides a way to achieve and manipulate alignment and, consequently, cell rearrangement in the tissue equivalents through variations in needle manipulation, needle location, and matrix concentration.

Proceedings of the ASME 2008 Summer Bioengineering Conference (SBC2008)
June 25-29, Marriott Resort, Marco Island, Florida, USA

SBC2008-192829

COLLAGEN CONTENT AND STIFFNESS AFFECT THE BIOMECHANICAL RESPONSE OF COLLAGEN GELS TO ACUPUNCTURE IN VITRO

MARGARET JULIAS (1), LOWELL T. EDGAR (2), DAVID I. SHREIBER (2), AND HELEN M. BUETTNER (1, 2)

(1) Department of Chemical and Biochemical Engineering
Rutgers, The State University of New Jersey
Piscataway, NJ

(2) Department of Biomedical Engineering
Rutgers, The State University of New Jersey
Piscataway, NJ

INTRODUCTION

Acupuncture is an ancient therapy that has been clinically proven for treating pain and nausea [1], though by unknown mechanisms. Recent in vivo and ex vivo studies demonstrate that acupuncture generates changes in the local tissue biomechanical environment, which may have been overlooked in previous neurophysiological studies [2].

During traditional acupuncture therapy, fine needles are inserted into specific points on the body and manipulated, typically in the form of needle rotation. Recent studies have shown that subcutaneous connective tissue winds around the needle during rotation [2-4], and that fibroblasts within the connective tissue are stimulated to change their morphology and remodel their cytoskeleton by the altered tissue mechanics [2, 3]. In addition to these changes, mechanical stress is known to induce cellular responses, including proliferation, apoptosis, migration, and ECM turnover [5, 6]. Hence, the stimulation of mechanotransduction pathways via tissue deformation may be an underlying contributor to the mechanisms of acupuncture. As such, local changes in tissue parameters that affect the mechanical response to acupuncture, such as collagen content, matrix composition, crosslinking, and tissue thickness, may ultimately influence the efficacy of acupuncture treatment.

To study these factors in a controlled setting, we are developing 3D in vitro models of acupuncture, where we can quantitatively examine elements of the tissue and cellular responses. We have established acellular type I collagen gels as our proof-of-principle model. We show that controlled needling of collagen gels produces fibril alignment consistent with the in vivo response, and that changes in the collagen concentration, degree of aldehyde-mediated crosslinking, gel thickness, and depth of needle insertion significantly affect the biomechanical response of collagen gels. Finally, using cell-populated tissue equivalents, we demonstrate morphological changes in cells subjected to acupuncture needling.

METHODS

Assay Preparation and Conditions: Collagen gels were prepared from lyophilized collagen (Elastin Products, Owensville, MO) [7] and cast in 35-mm glass bottom MatTek dishes (MatTek Corporation). Gels were prepared at 1.5, 2.0, or 2.5mg/ml with a centerline thickness of 4mm. At each concentration, some gels were crosslinked by incubating in 1ml of 10% neutral buffered formalin for 15min. Separate 2.0 mg/ml gels were prepared at centerline thicknesses of 4mm or 6mm, with the depth of needle insertion altered as described below. At least 6 gels were needled for each condition. A final set of fibroblast-populated gels (GFP-expressing rat dermal fibroblasts, 50,000 cell/ml) were allowed to compact for 2 days before needling. Cell morphology was examined prior to and 72hrs after needling.

In Vitro Acupuncture: Acupuncture was simulated with a computer controlled motor (MicroMo Electronics, Inc.) rotating a 250-μm stainless steel acupuncture needle (Seirin, Tokyo, Japan) inserted perpendicular to the surface of the gel. For collagen concentration and crosslinking studies, the needle was inserted 3mm deep. For collagen thickness/depth of insertion studies, needles were inserted between 1.5mm and 4.5mm deep, depending on the thickness of the gel. The needle was rotated at 0.3rev/s for 10 revolutions while viewing the gel with polarized light microscopy.

Polarization Light Microscopy (PLM): PLM was used to image fiber alignment continuously in real time. The gel was placed between two polarizers, which were positioned as 'cross-polars' with their respective angles of polarization 90° apart. Images were captured at 6 frames per second during needling and were analyzed using MATLAB

Copyright © 2008 by ASME

(Mathworks, Inc). A thresholding algorithm was developed to specifically evaluate the area of the 'clover-leaf' formation of birefringence [8], and was used to identify the failure point of the gels and to quantify the area of alignment.

RESULTS/DISCUSSION

In all conditions, significant alignment of collagen fibrils occurred, which was observed with PLM as a clover-leaf formation of birefringence consistent with radial and/or circumferential alignment (Fig 1A-D). The area of birefringence increased with needle rotation until gel failure, after which the area dropped sharply. Individual image sets were binarized using consistent criteria to identify the threshold pixel value [8], and the alignment area vs. revolutions curves were used to identify failure points and the degree of alignment. The area of alignment increased with increasing collagen concentration (Fig 1E), but decreased with crosslinking (Fig 2A – for clarity purposes, 2 mg/ml results were not included, however, they were consistent with the rest of results). Cone-and-plate rheometry demonstrated that the crosslinking increased the storage modulus in shear by an order of magnitude. No differences in the failure point were observed when changing collagen concentration. However, crosslinked collagen failed at significantly fewer needle revolutions than untreated gels (Fig 2B). These results suggest that stiffer tissues are less susceptible to acupuncture needling, which is consistent with published differences in the stiffness of loose connective tissue, which winds around the needle, and dermal tissue, which does not [3, 9].

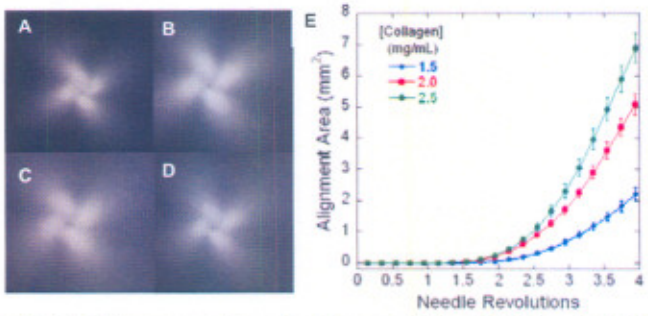

Fig 1. PLM images of peak alignment for (A)1.5mg/ml, (B) 2.0mg/ml, (C) 2.5mg/ml, and (D) 2.5mg/ml collagen crosslinked with formalin. (E) The area of alignment increases with collagen concentration.

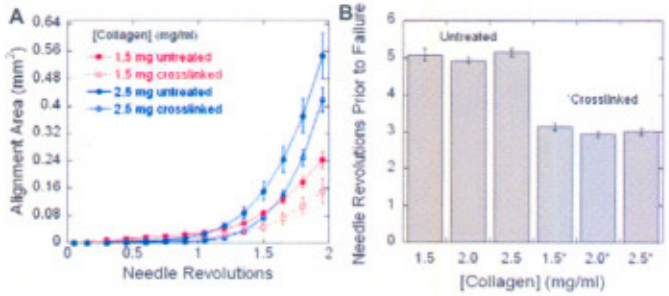

Fig 2. Crosslinked gels align less (A) and fail at fewer revolutions (B) than untreated collagen gels.

The thickness of the connective tissue layer is known to vary in vivo, and is especially thick at inter- and intra-muscular cleavage planes, which correlate anatomically to traditional acupuncture points and meridians [4]. We observed greater alignment after rotation of needles inserted deeper into collagen gels. However, for the same depth of insertion, we observed greater alignment in thinner gels (Fig 4). These results indicate that the amount of tissue and the fraction of the tissue in contact with the needle are important factors in the biomechanical response to needling.

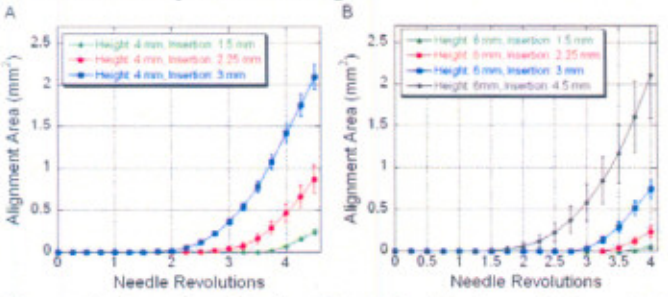

Figure 4. Insertion depth effects in (A) 4mm-thick and (B) 6mm-thick gels

The acupuncture-induced stress and strain fields in cell-populated collagen gels caused cellular expansion (Fig 5B) consistent with published reports from tissue explants [10]. This expansion occurred at minimum of 4 mm away from the acupuncture needle.

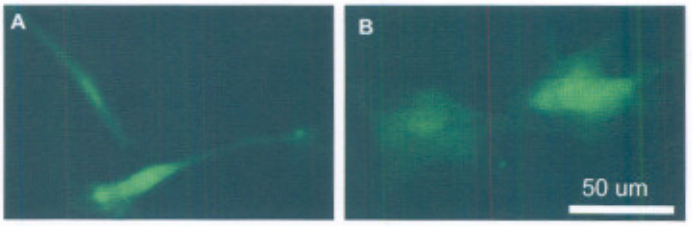

Figure 5. Cell morphology before (A) and after (B) needling

Collectively, these results demonstrate that our in vitro systems are capable of reproducing biomechanical and cellular features of acupuncture seen in explant models, and that our methods can identify quantitative differences in the response caused by controlled changes in tissue composition and geometry that may prove important in dictating the efficacy of acupuncture therapy.

ACKNOWLEDGEMENTS

This work is supported by the grant from National Institutes of Health (R03 EB006045-01A1) and a fellowship from the New Jersey Commission on Spinal Cord Research (05-2912-SCR-E-0).

REFERENCES

1. *Acupuncture*, NIH Consensus Statement Online. 1997 Nov 3-5. 15(5), 1-34.
2. Langevin, H., Churchill, DL., Wu, J., Badger, GJ., Yandow, JA., Fox, JR., and Krag, MH., FASEB Journal, 2002, 16, 872-4.
3. Langevin, H., D. Churchill, and M. Cipolla, FASEB Journal, 2001. 15: p. 2275-2282.
4. Langevin, H. and J. Yandow, The Anatomical Record (New Anat), 2002. 269: p. 257-265.
5. Grinnell, F., Trends in Cell Biology, 2003. 13(5): p. 264-269.
6. Elsdale, T. and J. Bard, J Cell Biol, 1972. 53(3): p. 626-637.
7. Shreiber, D., P. Enever, and R. Tranquillo, Experimental Cell Research, 2001. 266: p. 155-166.
8. Edgar, TE., et. al., submitted abstract SBC2008-192595.
9. Iatridis, JC., Wu, J., Yandow, JA., Langevin, HM., Connect Tissue Res. 44(5): 208-17, 2003.
10. Langevin, H., Bouffardi, NA., Churchill, DL., and Badger, GJ., J Altern Complement Med., 2007, 13(3): 355-60.

Copyright © 2008 by ASME

Proceedings of the ASME 2008 Summer Bioengineering Conference (SBC2008)
June 25-29, Marriott Resort, Marco Island, Florida, USA

SBC2008-XXXXXX

POLARIZED LIGHT MICROSCOPY FOR ANALYZING TISSUE MECHANICS DURING IN VITRO ACUPUNCTURE

Lowell Taylor Edgar (1)
Margaret Julias (2)
David I. Shreiber (1)
Helen M. Buettner (1, 2)

(1) Rutgers, The State University of New Jersey, Department of Biomedical Engineering

(2) Rutgers, The State University of New Jersey, Department of Chemical and Biochemical Engineering

INTRODUCTION: Acupuncture is a traditional therapy originating in China almost 2000 years ago. Acupuncture has slowly been growing in popularity in the West, and clinical evidence has shown the potential for acupuncture as a low-cost 'alternative' therapy for an assortment of ailments [1]. The practice of acupuncture involves inserting fine needles into the skin followed by needle manipulation, usually by rotation. Recent studies by Langevin et al demonstrate that this rotation causes the subcutaneous connective tissue to couple to and wind around the needle [2-4], which suggests that mechanotransduction in the connective tissue might play a role in the therapeutic mechanisms that underlay acupuncture [2, 3]. To begin to decompose and quantify this complex mechanism at the tissue level in a controlled setting, we have simulated acupuncture in type I collagen gels in vitro, and have developed algorithms to quantify the tissue response following imaging with polarized light microscopy (PLM).

METHODS: In vitro acupuncture was performed by casting a 3ml type 1 collagen gel (2.0mg/ml) in a 35mm MaTek Petri dish. Acupuncture needles (250μm) were inserted 3mm deep into the 4mm thick gel with a calibrated micromanipulator, and were rotated with a computer-controlled motor at 0.3rev/s. The evolution of collagen fiber alignment with needle rotation was observed with PLM and recorded in real-time with a USB digital camera. The collagen gel was situated between cross-polarizers. Prior to needling, PLM images were uniformly dark. As the needle was rotated, a pattern of birefringence emerged that resembled a '4-leaf clover' shape, which was caused by the radial and/or circumferential alignment of fibers that creates bright regions when aligned 45° off-axis to the cross-polars (Fig 1). The brightness and area of the clover increased with needle rotation until gel failure, after which it sharply declined.

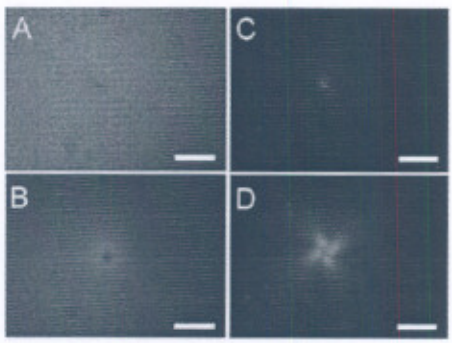

Figure 1: Images of gel before and after needling under bright field (A, B) and polarized light (C, D), where birefringence is observed when fiber alignment is 45° off-axis. Bar: 1mm.

To quantify the alignment, the raw images were binarized based on a threshold value specifically identified from each image set. First, the image set was binarized according to an arbitrary pixel grayscale value, and the area plotted against time to identify the frame at peak alignment. This frame was extracted and binarized at sequentially decreasing threshold values, beginning with the maximum intensity value in the image. As the threshold value decreased, the clover-shaped birefringence pattern began to emerge in the black-and-white images. The final threshold intensity level was identified when the binary image first contained a complete clover structure (Fig 2). Each image in the set was subsequently binarized with this threshold value, and the area of alignment determined.

Copyright © 2008 by ASME

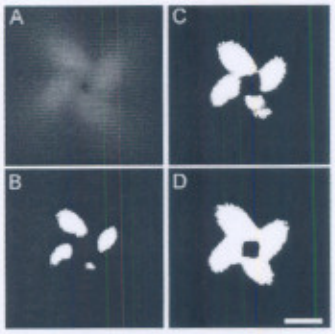

Figure 2: Identifying the threshold value for an image set. A raw image showing maximum alignment (B, C) As the threshold value is decreased, clover shape emerges (D) Final threshold value selected when a complete clover structure is observed.

RESULTS: The thresholding algorithm enabled continuous assessment of the area of alignment as well as a consistent and objective means of identifying the failure point (Fig 3). When applied to multiple data sets comprising different experimental conditions, the reproducible results were generated (Fig 4A), which allowed condition-dependent differences in the alignment and failure metrics to be identified. For example, decreasing collagen concentration caused a decrease in alignment with no change in the number of needle revolutions before failure. Crosslinking the gel for 15min with 10% buffered formalin prior to needling caused a decrease in alignment and in the failure point (Fig 4B).

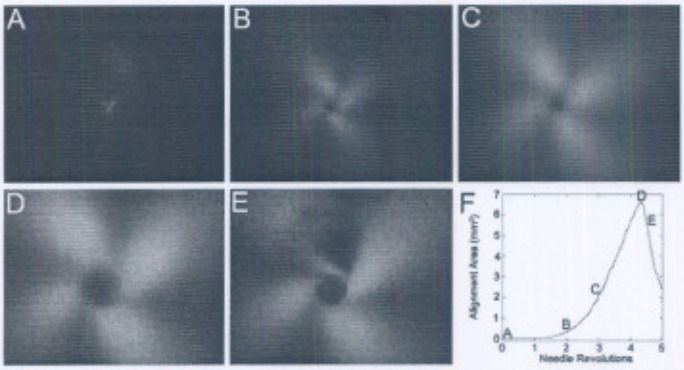

Figure 3: (A-D) The area of birefringence increases with needle revolutions until the stress in the gel causes failure (E). The revolutions for each image (A-E) are noted on (F).

DISCUSSION: The simple insertion and rotation of fine needles into the skin can produce an array of physical and biological changes including changes in tissue biomechanics. To study these biomechanical changes, and ultimately to examine their potential to induce cellular changes that could contribute to the benefits of acupuncture therapy, we are developing 3D in vitro models to impose defined experimental conditions in a controlled setting. PLM, combined with the image processing algorithms we developed, allows us to quantify elements of the biomechanical tissue response within minutes after an experiment. Using this system, we have found differences in the tissue response as a result of changing collagen concentration, crosslinking the gels, changing the depth of needle insertion, and changing the thickness of the collagen gel [5], and we have also used the technique to quantify the alignment response in cell-compacted collagen gels, which better mimic connective tissue in vivo. The system is simple yet robust, and can be used to examine differences in tissue mechanics imposed by different tissue and boundary conditions that may play a role in the efficacy of acupuncture therapy in a clinical setting.

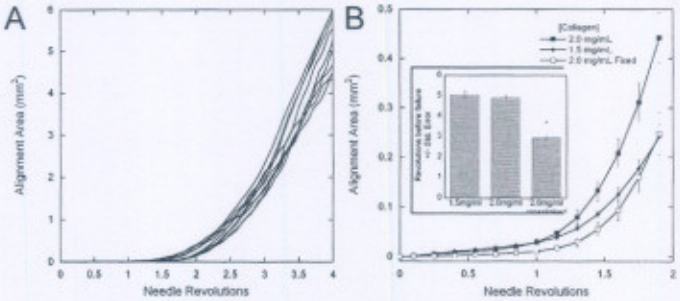

Figure 4: (A) Reproducibility of individual alignment curves for 2.0mg/ml collagen gels subjected to in vitro acupuncture. (B) Differences in alignment and/or failure (inset) are detected when the collagen concentration is changed or the gel is cross-linked.

The 'clover-leaf' pattern of birefringence results from fibers mis-aligned with the polarizer and analyzer, and peaks at 45°, which may be radial or circumferential alignment. The symmetry of the clover results from the symmetry of the circular MaTek chamber. From Fig 3E, it appears that the gels fail at an area where there is a transition from circumferential alignment near the needle to radial alignment away from the needle. With cross-polars, we can only identify the magnitude of birefringence and not the orientation of fiber alignment. By incorporating circularly polarized light and a second motor that rotates the analyzer through polarization states, both the magnitude and direction of alignment can be determined [6]. Such information could be especially valuable when gels and tissue with asymmetric boundary conditions are needled. The geometry of tissue at or near intermuscular cleavage planes is particularly variable, and these sites have been well correlated to the anatomical positions of traditional acupuncture points defined historically.

ACKNOWLEDGEMENTS: This work was supported by the National Institutes of Health (R03 EB006045-01A1) and ISURF (IGERT Summer Undergraduate Research Function) of Rutgers NSF IGERT on Biointerfaces DGE 0333196 (P.V. Moghe, Principal Investigator)

REFERENCES:

1. Acupuncture. NIH Consensus Statement Online. Nov. 3-5 15(5):1 34, 1997.
2. Langevin H., D. Churchill, and M. Cipolla. Mechanical Signaling through connective tissue: a mechanism for the therapeutic effect of acupuncture. FASEB Journal. 15: 2275-2282, 2001a.
3. Langevin H., D. Churchill, J. Wu, G. Badger, J. Yandow, J. Fox, and M. Krag. Evidence of connective tissue involvement in acupuncture. FASEB Journal. 16(872-874): June, 2002a.
4. Langevin H. and J. Yandow. Relationship of acupuncture points and meridians to connective tissue planes. The Anatomical Record (New Anat). 269: 257- 265,2002b.
5. Julias M. et al. In Vitro System to Study the Mechanism of Acupuncture Needling. Submitted to ASME SBC 2008.
6. Tower T. and R. Tranquillo. Alignment Maps of Tissues: I. Microscopic Elliptical Polarimetry. Biophysical Journal Vol. 81 2954–2963: November 2001.

Copyright © 2008 by ASME

Proceedings of the ASME 2009 Summer Bioengineering Conference (SBC2009)
June 17-21, Resort at Squaw Creek, Lake Tahoe, CA, USA

SBC2009-206519

EMULATING THE ANATOMY OF ACUPUNCTURE POINTS WITH IN VITRO MODELS

Margaret Julias[1], Lowell T. Edgar[2], Helen M. Buettner[1,2], and David I. Shreiber[2]

(1) Department of Chemical and Biochemical Engineering
Rutgers, the State University of New Jersey
New Brunswick, NJ

(2) Department of Biomedical Engineering
Rutgers, the State University of New Jersey
New Brunswick, NJ

INTRODUCTION

In traditional acupuncture, fine needles are inserted and rotated at specific locations on the body that correspond to specific therapeutic effects, which can occur locally or at a distance from the needling point. The majority of acupuncture points co-align with fascial planes under the skin, which present more subcutaneous connective tissue [1] (Fig 1). Needle insertion and rotation induces this connective tissue to couple to and wind around the needle, forming a whorl of alignment and generating measurable force on the needle that is significantly higher at fascial planes in comparison to insertion above a muscle [2, 3]. However, the effects of the varying tissue anatomy at fascial planes on fiber winding are not known. At these planes, the tissue is bounded on two sides by skeletal muscle and generally becomes narrower with increasing depth, presenting distinct boundary conditions compared to locations above a muscle, which resembles an infinite plane.

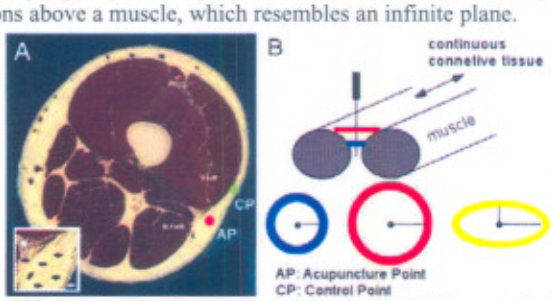

Fig 1. (A) Anatomical section of a thigh [1]. Arrows indicate subcutaneous connective tissue. (B) Simple geometries are used to emulate aspects of the connective tissue plane

We used a simple in vitro approach to study the effects of the basic elements of fascial plane geometry on fiber winding and cell alignment in a controlled setting [4]. We prepared circular gels of different radii to emulate the narrower boundary within the intermuscular plane, and elliptical gels to model the anisotropic boundary conditions presented within these planes (Fig 1). The alignment behavior of acellular collagen gels was examined quantitatively using polarized light microscopy. The orientation response of fibroblasts – the major cell type in the connective tissue layer – was examined in cell-populated gels. We found that fibers align faster in the smaller circular gels, and that fiber and cell alignment occurs preferentially in the direction of the minor axis of the ellipse, which represents across the tissue plane.

MATERIALS AND METHODS

Collagen gel preparation Collagen solutions were prepared to achieve a final concentration of 2.5mg/ml [5]. A 3-ml gel solution was poured into a 35-mm glass bottom MatTek dish (MatTek Corporation) containing annular circular (1.125" or 0.75" i.d.) or elliptical (1.125" major axis, 0.75" minor axis) porous polyethylene (PPE) inserts and incubated at 37°C for 4hr to ensure complete fibril formation. Cell populated gels were prepared using primary rat dermal fibroblasts isolated from rat pups that constitutively express green fluorescent protein (GFP). Cells were resuspended in a 2 mg/ml collagen solution at a cell density of 100,000 cells/ml. Cells became entrapped in the fibrillar gel after self-assembly.

In vitro acupuncture A computer controlled motor (MicroMo Electronics, Inc.) was used to needle the collagen gels. A 250-μm stainless steel acupuncture needle (Seirin, Tokyo, Japan) was attached to the motor and inserted perpendicular to the surface of the gel to a depth of 3mm using a calibrated micromanipulator. The needle was rotated at 0.3rev/s for 10 revolutions. The cellular gels were needled for 2 revolutions to prevent gel tearing and allow the observation of cell alignment after rotation with epifluorescence microscopy.

Copyright © 2009 by ASME

Fiber and cell alignment: Polarization light microscopy (PLM) [4] was used to examine fiber alignment. The gels were placed between two polarizers, which were positioned as 'cross-polars'. To capture alignment during needling, images were captured at 6 frames per second during needle rotation and analyzed with MATLAB (The Mathworks, Inc, Natick, MA) [4]. Both the polarizer and analyzer were then rotated manually to 22.5° and 45° off the ellipse's major axis to examine fiber anisotropy. In cell populated gels, fiber alignment was captured with PLM at 45° off the ellipse's major axis, and cell alignment was measured following epifluorescent imaging by determining $\cos^2\theta$ for each cell, where θ is the angle of a cell with respect to a radius from the needle to the center of the cell.

RESULTS/DISCUSSION

In general, PLM revealed alignment as a result of needle rotation in the form of a '4-leaf clover'. Alignment area increased with the number of needle rotations. At the same number of revolutions, the average alignment area was greater in the small, 0.75" circular gels than the large 1.125" circular gels (Fig 2A). Rotations-to-failure was inversely correlated to alignment, with failure occurring earlier in the smaller gels (Fig 2B). The alignment and failure points for the elliptical geometry, which had a major axis matching the large circular gel and a minor axis matching the small one, fell in between the large and small circular gels. Failure points for the different geometries were significantly different from each other (ANOVA followed by Scheffe's post hoc test, $P<0.001$).

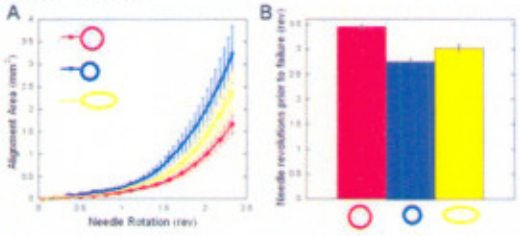

Fig 2. Effects of geometry on the alignment area (A) and gel failure (B)

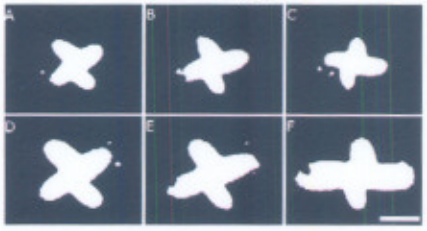

Fig 3. Binarized PLM images of the clover leaf pattern after 2.5 rev of 1.125" circular gels (A-C) and oval gels (D-F) at 0° (A, D), 22.5° (B, E), and 45° (C, F). Bar 1mm

To examine if the elliptical geometry caused non-uniform fiber alignment, the axis of the polarizer/analyzer was rotated different degrees off of the major axis of the ellipse. As expected, the size and shape of the clover pattern was conserved for circular gels (Fig 3 A-C), indicated uniform, axisymmetric radial alignment. However, for the ellipse, the shape and size of the clover pattern changed with the axis of polarization (Fig 3 D-F). Radial alignment was greater in the direction of the minor axis. In cell-populated gels, fibroblast alignment followed fiber alignment (Fig 4). As with fiber alignment, cell alignment was uniformly radial in circular gels, but was more extensive in the direction of the minor axis for elliptical gels (Fig 5).

Fiber alignment during acupuncture needling is indicative of tissue tension, which can stimulate resident fibroblasts mechanically. The stimulated fibroblasts may in turn affect the neighboring cells through cell-cell interactions [6] and modification of the surrounding matrix via collagen deposition or matrix degradation, to propagate the effects of the local perturbation as well as produce longer term changes. The alignment of fibers and cells may also serve to transmit signals in a preferred direction, in addition to adding important structural changes that could also influence transport and healing.

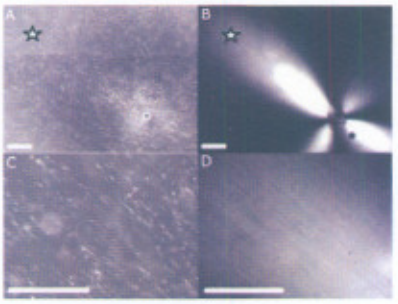

Fig 4. Cell alignment (A) and corresponding PLM image (B) after 2 needle rotation in an elliptical gel. (C, D) Higher magnification of the starred areas show alignment as far as 5mm away from the needle. Bar 1mm

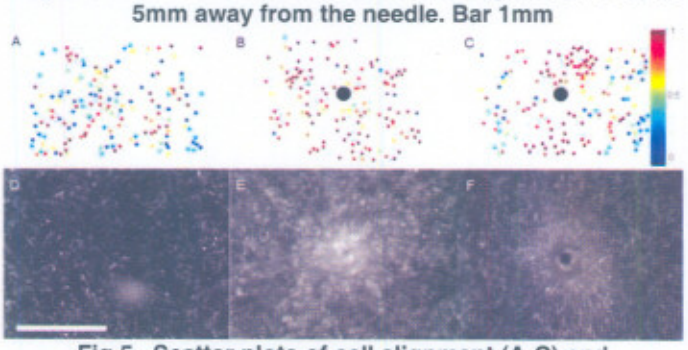

Fig 5. Scatter plots of cell alignment (A-C) and corresponding epifluorescent image (D-F). Each circle is a separate cell, and the black circle represents the needle. Red/blue indicates radial/circumferential alignment. Before needling (A, D), cells are randomly aligned. After needling, radial alignment is nearly uniform for circular gels (B, E). Radial alignment occurs preferentially along the minor axis for elliptical gels (C, F). Bar 1mm

ACKNOWLEDGEMENTS

This work is supported by the grant from National Institutes of Health (R03 EB006045-01A1) and a fellowship from the New Jersey Commission on Spinal Cord Research (05-2912-SCR-E-0). Data from the Visible Human Project Initiative was made available through the National Library of Medicine and the University of Colorado.

REFERENCES

1. Langevin, HM and J. Yandow, The Anatomical Record (New Anat), 2002. 269: p. 257-265.
2. Langevin, HM, Churchill, DL., Wu, J., Badger, GJ., Yandow, JA., Fox, JR., and Krag, MH., FASEB Journal, 2002, 16, 872-4.
3. Langevin, HM., Churchill, DL., Fox, JR., Badger, GJ., Garra, BS., and Krag, MH., J Appl Physiol, 2001, 91, 2471-2478.
4. Julias, M, Edgar, LT., Buettner, HM., Shreiber, DI., Biomedical Engineering Online 2008, 7:19.
5. Shreiber, D., P. Enever, and R. Tranquillo, Experimental Cell Research, 2001. 266: p. 155-166.
6. Langevin, HM., Cornbrooks, CJ., and Taatjes, DJ., Histochem Cell Biol, 2004, 122: 7-15.

Copyright © 2009 by ASME

Proceedings of the ASME 2010 Summer Bioengineering Conference (SBC2010)
June 16-19, Grande Beach Resort, Naples Florida, USA

SBC2010-19221

THE BIOPHYSICAL RESPONSE OF COLLAGEN-FIBRIN COMPOSITE GELS TO IN VITRO ACUPUNCTURE

Margaret Julias[1], Helen M. Buettner[1,2], David I. Shreiber[1]

1. Department of Chemical & Biochemical Engineering
2. Department of Biomedical Engineering
Rutgers, The State University of New Jersey, Piscataway, NJ, USA

INTRODUCTION

Therapeutic acupuncture involves the insertion and manipulation of fine needles at specific points. Although acupuncture has been proven effective for a number of conditions, the mechanisms that underlay these effects remain unknown. A critical first step is to identify the local changes that occur during needle manipulation, which can then be related to longer-term and more remote consequences. In vivo and ex vivo studies have demonstrated that loose collagenous subcutaneous connective tissue couples to needles during therapeutic manipulation, which deforms the tissue and exposes resident cells to altered mechanics and triggers morphologic and phenotypic changes[1]. The resultant alignment of the tissue and cells may additionally help to propagate signals along acupuncture meridians.

We have developed a 3D in vitro model that emulates loose connective tissue in a highly controlled setting[2]. Herein, we use the model to preliminarily examine the role of matrix composition on the biophysical response of tissues to acupuncture needle rotation. Though the primary structural component is type 1 collagen, little else has been reported regarding the composition of the loose fascia that specifically interacts with the needle during therapy. We prepared composite gels comprising type I collagen mixed with fibrin. Fibrin is found within injured tissues and wounds that are unable to heal or heal properly, and may also be present near 'leaky' vessels that are dilated because of a local inflammatory response. Acupuncture is often applied to treat such disorders[3], and punctures the skin to cause a wound (albeit very minor) during therapy. Collagen-fibrin composite gels have been also made as tissue engineered biocompatible scaffolds[4]. In the current research, we varied the composition of collagen-fibrin gels as a simple model of a gel comprising 2-fibril forming components, and quantified the rate and degree of fiber alignment, the failure of the gels, and the mechanical properties of the gels.

MATERIALS AND METHODS

Composite Gel Preparation Stock solutions for collagen-fibrin composites were prepared for easy preparation of gels with different compositions: a) 6mg/ml bovine type 1 collagen in 0.02N acetic acid, b) 42.5 mg/ml fibrinogen in M199, and c) 5 unit/ml thrombin in 10xMEM. Composite gels were prepared following the collagen gel preparation as previously described[5]. Briefly, collagen solutions were neutralized with 1N NaOH and diluted to the desired final concentration using M199 and MEM containing fibrinogen and thrombin (0.1 unit/mg fibrinogen) to reach final concentrations as listed in Table 1, and supplemented with 0.3 Ca2+ to facilitate enzymatic cleavage of fibrinogen to fibrin. Gels were cast in 35-mm MatTek dishes containing porous polyethelyne rings (28.6mm i.d.) and incubated at 37°C for 4hr. The solution intercalated within the pores to produce a fixed boundary condition at the perimeter of the 4-mm thick gel.

In Vitro Acupuncture A 250-μm stainless steel acupuncture needle was attached to a computer-controlled motor and inserted 3mm into perpendicular gels using a calibrated micromanipulator. The needle was rotated at 0.3rev/s for 10 revolutions. The evolution of fiber alignment was captured in real-time with polarized light microscopy (PLM) and quantified with image analysis algorithms that normalize for differences in inherent birefringence as previously described[2].

Mechanical Testing The stiffness of composite gels was assessed by measuring the displacement of a small, metallic bead under a controlled magnetic force using methods previously described[6]. Briefly, a 1/32" diameter chrome-steel bead was entrapped within a gel in a 0.5ml microcentrifuge tube. Images were taken to acquire the bead displacement as voltage was altered to incrementally change the applied magnetic field and generate a force-deflection curve. The force-deflection curve was then related to the elastic modulus[6].

Copyright © 2010 by ASME

Total Protein	%F						
	0	20	33	50	67	80	100
2 mg/ml	2C0F			1C1F			0C2F
2.5 mg/ml	2.5C0F	2C0.5F				0.5C2F	0C2.5F
3 mg/ml	3C0F		2C1F	1.5C1.5F	1C2F		0C3F
4 mg/ml				2C2F			

Table 1: List of gel compositions. Index prior to C (collagen) or F (fibrin) indicates concentration (mg/ml)

RESULTS

With PLM, changes in brightness surrounding the needle indicated that alignment occurred immediately after the start of needle rotation. A '4 leaf clover' was observed following needle rotation, which represented both radial and circumferential alignment (Fig 1- 2mg/ml total concentration shown). In collagen-fibrin composites, Regardless of fibrin content, alignment increased with increasing total protein concentration (ANOVA, $P<0.001$). Although the rate of alignment was increased with the relative fraction of collagen, gels with higher fibrin content were more resistant to failure and ultimately generated significantly more alignment, but only when the fibrin percentage was greater than 50% (ANOVA, $P<0.001$) (Fig 2). The stiffness of the gels decreased significantly with increasing percentage of fibrin and increased with increasing total protein concentration (ANOVA, $P<0.001$). Collagen and fibrin fiber formation and general alignment were confirmed using confocal microscopy with FITC-tagged collagen and TRITC-tagged fibrin (data not shown).

DISCUSSION

Composites gels with relatively higher collagen content had a higher alignment rate, but once collagen content dropped below 1mg/ml, composite gels behaved similar to pure fibrin gels in terms of both failure and alignment. We found that inclusion of fibrin in collagen gels decreased the stiffness of gels, which was consistent with previous reports by Rowe and Stegemann[4]. The less flexible collagen fibers will be forced to rotate and align faster than the fibrin fibers, but will also fail earlier. We believed that collagen fibers generally play a dominant role in gel failure only when the concentration within composite gels is at least ~0.8 - 1mg/ml, which is approximately the minimum concentration necessary for collagen to form a hydrogel that can support its own form. Clinically, the results suggest that recently wounded or inflamed tissue may be particularly responsive mechanically to acupuncture because the prevalence of fibrin would enable more tissue to align.

ACKNOWLEDGMENTS

Funding was provided by the NIH (R03 EB006045-01A1) and New Jersey Commission on Spinal Cord Research (05-2912-SCR-E-0).

REFERENCES

1. Langevin et al.. 2006. J Cell Physiol 207(3): 767-74.3.
2. Julias et al 2008.. Biomed Eng Online 7:19.
3. Pretorius, E, 2009. Acupunct Electrother Res 34(1-2): 15-26
4. Rowe and Stegemann, 2006. Biomacromolecules 7(11): 2942-8.
5. Shreiber et al, 2001. Exp Cell Res 266:155-166.
6. Lin et al.,. 2005. J Biomech Eng 127(4): 571-9.

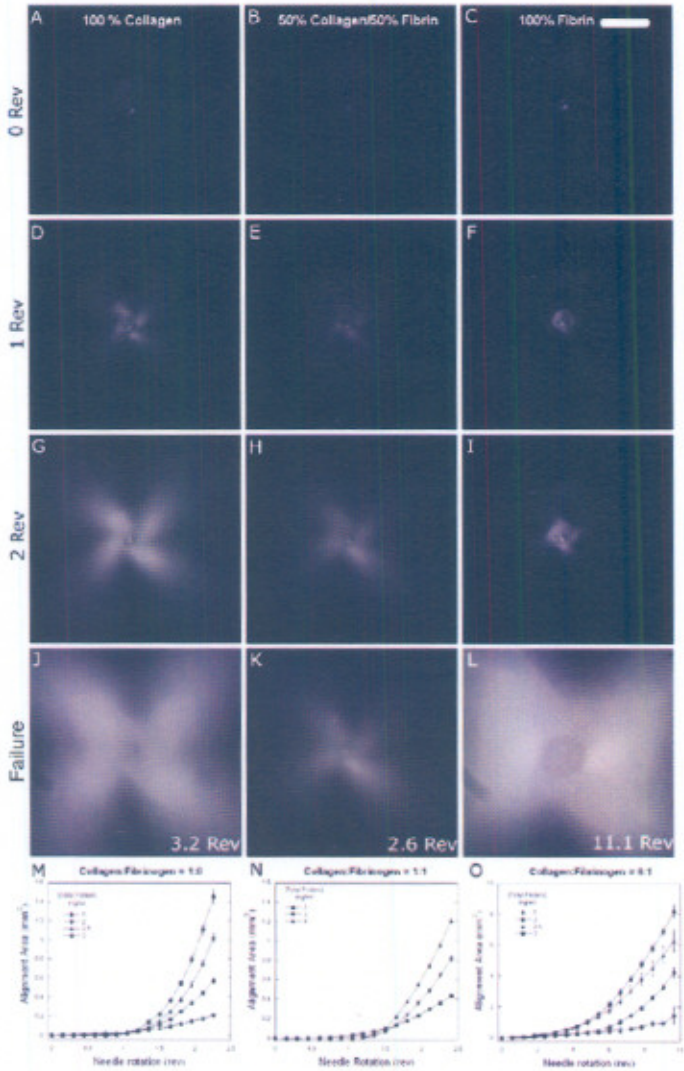

Figure 1: Alignment in collagen-fibrin composite gels.

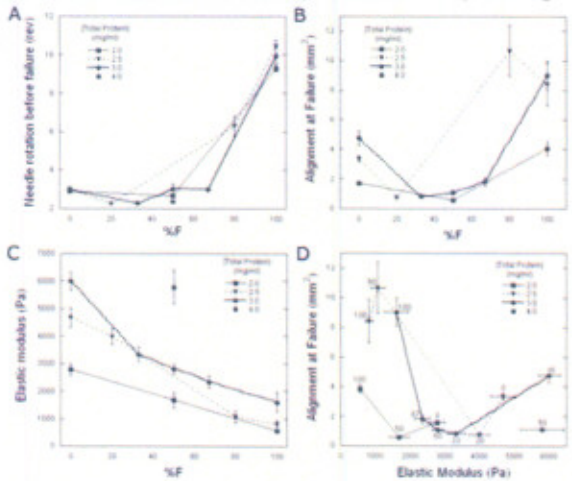

Figure 2: Relationships among stiffness, alignment, failure, and composition in collagen-fibrin gels. The percentage of fibrin is indicated for individual points in (D).

Copyright © 2010 by ASME

Proceedings of the ASME 2010 Summer Bioengineering Conference (SBC2010)
June 16-19, Grande Beach Resort, Naples Florida, USA

SBC2010-19350

THE GEOMETRY OF CONNECTIVE TISSUE PLANES ACCENTUATES THE BIOPHYSICAL RESPONSE TO TRADITIONAL ACUPUNCTURE: AN IN VITRO STUDY

Margaret Julias[1], Helen M. Buettner[1,2], David I. Shreiber[2]

1. Department of Chemical & Biochemical Engineering
2. Department of Biomedical Engineering
Rutgers, The State University of New Jersey, Piscataway, NJ, USA

INTRODUCTION

In traditional acupuncture, fine needles are inserted and rotated at defined points that correspond to specific therapeutic effects, which can occur locally or at a distance from the needling point. The majority of acupuncture points co-align with fascial planes under the skin, which present more subcutaneous loose connective tissue [1] (Fig 1 – black dot). Needle rotation induces this connective tissue specifically to couple to and wind around the needle, forming a whorl of alignment and generating measurable force on the needle that is significantly higher at fascial planes in comparison to insertion above a muscle (Fig 1A – black dot) [2, 3]. At these planes, the loose connective tissue is bounded on two sides by skeletal muscle and generally becomes narrower with increasing depth, presenting distinct geometry and boundary conditions compared to locations above a muscle, which resembles an infinite plane (Fig 1B&C).

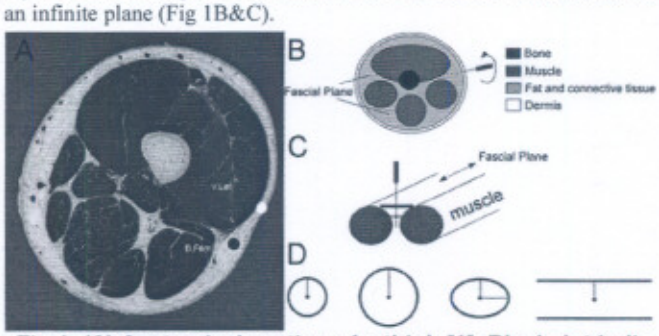

Fig 1. (A) Anatomical section of a thigh [1]. Black dot indicates an acupuncture point, white dot a control point. (B) & (C) Simplified schematics. (D) Simple geometries are used to emulate aspects of the connective tissue plane.

We used a simple in vitro approach [4] to study the effects of the basic elements of fascial plane geometry on fiber winding in a controlled setting. We prepared circular gels of different radii to emulate the narrower boundary within the intermuscular plane, and elliptical gels and 'planar' gels between two parallel strips to model the anisotropic boundary conditions presented within these planes (Fig 1D). The alignment behavior and failure of acellular collagen gels were examined quantitatively using polarized light microscopy.

MATERIALS AND METHODS

Collagen gel preparation Collagen solutions were prepared to achieve a final concentration of 2.5 mg/ml [5] and were poured into a 35-mm glass bottom MatTek dish containing annular circular (1.125" or 0.75" i.d.) or elliptical (1.125" major axis, 0.75" minor axis) porous polyethylene (PPE) inserts, or two 35-mm long thin strips of PPE placed 0.75" apart (to create planar gels) and incubated at 37°C for 4hr to ensure complete fibril formation. Since the signal from polarized light microscopy (PLM - see below) depends on sample thickness, the volume of collagen solution added was adjusted to maintain a 4-mm centerline height.

In vitro acupuncture A computer controlled motor was used to needle the gels. A 250-μm stainless steel acupuncture needle was attached to the motor and inserted perpendicular to the surface of the gel to a depth of 3 mm using a calibrated micromanipulator. The needle was rotated at 0.3 rev/s for 10 revolutions. The cellular gels were needled for 2 revolutions to prevent gel tearing and allow the observation of cell alignment after rotation with epifluorescence microscopy.

Fiber alignment: PLM was used to examine fiber alignment [4]. The gels were placed between two polarizers, which were positioned as 'cross-polars'. Images were captured at 6 frames per second during needle rotation and analyzed with MATLAB [4]. Both the polarizer

Copyright © 2010 by ASME

and analyzer were then rotated manually to 22.5° and 45° off the ellipse's major axis to examine fiber anisotropy

RESULTS/DISCUSSION

PLM revealed 'four-leaf clover' patterns of alignment following in vitro acupuncture (Fig 2). Fig 2A-D depicts alignment at 2.4 revolutions (the lowest number of revolutions across all conditions). Fig 2E-H shows alignment at failure, with number of revolutions indicated in lower-left hand corner. At 2.4 revolutions, alignment-induced birefringence is clearly weaker in the large circular gels (Fig 2A) and small circular gels (Fig 2B) when compared to elliptical gels (Fig 2C) and planar gels (Fig 2D). At failure, alignment was stronger in large circular gels (Fig 2E) than small circular ones (Fig 2F) and approached that in elliptical gels (Fig 2G). Planar gels (Fig 2H) demonstrated the strongest field of alignment at failure.

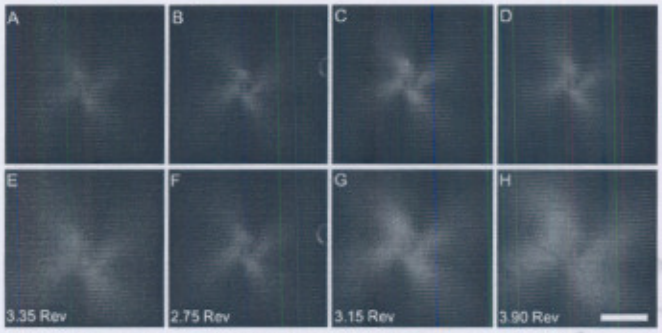

Fig 2: PLM-generated 'four-leaf clover' pattern of alignment following in vitro acupuncture. Bar: 1mm.

The effects of assay geometry on gel failure and fiber alignment were determined from image analysis of the clover leaf patters (Fig 3). Small diameter circular gels generated more alignment per revolution than larger gels, but also failed earlier, and the alignment at failure was greater for the larger gels. Introducing a non-uniform boundary condition significantly affected both alignment and failure (ANOVA, followed by Tukey's test, $P<0.02$) (Fig 3A). Fibers in the elliptical geometry aligned faster than in either circular assay but failed in between the two (Fig 3B). The net alignment at failure was the same statistically as that produced in the large circles (Fig 3C). When the anisotropy was increased with the planar gels, gels aligned at the same rate as in the ellipses, but were able to withstand the most number of revolutions before failure ($P<0.001$), which enabled the planar gels to demonstrate the greatest alignment at failure ($P<0.001$).

To examine if the elliptical geometry caused non-uniform fiber alignment, the axis of the polarizer/analyzer was rotated different degrees off of the major axis of the ellipse (indicated by the orientation of the cross in the upper right-hand corner of Fig 4A-F). Shown are the large circle (Fig 4A-C) and ellipse (Fig 4D-F). Within circular gels with uniform boundaries, the clover leaf patterns remained symmetric regardless of the polarization axes. Patterns within elliptical and planar gels were symmetric when the axes were coincident with the major and minor axes (Fig 4D), but became increasingly asymmetric as the angle was changed to 22.5° (Fig 4E) and 45° (Fig 4F). The degree of asymmetry was expressed as the ratio of the length of perpendicular leafs in each assay geometry (Fig 4G). The elliptical and planar geometries became increasingly asymmetric as the polarization axis was rotated (* - significantly different than 0°, # - significantly different than 22.5°, ANOVA followed by Tukey's pairwise comparisons).

DISCUSSION

Using simple in vitro analogs, we demonstrated that the geometrical constraints present in the narrowing channels of connective tissue at fascial cleavage planes may act to accentuate the mechanical response of the tissue to needle manipulation. In the elliptical and in particular the planar assays, fibers aligned faster and were more resistant to failure. We previously demonstrated that, when cells are included in these assays, they follow the orientation of the fibers [6]. Fiber alignment during acupuncture needling is indicative of tissue tension, which can stimulate resident fibroblasts mechanically. The stimulated fibroblasts may in turn affect the neighboring cells through cell-cell interactions [7] and modification of the surrounding matrix via collagen deposition or matrix degradation to propagate the effects of the local perturbation as well as produce longer term changes. The alignment of fibers and cells may also serve to transmit signals in a preferred direction, in addition to adding important structural changes that could also influence transport and healing.

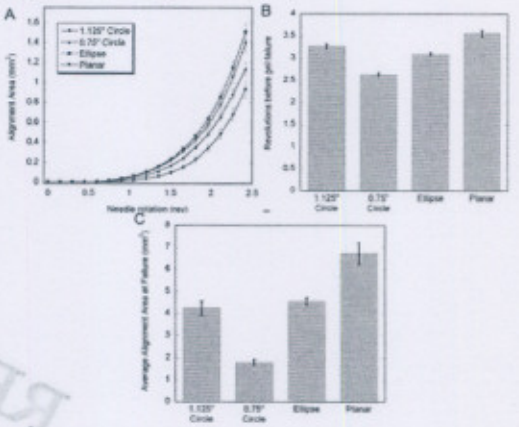

Fig 3. Evolution of alignment area up to 2.4 revolutions (B) Revolutions before gel failure. (C) Alignment area at failure. Results are average +/- std error.

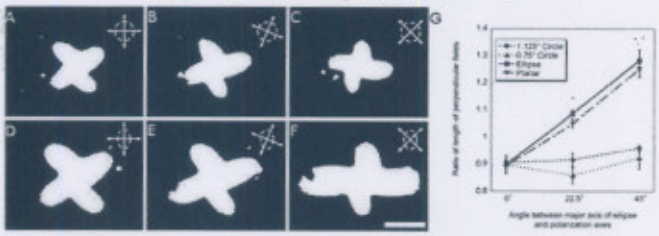

Fig 4. Alignment is isotropic in circular gels (A-C) but anisotropic in elliptical gels (D-F). Stronger alignment is in the direction of the minor axis. The degree of anisotropy was significantly greater for elliptical and planar gels, compared to circular gels (G).

ACKNOWLEDGEMENTS

Funding was provided by the NIH (R03 EB006045-01A1) and New Jersey Commission on Spinal Cord Research (05-2912-SCR-E-0). Data from the Visible Human Project Initiative was made available by the National Library of Medicine and the University of Colorado.

REFERENCES

1. Langevin, HM and J. Yandow, Anat Record (New Anat), 2002. 269: p. 257-265.
2. Langevin, HM et al. FASEB Journal, 2002, 16, 872-4.
3. Langevin, HM et al. J Appl Physiol, 2001, 91, 2471-2478.
4. Julias, M et al. Biomed Eng Online 2008, 7:19.
5. Shreiber, DI et al Exp Cell Res, 2001. 266: p. 155-166.
6. Julias M et al. 2009 SBC, #SBC2009-206519.
7. Langevin, HM et al. Histochem Cell Biol, 2004, 122: 7-15.

Copyright © 2010 by ASME